THESIS FOR THE DEGREE OF DOCTOR OF PHILOSOPHY

Preventing decoherence with giant atoms

ARIADNA SORO

Department of Microtechnology and Nanoscience (MC2)
Applied Quantum Physics Laboratory
Chalmers University of Technology
Gothenburg, Sweden, 2025

Preventing decoherence with giant atoms
ARIADNA SORO

ISBN 978-91-8103-220-8

Doktorsavhandlingar vid Chalmers tekniska högskola
Ny serie nr 5678
ISSN 0346-718X

Chalmers University of Technology
Department of Microtechnology and Nanoscience (MC2)
Applied Quantum Physics Laboratory
SE–412 96 Gothenburg, Sweden
Telephone +46 (0)31-772 1000

Cover: Two braided giant atoms coupled to a two-dimensional structured bath, which is depicted as a lattice of coupled cavities. This is one of the setups studied in Paper C.

Chalmers Digitaltryck
Gothenburg, Sweden, 2025

Preventing decoherence with giant atoms
ARIADNA SORO
Department of Microtechnology and Nanoscience (MC2)
Applied Quantum Physics Laboratory
Chalmers University of Technology

Abstract

Giant atoms have emerged as a new paradigm in quantum optics during the last decade. These are quantum emitters that couple to light—or other bosonic fields—at multiple discrete points, which can be spaced wavelengths apart. In the short time since the giant-atom regime was first reached, it has been shown that they offer more possibilities for design, control, and tunability than small atoms do, which makes them promising assets for quantum technologies. At the same time, due to the novelty of the field, most works have only studied giant atoms in relatively simple setups, e.g., coupled to open continuous waveguides. Thus, the papers appended here are an attempt to broaden the field by studying giant atoms in environments that have not been explored in depth before: continuous waveguides with chiral coupling and structured baths.

In this thesis, we contextualize the papers with regards to previously existing knowledge and future applications in the fields of quantum optics and quantum technology. We also provide a detailed description of the analytical tools that are necessary to derive the results of the appended papers: we delve into Lindbladian master equations, SLH formalism, and resolvent formalism, and we focus particularly on the underlying assumptions and approximations behind these techniques.

Keywords: Quantum optics, waveguide quantum electrodynamics, open quantum systems, giant atoms, artificial atoms, continuous waveguides, structured waveguides, master equation, SLH formalism, resolvent formalism

Acknowledgments

First and foremost, I would like to express my deep gratitude to Anton Frisk Kockum, my main supervisor, for his support, guidance, motivation and constructive criticism. Thank you for encouraging me to teach, attend courses and summer schools, present at conferences, ask for grants, and all those things that help me become a well-rounded researcher and individual. This thesis would not have been possible without you.

I would also like to thank Carlos Sánchez Muñoz, Alejandro González-Tudela, Alejandro Vivas-Viaña, and the people at Quinfog (CSIC), for welcoming me during my research stay, despite the difficult circumstances. More thanks go to my brilliant master's students, Emil Raaholt Ingelsten and Walter Rieck, who made me adore every second of my role as supervisor.

Special thanks to Aziza Almanakly, who took my utopian theory and brought it down to Earth, to the real world, so that I could learn about *actual* decoherence, noise sources, fabrication delays, and other real-life problems. It has been a great pleasure to work and hang out with you—hope we can do it again!

I finish the research acknowledgments by expressing my sincerest gratitude to Guangze Chen who, from the moment we met in Quantum Connections, has done nothing but restore the fun and joy I used to feel for physics. Your incessant questions and brilliant intuitive reasoning have been one of the highlights of my PhD.

Now, those who know me, know that research has only been a portion of my PhD. In fact, a big part of my time at Chalmers has been dedicated to building a better working environment for PhD students. I am thankful to all those who have crossed paths with me at the MC2 PhD student council, the DS board and Jägr, for sharing my belief that academia doesn't have to be toxic, and for trying to do something about it. Special thanks go to Núria, Nermin, Ivo, Vittorio, Junjie and Yiting, among whom I found more than purpose: I found community.

And speaking of community, I can honestly say I could not have finished the PhD without the incommensurable support of the badass women I have met in this journey. I am deeply grateful to Irina Pettersson, one of the strongest people I know, for being the absolute best mentor and role model I could ever ask for. I am also thankful for my AQP family: Therese, Hanna, Laura, Emely, Maryam, and my sisters from Physics: Adriana, Pantea, Emelie, Laura, Julia,

Kajsa, Mirna, Rebecka. Time and time again, you have shown me the most beautiful blend of strength, resilience, intelligence, fun, compassion, empathy, and love. I am in awe of all of you, and in eternal gratitude to Adriana for bringing us together. Keep shining bright!

Next, I would like to thank those who didn't have to, but went above and beyond to create warm and safe spaces for me. To Linda Brånell, she who has all the answers: your diligence alone would be reason enough to thank you. But what I appreciate the most is how much you care about others and always create the best environment around you. Thanks for welcoming us to your home, your office and your lunch breaks, and for helping us navigate this foreign language and culture that we now call our own. To the staff at Wijkanders, thank you not only for making me safe lunch and adapting to my changing needs without complaint, but also for knowing my order, receiving me with open arms, laughs and even silly little dances. You have no idea the amount of hours you've saved me in lunchbox prep! *Tusen tack* to Mats and Madeleine, who have given me a home away from home, a refuge, a shelter. A place where I can disconnect, recharge, and where every day feels like spa day. Finally, *infinites gràcies* to my parents, Arpi and Clàudia, as well as to Carlos Moreno and Vela, for always believing in me, even when I didn't. *Gracias de todo corazón.*

Last but not least, to Simon, the love of my life. Thanks for your unwavering support, love, and radical compassion. I could have done this without you (strong independent woman and all that jazz), but I'm really glad I didn't have to. Everything is undoubtedly better with you by my side.

Ariadna Soro, Gothenburg, May 2025

Publications

This thesis is based on the following papers:

A **Chiral quantum optics with giant atoms**
Ariadna Soro and Anton Frisk Kockum
Physical Review A **105**, 023712 (2022)

B **Interaction between giant atoms in a one-dimensional structured environment**
Ariadna Soro, Carlos Sánchez Muñoz, and Anton Frisk Kockum
Physical Review A **107**, 013710 (2023)

C **Avoiding decoherence with giant atoms in a two-dimensional structured environment**
Emil Raaholt Ingelsten, Anton Frisk Kockum, and Ariadna Soro
Physical Review Research **6**, 043222 (2024)

D **Two-photon quantum gates with giant atoms in structured waveguides**
Walter Rieck, Ariadna Soro, Anton Frisk Kockum, and Guangze Chen
In preparation (not appended)

E **Driven-dissipative entanglement with separate giant atoms**
Aziza Almanakly, Ariadna Soro, et int., Anton Frisk Kockum, and William D. Oliver
In preparation (not appended)

Other papers that are outside the scope of this thesis:

I **Giant Rydberg excitons in Cu_20 probed by photoluminescence excitation spectroscopy**
Marijn A. M. Versteegh, Stephan Steinhauer, Josip Bajo, Thomas Lettner, Ariadna Soro, Alena Romanova, Samuel Gyger, Lucas Schweickert, André Mysyrowicz, and Val Zwiller
Physical Review B **104**, 245206 (2021)

II **Lecture notes on quantum computing**
Anton Frisk Kockum, Ariadna Soro, Laura García-Álvarez, Pontus Vikstål, Tom Douce, Göran Johansson, Giulia Ferrini
arXiv.2311.08445 [quant-ph]

Contents

Prologue

El prólogo, para los de la
LOGSE: lo que hay al principio
de los libros que no son las tapas.

Goyo Jiménez (2011)

What is quantum?—asked Vitaly, in a thick Slavic accent and a skeptical tone, on one of my first days as a PhD student. Not the question you expect to hear from the most senior member of the Applied *Quantum* Physics division, yet I have heard him ask it many times since, to all sorts of speakers—from students to renowned researchers. *Vot is qvantum?*

To borrow from Elyse Myers, *that's a great question, I'd love to tell you.*

1 Introduction

> In this field, almost everything is already discovered, and all that remains is to fill a few holes.
>
> Philipp von Jolly, Max Planck's professor (1878)

At the end of the nineteenth century, scientists seemed to have understood the most fundamental principles of nature: from the motion of bodies, to the propagation of electromagnetic fields, or the laws of thermodynamics. Little did they know that the understanding of physics was about to drastically change at the turn of the century, once they started delving into the atomic and subatomic scales. Many novel counterintuitive ideas were postulated and subsequently proved: energy comes in discrete quantities known as quanta, objects have characteristics of both particle and waves, and there are limits to how accurately the value of a physical quantity can be predicted prior to its measurement. Under these principles, quantum mechanics was established, and many great inventions were created, such as the transistor, the laser, and the atomic clock. In turn, these inventions later gave us computers, optical fiber communication, and the global positioning system (GPS), all of which are vital to the world as we know it today. This is what we call the *first quantum revolution* [1, 2].

Now a *second* revolution is underway—this one centered on the applicability of more complex quantum phenomena, such as superposition, entanglement, or squeezing. In this era, we not only talk about quantum mechanics or physics, but also of quantum technologies, which can be divided in four main fields according to their purpose. Quantum computing [3] aims at speeding up computation on important optimization problems; quantum simulation [4] pursues simulating complex physical systems, such as molecules for medical and chemical applications; quantum communication [5] wants to provide secure encryption and communication channels; and quantum sensing and metrology [6] aims at increasing precision and speed for a large variety of measurements.

Most of these quantum technologies have something in common: they rely on the manipulation and generation of non-classical states of light. And in order to achieve such control, it is essential to first achieve a deep understanding of

quantum optical phenomena, i.e., of phenomena concerning the interactions between light and matter at the scale of individual quanta of light (photons). It was, in fact, quantum optics that kickstarted the first quantum revolution, with the modeling of the blackbody radiation spectrum by Max Planck in 1899. Since then, the field has expanded—and keeps expanding—into many directions, in part aided by emerging technologies that keep opening the door to unexplored physical paradigms.

In this thesis, we focus on a specific platform to study quantum optics: waveguide quantum electrodynamics (QED) [7]. As the name suggests, a waveguide is a structure that guides waves with minimal energy losses by restricting the transmission of energy to one dimension. Thus, waveguide QED is concerned with the interaction between photons propagating in a waveguide and localized quantum emitters, such as cold atoms or superconducting qubits, which are capable of emitting and absorbing single photons. More in particular, in this thesis, we use waveguide QED to study a new kind of quantum emitters: *giant atoms*. These emitters can couple to light at multiple discrete points, spaced wavelengths apart, and give rise to fascinating interference effects.

Contrary to *small* atoms, which is the standard paradigm of matter in quantum optics, giant atoms offer more possibilities for design, control, and tunability than small atoms do, which makes them promising assets for quantum technologies. At the same time, the field is still very new, meaning that at the beginning of this thesis, most works had only studied giant atoms in relatively simple setups. Thus, the papers upon which this thesis is based are an attempt to broaden the field by studying giant atoms in environments that either had not been explored before, or not in sufficient depth: continuous waveguides with chiral coupling (Paper A), one-dimensional structured waveguides (Papers B and D) and two-dimensional structured lattices (Paper C). Paper E is the experimental implementation of one of the results found in Paper A.

1.1 Outline of the thesis

This thesis is structured as follows.

In Chapter 2, we introduce the building blocks of the setups that we study in the appended papers: giant atoms as the system, and continuous and structured waveguides as the environment. We describe them from the standpoint of both theory and experiment, and we contextualize them with state-of-the-art technologies.

In Chapter 3 and Chapter 4, we present the formalism that we use to describe giant atoms coupled to open *continuous* waveguides—the setup studied in Papers A and E. In particular, in Chapter 3, we introduce the density operator to discuss pure and mixed states, entanglement measures, and decoherence mechanisms. We then use the density operator to derive a Lindbladian master equation which describes the Markovian dynamics of a quantum emitter coupled to a waveguide. In Chapter 4, we introduce the SLH formalism, which we use in

conjunction with the Lindblad master equation to model cascaded systems such as the setup in Paper A, where an atom (or an ensemble) is chirally coupled to the waveguide. We also lean on the more applied side of the theory to discuss chiral interfaces, as well as interference effects for preventing decoherence and for implementing quantum logic gates.

In Chapter 5, on the other hand, we delve into the analytical methods used to describe giant atoms coupled to *structured* baths, which is the environment studied in Papers B, C, and D. In particular, we discuss the limitations of the tools presented in the previous chapters, and introduce the resolvent formalism and other complex-analysis techniques to overcome them. We then exemplify the use of these methods to the spontaneous emission of a giant atom coupled to a one- and a two-dimensional structured environment, specifically focusing on harnessing bound states to prevent decoherence. We round off by discussing the non-Markovian effects that arise in these setups.

Finally, in Chapter 6, we give an overview of the papers upon which this thesis is based, and we conclude with final remarks and an outlook on future research in Chapter 7.

2 The system and its environment

Yo soy yo y mi circumstancia.

José Ortega y Gasset (1914)

In this chapter, we introduce the building blocks of the setups that we study in the appended papers: giant atoms as the system, and continuous and structured waveguides as the environment. We describe them from the standpoint of both theory and experiment, and we contextualize them with state-of-the-art technologies.

2.1 The system – giant atoms

Historically, when studying light-matter interactions at the smallest scale, we have assumed the matter to be natural atoms. And since the radius of natural atoms ($r \approx 10^{-10}$ m) is orders of magnitude smaller than optical ($\lambda \approx 10^{-7} - 10^{-6}$ m) or microwave wavelengths ($\lambda \approx 10^{-2} - 10^{-1}$ m), we have typically assumed that atoms are *small* compared to the light they interact with [8]. Even Rydberg atoms, which are considerably larger ($r \approx 10^{-8} - 10^{-6}$ m), are still small with respect to the microwaves they typically interact with [9]. This is known as the dipole approximation ($r \ll \lambda$) [10].

However, in the last decades, quantum optics has expanded to systems with artificial atoms, such as quantum dots ($r \approx 10^{-9}$ m) [11] and superconducting qubits ($r \approx 10^{-4} - 10^{-3}$ m) [12, 13], which are engineered to have some of the properties of natural atoms: quantized energy levels and the ability to emit and absorb energy in those quanta. This grants both natural and artificial atoms the name of *quantum emitters*.

In particular, in 2014, it was thanks to artificial atoms when an experiment [14] showed that the dipole approximation can break down in circuit

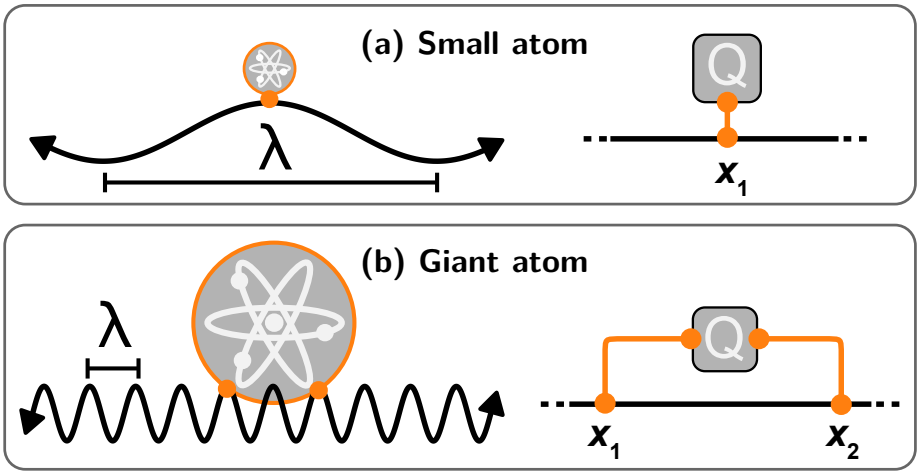

Figure 2.1: (a) A small atom, treated as a point-like object because it is much smaller than the wavelength λ of the field it interacts with. (b) A giant atom, formed by coupling a small atom to a mode at two discrete locations, spaced wavelengths apart. Figure adapted with permission from Ref. [20].

QED[1]. This feat was achieved coupling a superconducting transmon qubit [17] to surface acoustic waves [18] ($\lambda \approx 10^{-6}$ m) at multiple discrete points, spaced $\lambda/4$ apart. A subsequent theoretical study [19] coined the term *giant atom* (GA), in contrast to a *small* atom, to refer to a paradigm where a quantum emitter is large compared to the wavelength of the field it interacts with, and where the multiple coupling points lead to interference effects. A sketch illustrating the difference between a small and a giant atom is shown in Fig. 2.1: on the left, the atoms couple to the field in free space; on the right, the emitters are qubits which interact with the field by coupling to a waveguide at a single or multiple points.

Looking at the illustration of the GA in Fig. 2.1(b), one can see that, if GAs can emit and absorb energy at each of their coupling points, there can be interference between those paths. Therefore effectively, GAs interfere with themselves, which allows them to exhibit physical phenomena that are generally unattainable with small atoms. Some of these phenomena, such as frequency-dependent relaxation rates and decoherence-free interaction, will be explained in the next section and derived in more detail throughout the thesis.

It should be noted, however, that some particular cases of GAs can indeed be reproduced by using small atoms. For instance, a small atom in front of a

[1]We refer to the dipole approximation breakdown as the fact that $r \gtrsim \lambda$, which means there may be variations of the electromagnetic field across the atom that lead to self-interference effects. We do not imply that higher multipole effects should be considered, as may be the case in other subfields of atomic and molecular physics [15, 16]; nor that this was the first experiment ever to break the dipole approximation (only in the context of circuit QED).

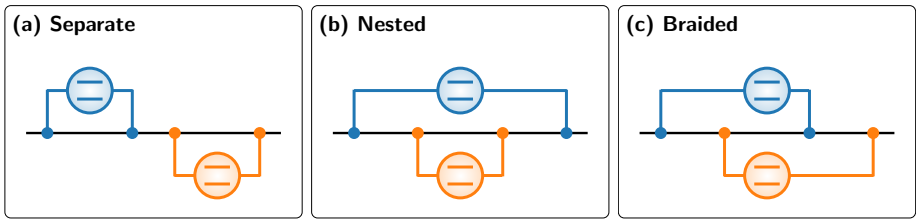

Figure 2.2: Different arrangements of two giant atoms with two coupling points each. Figure adapted from Paper B.

mirror [21–36] can simulate a GA with two coupling points in a unidirectional waveguide. That said, the small-atom setup poses many design limitations, since it is not possible to increase the number of coupling points, to have different coupling strengths at different points, or to have more advanced scattering.

In fact, in general, it has been shown that GAs offer more possibilities for design, control, and tunability than small atoms do. This can be intuitively understood by picturing the different ways in which two GAs with two coupling points each can couple to a common waveguide. In Fig. 2.2, we can see that with such a simple setup, there already exist three possible arrangements: the *separate* configuration, where the points of the second atom come sequentially after the ones of the first atom; the *nested* configuration, where the points of the first atom enclose those of the second atom; and the *braided* configuration, where the points of the two atoms are interleaved. Now, it is straightforward to see that by increasing the number of atoms and coupling points, the amount of possible configurations increases too, and with it, the amount of design parameters.

This freedom in design, control and tunability that GAs offer, makes them appealing both for the pursuit of fundamental understanding of light-matter interactions, and for their potential applications in the fields of quantum computing [3] and quantum simulation [4, 37].

2.2 The environment

Because the size of a quantum emitter is defined with respect to the field it interacts with, it does not make sense to talk about a GA as a closed system. Instead, it should be considered an *open quantum system*, i.e., a quantum-mechanical system that is coupled to a surrounding *environment*, often called a *bath* or a *reservoir*. In general, this interaction changes the dynamics of the system and results in dissipation, such that the information contained in the system is lost to its environment.

2.2.1 Continuous waveguides

In waveguide QED experiments, an open quantum system typically consists of one or more quantum emitters (natural or artificial atoms) coupled to an optical fiber or to a microwave transmission line (chip-integrated coaxial cable). These are types of one-dimensional (1D) *continuous waveguides*, which support a continuum of *propagating modes* that can be modeled by the following Hamiltonian ($\hbar = 1$ throughout this thesis):

$$H = \sum_k \omega_k \, a_k^\dagger a_k, \tag{2.1}$$

where ω_k is the frequency of each mode, and $a_k^\dagger, a_k$ are the creation and annihilation operators, respectively [7, 38–40]. Since the sum is infinite[2] and mode spacing is infinitesimal, it is sometimes convenient to rewrite the Hamiltonian as an integral:

$$H = \int_0^\infty d\omega \, \omega \, a_\omega^\dagger a_\omega = \int_0^\infty dk \, \omega_k v_p \, a_k^\dagger a_k, \tag{2.2}$$

where v_p is the phase velocity. The dispersion relation of the bath is given by $\omega(k) = k \cdot v_p(k)$, with k being the wave number, which sets the density of states $D(\omega) = |\partial\omega(k)/\partial k|^{-1}$ [40]. Continuous waveguides usually have trivial dispersion relations, often considered linear [38, 39, 41].

When coupling a small excited atom to a continuous waveguide, the atom will relax, i.e., it will spontaneously emit a photon at a rate given by Fermi's golden rule, which is proportional to the density of states $D(\omega)$ [40, 42]. The photon, of frequency equal to the spacing between the atomic energy levels, will then propagate through the waveguide with little to no dissipation, at a speed given by the phase and group velocities ($v_p = v_g$ in the case of linear dispersion).

When coupling a single GA or multiple small or giant atoms to a continuous waveguide, interference effects may amplify or suppress the spontaneous emission process. We present below two consequences of such effects.

Tunable frequency-dependent relaxation rates

In the first theory paper on GAs back in 2014, it was shown that interference between the coupling points of a GA leads to frequency-dependent relaxation rates [19]. This dependence can be engineered with a number of design parameters (e.g., coupling strength at each point, distance between coupling points) that increases linearly with the number of coupling points. What is more, in some experimental platforms—for instance, by using superconducting qubits or ferromagnetic spin ensembles as GAs (see Sec. 2.3.1)—the atomic frequency can be tuned in situ, making it possible to move between regions with high and low relaxation rates during an experiment, as demonstrated in Refs. [20, 43, 44].

[2] In reality, most waveguides have a cutoff frequency after which modes can no longer propagate. However, when operating at frequencies far off the cutoff, the dynamics mimic those of an infinite continuum of propagating modes.

If we consider more than two atomic levels, other interesting applications of the frequency-dependent relaxation rate open up. For instance, it is possible to engineer different relaxation rates for different transitions, thus allowing population inversion and lasing, which in turn, can enable electromagnetically induced transparency, as shown in Refs. [43, 45].

Waveguide-mediated decoherence-free interaction

Probably the most intriguing property yet found in GAs is their ability to interact though a waveguide without decohering—a feature demonstrated both theoretically [46–48] and experimentally [20]. By arranging two or more giant atoms in the braided configuration, i.e., with their coupling points interleaved [see Fig. 2.2(c)], it is possible to suppress their relaxation rates while maintaining their exchange interaction. In this way, they can exchange an excitation back and forth without ever losing it into the waveguide, which is something small atoms cannot do.

Thus, this property is of great interest in the field of quantum computing, where a major hurdle is preventing operation errors arising from decoherence and dissipation.

At the beginning of this thesis, the two features above had only been shown for GAs coupled to 1D bidirectional waveguides. In the appended papers, we extended their applicability to continuous waveguides with chiral coupling (Paper A), through the formalism provided in Chapter 3 and Chapter 4; and to 1D and 2D structured baths (Papers B and C), through the formalism in Chapter 5.

2.2.2 Structured waveguides

Structured waveguides are those which, contrary to continuous waveguides, have nontrivial dispersion relations, such as band edges and band gaps. A simple example is an array of coupled cavities, which creates a finite propagating band with a speed of light that is controlled by the tunneling between neighboring cavities and thus can, in principle, be made arbitrarily small. This is why structured waveguides are also known as *slow-light waveguides* [49]. Other commonly used names are *photonic crystal waveguide* or *coupled-resonator array*.

As shown in Fig. 2.3, an atom coupled to a structured environment with its transition frequency tuned to the propagating band shows the typical exponential decay of spontaneous emission (similar to a continuous waveguide). Conversely, when the atom is detuned away from the band, i.e., when it is tuned to the band gap, it does not decay. This occurs because atom-photon bound states are formed in the band gaps, where photons become exponentially localized in the vicinity of the atoms, inhibiting their decay [49–52]. Even at the band edge of the continuum of propagating modes, atoms show fractional decay due to the influence of bound states [53–56]. Furthermore, multiple atoms coupled to the band gap of the same reservoir can interact through the overlap of their bound-state photonic wavefunctions [57–59], without losing their excita-

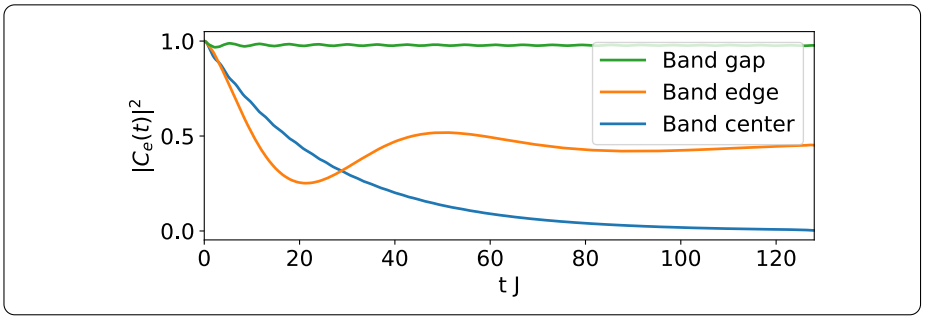

Figure 2.3: Population dynamics of a two-level atom coupled to a structured waveguide. The atom shows no relaxation when tuned to the band gap (green line), fractional decay when tuned to the band edge (orange line) and exponential relaxation when tuned to the band (blue line).

tions to the environment. These interactions can be tuned during experiments by modifying the frequencies of the atoms and their coupling strengths to the bath, which opens doors for applications in quantum computation and quantum simulation of many-body physics [60, 61].

1D arrays

Mathematically, a 1D structured waveguide can be modeled with the same Hamiltonian as a continuous waveguide [Eq. (2.1)], but with a different dispersion relation. For example, in Paper B, we use that the bath Hamiltonian rotating at the bath frequency can be expressed as $H_b = \sum_k \omega(k) a_k^\dagger a_k$, with

$$\omega(k) = -2J\cos(k), \tag{2.3}$$

where J is the hopping rate between coupled cavities. This describes a continuum of modes confined in an energy band $E \in [-2J, 2J]$, where the dispersion is linear around the middle of the band [$\omega(\pm\pi/2+\varepsilon) = \pm 2J\sin(\varepsilon) \approx \pm 2J\varepsilon$] and parabolic close to the band edges [e.g., $\omega(\varepsilon) \approx -2J(1-\varepsilon^2/2)$]. In turn, this translates into a density of states

$$D(E) = \left|\frac{\partial\omega(k)}{\partial k}\right|^{-1}_{\omega(k)=E} = \frac{1}{\pi\sqrt{4J^2 - E^2}}\Theta(2J - |E|), \tag{2.4}$$

that is nearly constant around the middle of the band (i.e., for energies $E \approx 0$) and diverges at the band edges ($|E/J| \approx 2$) [62]—as shown in Fig. 2.4(a).

2D lattices

The formulation for the 1D array can organically be extended to a two-dimensional (2D) square lattice with the following dispersion relation:

$$\omega(\vec{k}) = -2J(\cos k_x + \cos k_y), \tag{2.5}$$

which we use to describe the setup in Paper C. Although describing a fairly simple 2D structured bath, Eq. (2.5) gives rise to some very interesting properties. First and foremost, it results in an broader energy band than the 1D case, now in the range $E \in [-4J, 4J]$. Within this band, the energy dispersion varies widely: it is isotropic close to the band edges, meaning that excitations in the lattice propagate equally in all directions. However, the dispersion becomes highly anisotropic at the band center [i.e., at $\omega(\vec{k}) = 0$] [62], which is easy to see from the definition of group velocity:

$$\vec{v}_g = \vec{\nabla}\omega(\vec{k})\Big|_{\omega(\vec{k})=0} = 2J \sin k \begin{bmatrix} 1 \\ \pm 1 \end{bmatrix} \tag{2.6}$$

for any $k \in [-\pi, \pi)$. Thus, at the band center, excitations can only propagate along the two orthogonal diagonals $\left[\begin{smallmatrix} 1 \\ \pm 1 \end{smallmatrix}\right]$. Furthermore, note that $\vec{v}_g$ vanishes for $k = \{0, \pm\pi\}$, which yields a divergent density of states, i.e., a type of Van Hove singularity present in many 2D structured baths [62, 63]. In particular, the density of states in this case satisfies

$$D(E) = \frac{1}{(2\pi)^2} \iint d\vec{k}\, \delta[E - \omega(\vec{k})], \tag{2.7}$$

with $\omega(\vec{k})$ given in Eq. (2.5). We plot this expression in Fig. 2.4(b), computed by Monte Carlo integration.

The singularities that appear in the density of states, both in 1D and 2D, lead to non-Markovian dynamics, such as the aforementioned appearance of atom-photon bound states and fractional decay at the band edges. These non-Markovianities prevent us from using the analytical tools described in Chapter 3 and Chapter 4, so in order to accurately describe the dynamics of the system, we instead resort to the complex-analysis techniques shown in Chapter 5.

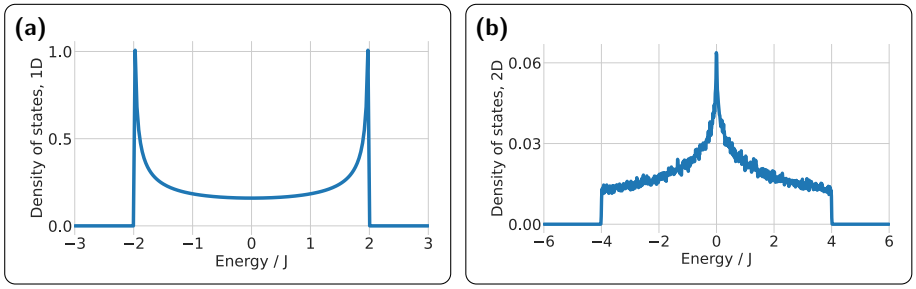

Figure 2.4: Density of states as a function of energy for (a) a 1D structured bath, as given by Eq. (2.4); and (b) a 2D structured bath, as given by Eq. (2.7).

2.3 Experimental implementations

Since the first experiment in 2014, several other demonstrations of GAs have been achieved, both with superconducting qubits coupled to surface acoustic waves [14, 45, 64–73] and to microwave waveguides [20, 43, 74], and many other implementations have been proposed [75–78]. Recently, giant-atom physics have also been explored beyond the atomic paradigm (natural or artificial few-level systems) into giant molecules [79–83], giant spin ensembles [44, 84], and giant superatoms [85]. Here, we give an overview of how giant atoms can be implemented in experiments.

2.3.1 Giant atoms in continuous waveguides

Transmon qubits coupled to transmission lines

While it is clear that superconducting qubits ($r \approx 10^{-4} - 10^{-3}$ m) fall in the giant-atom regime when coupled to SAWs ($\lambda \approx 10^{-6}$ m), it may not be straightforward to see how they reach this regime when coupled to microwave waveguides ($\lambda \approx 10^{-2} - 10^{-1}$ m). The answer lies in meandering the waveguide between the coupling points of the qubit long enough to enter the giant-atom regime [20, 43, 86], as shown in Fig. 2.5(a), which is the approach we envisioned in Paper A and brought to experiment in Paper E.

In Paper E, we used two frequency-tunable *transmon qubits* [17] acting as separate giant atoms, as shown in Fig. 2.5(b). Transmons are superconducting qubits whose energy spectrum can be modeled as an anharmonic potential. The uneven spacing between energy levels means that we can control which energy transition we want to target, and we choose to use the two lowest levels to define our qubit, i.e., to encode the logical $|0\rangle$ in the ground state $|g\rangle$, and the logical $|1\rangle$ in the first excited state $|e\rangle$. It is important to note that reducing the anharmonic oscillator to its two lowest energy levels only makes sense in the low-power regime, where the probability of exciting higher levels is negligible. This is why modeling the giant atoms as two-level systems—which we do in Papers A, B, C—is strongly tied to studying these systems in the single- or few-photon regime. In Paper E, however, the choice of experimental parameters requires us to use stronger drive powers, which can surpass the anharmonicity and eventually populate the third energy level—typically referred to as $|2\rangle$ or $|f\rangle$. We should note that populating higher states is not always undesired, on the contrary, it can be necessary for the implementation of quantum gates such as the CZ gate [87, 88], as is the case in Paper D.

Analytically, the atom as an anharmonic three-level system (3LS) is described by the following Hamiltonian:

$$H_{\mathrm{3LS}} = \omega_{01} a^\dagger a + \frac{\alpha}{2} a^\dagger a^\dagger a a, \tag{2.8}$$

where ω_{01} and ω_{12} are the the two lowest transition frequencies, $\alpha = \omega_{12} - \omega_{01}$ is the anharmonicity, and a and $a^\dagger$ are the annihilation and creation operators

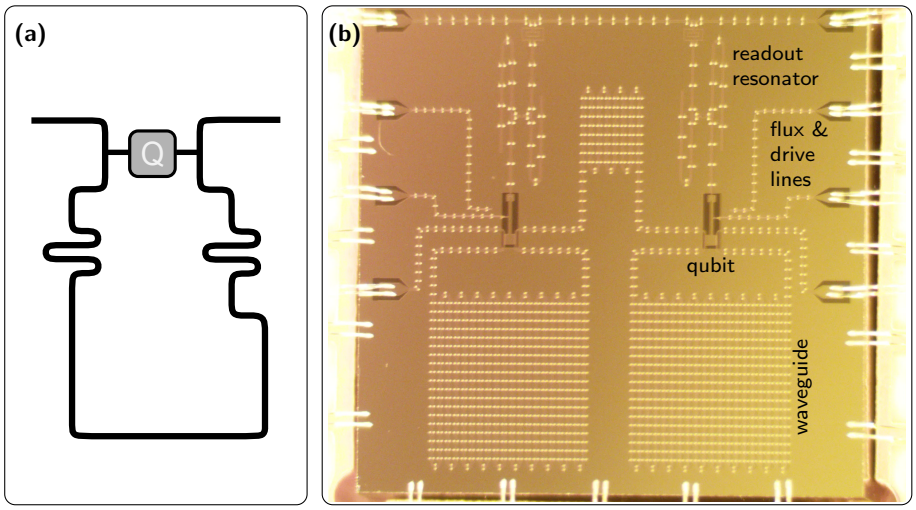

Figure 2.5: (a) A giant atom coupled to a meandering transmission line. Figure adapted with permission from Ref. [20] (b) A picture of the chip used in Paper E, with two separate giant atoms coupled to a common transmission line. The giant atoms are flux-tunable transmon qubits with their own flux and drive lines, and they are coupled to readout resonators.

of the harmonic oscillator. In the two-level system (2LS) approximation, we disregard all higher levels, and $a^\dagger a$ in Eq. (2.8) becomes $\sigma_+\sigma_- = (1+\sigma_z)/2$, with σ_z being the Pauli-Z matrix[3]. Hence, the Hamiltonian reads:

$$H_{\text{2LS}} = \frac{\omega_{01}}{2}\sigma_z. \tag{2.9}$$

Regardless of their analytical description, and as we can see in Fig. 2.5(b), the transmons are coupled to a *transmission line*, which is a continuous 1D coplanar waveguide that follows the description in Sec. 2.2.1. The transmission line may carry the microwave pulses that excite the qubits (in Fig. 2.5(b) each qubit also has its own drive line), as well as the excitations emitted by them, and therefore mediates their interaction. The qubit frequencies are tuned via flux lines, which allows us to tune the phase shift between the coupling points of the atoms, and thus control their relaxation rate and other interference effects during the experiment. Finally, the state of the qubits are measured through *readout resonators*, which are shorted transmission line that can be modeled as harmonic oscillators. State readout is possible by dispersively coupling the qubit and the resonator, i.e., by detuning them significantly, until the state of the qubit imprints a frequency shift in the resonator that is measurable.

[3]In the basis $\{|e\rangle, |g\rangle\}$, which is more common in atomic, molecular and optical physics, these operators are defined as: $\sigma_- = |g\rangle\langle e|$, $\sigma_+ = |e\rangle\langle g|$, and $\sigma_z = |e\rangle\langle e| - |g\rangle\langle g|$. In quantum computing, however, they are typically defined the other way around, e.g., $\sigma_z = |0\rangle\langle 0| - |1\rangle\langle 1|$. In this thesis, we use the former definition, unless stated otherwise.

Spin ensembles in waveguide magnonics

Using superconducting qubits as giant atoms means that experiments have to take place at cryogenic temperatures. However, a different approach has made it possible to reach the giant-atom regime at room temperature in the microwave spectrum [44]. The trick is to substitute the qubit for a ferromagnetic spin ensemble in the form of a rotating sphere and couple it to a meandering waveguide at two discrete points, in a similar way as in superconducting experiments. This demonstration has been able to reproduce frequency-dependent relaxation rates and characterize giant nested atoms in agreement with theory.

Optical spectrum

In the optical spectrum, meandering the waveguide around the atom is nontrivial: natural atoms are three to four orders of magnitude smaller than optical wavelengths, and optical waveguides such as nanofibers have a physical limitation to how much they can be bent. However, one can get around that by going beyond the atomic paradigm and using free-space light instead of waveguides. For instance, in a setup reminiscent of giant braided atoms, room-temperature decoherence-free interaction has been demonstrated between an optomechanical system and an atomic ensemble [47, 84].

2.3.2 Giant atoms in structured environments

Many different platforms have been used to demonstrate phenomena arising from the interaction between a small atom and a structured environment [89].

In the optical domain, these include cold atoms coupled to a photonic crystal waveguide [90–93] or to an optical lattice [94, 95], and quantum dots coupled to a photonic crystal waveguide [96, 97]. While it seems unlikely that many of these architectures can be adapted to reach the giant-atom regime, a proposal exists for ultracold atoms in 2D optical lattices [75]—which prompted us to study the setup in Paper C. In this proposal, the atom is localized in a deep lattice site and it is coupled by a laser to a shallower lattice which lets matter-wave propagate at rate J. Then, by moving the relative position between the potentials fast enough, the GA couples effectively to several bath positions. An experimental implementation of such a proposal remains elusive to date.

In the microwave domain, the interaction between a small atom and a structured environment has been realized with superconducting qubits coupled to microwave photonic crystals [98–100], to superconducting metamaterials [60, 101–104], and to compact resonator arrays [105–107]. In particular, microwave photonic crystals were first created to emulate their optical counterparts: by periodically modulating coplanar waveguides with a lattice constant on the order of the wavelength. However, this translated to a device size of approximately a few centimeters for complete confinement of the evanescent fields in the frequency range of microwave qubits. Such a restriction significantly limited the scaling in this approach, both in qubit number and qubit connectivity. To overcome this

limitation, a new approach started to gain traction: metamaterials with sublattice constants, where photonic excitations could be more strongly confined. While metamaterials had been studied for many years, their use in quantum optical experiments had been fairly unexplored, due to the lossy nature of the subwavelength components. Fortunately, technological improvements in recent years have made them very suitable for studying quantum phenomena. An even smaller lattice footprint has been achieved with compact lumped-element resonator arrays, for instance, by replacing the geometric inductance for Josephson inductance [105, 107], or for thin films of high kinetic inductance [106].

Since all of the 1D microwave arrays above use superconducting qubits as the quantum emitter, they are all adaptable to study giant-atom physics. To do that, the capacitive couplings between the atom and the resonator need to be made longer, so that the atom couples to several resonators instead—thus becoming giant. Extending these architectures to 2D may prove a bit more challenging, but still feasible: arranging for the multiple coupling points may be aided by flip-chip technology [108–110].

3 Density operator and master equation

Are we human or are we *denser*?

The Killers (2008)

In this chapter, we introduce the density-operator formalism to discuss pure and mixed states, entanglement measures, and decoherence mechanisms. Then, we use the formalism to derive a Lindbladian master equation, which allows us to examine the Markovian dynamics of a qubit coupled to a waveguide. The framework in this chapter is used in Papers A and E.

3.1 Density-operator formalism

In quantum optics and the study of open quantum systems, the density-operator formalism provides a robust framework for describing statistical mixtures, entanglement, and the effects of decoherence. While the terms *density matrix* and *density operator* are often used interchangeably, in reality, the density operator ρ is an object acting on a Hilbert space, whereas the density matrix is the matrix representation in a chosen basis.

A general quantum state is described by a density operator [3]

$$\rho \equiv \sum_{\psi} p_{\psi} \left|\psi\right\rangle\!\left\langle\psi\right|, \tag{3.1}$$

where $\{|\psi\rangle\}$ are pure states that occur with a probability $p_{\psi} \in [0,1]$, and the probabilities add up to one ($\sum_{\psi} p_{\psi} = 1$). This decomposition is not unique, and the operator ρ is Hermitian and has unit trace.

Given an orthonormal basis $\{|i\rangle\}$, the pure states can be written as $|\psi\rangle = \sum_i c_{\psi,i} |i\rangle$, and the density matrix elements become

$$\rho_{ij} \equiv \langle i|\rho|j\rangle = \langle i| \left(\sum_{\psi} p_{\psi} \sum_{k,l} c_{\psi,k} c^*_{\psi,l} \left|k\right\rangle\!\left\langle l\right| \right) |j\rangle = \sum_{\psi} p_{\psi} c_{\psi,i} c^*_{\psi,j}. \tag{3.2}$$

These elements carry physical meaning: on the one hand, the diagonal elements $\rho_{ii} \in \mathbb{R}$ are the *populations* of the states, i.e., the probabilities of measuring the system in state $|i\rangle$. On the other hand, the off-diagonal elements $\rho_{ij} \in \mathbb{C}$ with $i \neq j$ are the so-called *coherences*, which capture phase information and quantum interference between basis states.

To describe subsystems of composite quantum systems, we often use the *reduced density operator*, which is obtained by tracing out one of the subsystems. For instance, let us take systems A and B, whose state is given by the density operator ρ_{AB}. Then, the reduced density operator for system A is [3]

$$\rho_{\mathrm{A}} \equiv \mathrm{Tr}_{\mathrm{B}}(\rho_{\mathrm{AB}}), \tag{3.3}$$

where Tr_{B} is the *partial trace* over system B.

3.1.1 Purity, fidelity, and entanglement

A measure of coherence in noisy quantum systems, which we use in Paper E, is the *purity*, defined as the trace of the density operator squared [111]:

$$\mathcal{P} \equiv \mathrm{Tr}\big(\rho^2\big), \tag{3.4}$$

which takes values $1/d \leq \mathcal{P} \leq 1$, with d being the dimension of the Hilbert space in which ρ is defined.

We say that a state is *pure* if it can be written as $\rho = |\psi\rangle\langle\psi|$, which means that $\rho^2 = \rho$ and $\mathcal{P} = 1$. In this case, according to Eq. (3.2), the density matrix elements become simply $\rho_{ij} = c_{\psi,i}c^*_{\psi,j}$. Consequently, since the populations $\rho_{ii} = c_{\psi,i}c^*_{\psi,i}$ describe the probabilities of the system being in state $|i\rangle$, we commonly refer to $c_{\psi,i}$ as the *probability amplitudes*.

In contrast, a state is *mixed* or in a *mixture of pure states* when $\rho = \sum_\psi p_\psi |\psi\rangle\langle\psi|$ cannot be simplified, and thus $\rho^2 \neq \rho$ and $\mathcal{P} < 1$.

Remarkably, in composite systems, even if the global state ρ_{AB} is pure, the reduced state ρ_{A} can be mixed [3]. This happens, for instance, when ρ_{AB} is entangled, such as in the Bell state

$$\big|\Psi^+\big\rangle_{\mathrm{AB}} = \frac{1}{\sqrt{2}}(|01\rangle + |10\rangle). \tag{3.5}$$

Here, the global system is perfectly known, but if we trace out system B,

$$\rho_{\mathrm{A}} = \mathrm{Tr}_{\mathrm{B}}\left(\big|\Psi^+\big\rangle_{\mathrm{AB}}\big\langle\Psi^+\big|\right) = \frac{1}{2}|0\rangle\langle 0| + \frac{1}{2}|1\rangle\langle 1|, \tag{3.6}$$

we obtain a statistical mixture, i.e., we have no information about A individually; on the contrary, it looks maximally uncertain.

One way to quantify entanglement is to use the measure of concurrence. For a two-qubit mixed state ρ, the *concurrence* $C(\rho)$ is defined as [112]

$$C(\rho) \equiv \max\{0,\, \lambda_1 - \lambda_2 - \lambda_3 - \lambda_4\}, \tag{3.7}$$

where $\{\lambda_i\}$ are the eigenvalues (in decreasing order) of the Hermitian matrix

$$R = \sqrt{\sqrt{\rho}\tilde{\rho}\sqrt{\rho}}; \quad \tilde{\rho} = \rho\,(\sigma_y \otimes \sigma_y)\,\rho^*\,(\sigma_y \otimes \sigma_y), \tag{3.8}$$

where σ_y is the Pauli-Y matrix, and ρ^* is the complex conjugate of ρ in the σ_z basis. Concurrence ranges from 0 for separable states, to 1 for maximally entangled Bell states.

Another approach to "quantifying" entanglement, is to use the measure of fidelity to see how close a state is to a specific maximally entangled state, such as $|\Psi^+\rangle$ above. In general, the *fidelity* between two quantum states ρ and σ quantifies how close the states are to each other. It is defined as [113, 114]

$$\mathcal{F}(\rho,\sigma) \equiv \left[\mathrm{Tr}\left(\sqrt{\sqrt{\rho}\sigma\sqrt{\rho}}\right)\right]^2, \tag{3.9}$$

and it can take values from zero, when the states are orthogonal, to one, when the states are identical. For pure states $\rho = |\psi\rangle\langle\psi|$ and $\sigma = |\phi\rangle\langle\phi|$, this reduces to their overlap:

$$\mathcal{F}(\rho,\sigma) = |\langle\psi|\phi\rangle|^2. \tag{3.10}$$

It is important to note that sometimes an alternative definition of fidelity is used: $\mathcal{F}' := \sqrt{\mathcal{F}}$, where $\mathcal{F}'$ is instead called fidelity. That is, for instance, the case for QuTiP's `fidelity` function [115]—but we stick to the definition in Eq. (3.9).

In Paper E, where we want maximize the entanglement between two GAs, we use the fidelity between the steady-state of the system and the Bell state $|\Psi^+\rangle$ to optimize the experimental parameters. However, we remark that the fidelity is not a measure of entanglement. While, in the case of Paper E, the fidelity to the $|\Psi^+\rangle$ state yields very similar values to the concurrence, this is not always the case. For instance, if our entangled state would be rotated by a local unitary, fidelity to $|\Psi^+\rangle$ could drop significantly, while the concurrence would remain high.

3.1.2 Decoherence mechanisms

In open quantum systems, the interactions with the environment lead to *decoherence*, i.e., loss of the quantum information stored in the system. In the context of qubits or two-level systems, decoherence can be understood via the Bloch sphere representation, where pure states lie on the surface and mixed states lie inside. In these systems, we distinguish two decoherence paths: energy relaxation, and loss of phase coherence (dephasing) [88]. These mechanisms, as well as their combination, are depicted on the Bloch sphere in Fig. 3.1.

Relaxation

Also called *amplitude damping*, *longitudinal decay*, or *dissipation*. It is the system's loss of energy to the environment, which is reflected in the density matrix

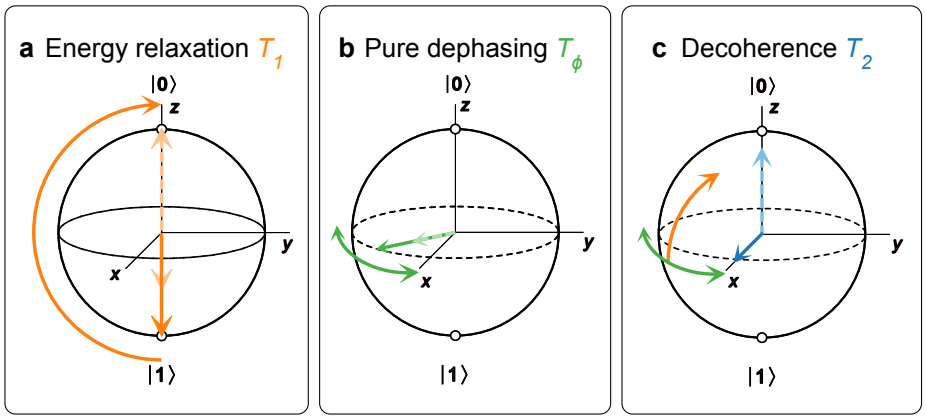

Figure 3.1: Representation of the decoherence mechanisms on the Bloch sphere, assuming the definition $\sigma_z = |0\rangle\langle 0| - |1\rangle\langle 1|$. (a) Energy relaxation, as a contraction of the state vector along the Z-axis. (b) Pure dephasing, as a contraction of the state vector in the XY-plane. (c) Decoherence, as a combination of relaxation and pure dephasing, makes the qubit decay to a mixed state. Figure adapted with permission from [116].

as changes in the populations. For a qubit, this corresponds to decay from the excited state $|1\rangle$ to the ground state $|0\rangle$, with populations evolving as

$$\rho_{11}(t) \to \rho_{11}(0)\, e^{-t/T_1}, \tag{3.11}$$

where T_1 is the *relaxation time* [88]. In fact, relaxation is caused by *transverse noise*, via the X- or Y-axis, with the intuition that off-diagonal elements of an interaction Hamiltonian are needed to connect and drive transitions between states $|0\rangle$ and $|1\rangle$. On the Bloch sphere, transverse noise can be pictured as fluctuations that kick the state vector out of the pole. On average, these fluctuations lead to a contraction along the Z-axis, with $\langle\sigma_z(t)\rangle$ decaying to its equilibrium value [see Fig. 3.1(a)].

Note that, in the literature, it is common to represent this phenomenon by drawing the state vector moving away from the pole *on* the surface of the Bloch sphere, without shrinking (e.g., Refs. [116, 117]). This may lead the reader to misinterpret relaxation as the trajectory that connects the poles through the surface of the sphere, instead of through its center—a notion that is incorrect.

Physically, relaxation is the sum of *radiative* decay, where the energy is dissipated in the form of a photon (e.g., spontaneous emission), and *non-radiative* decay, where the energy is dissipated to the environment in other ways, like phonons or heat [20, 118]: $T_1^{-1} = \gamma_\mathrm{r} + \gamma_\mathrm{nr}$.

Pure dephasing

Caused by *longitudinal noise* that couples to the qubit via the Z-axis, pure dephasing describes depolarization in the XY-plane on the Bloch sphere at a rate $\Gamma_\phi = 1/T_\phi$ [see Fig. 3.1(b)]. The longitudinal noise causes the qubit frequency to fluctuate, such that it is no longer equal to the rotating-frame frequency, and causes the Bloch vector to precess in the rotating frame [88]. This makes it common to represent pure dephasing as a state vector that points to the surface of the Bloch sphere and moves along its equator [88, 116, 117]. However, on average, these stochastic fluctuations result in a contraction of the Bloch vector in the XY-plane.

In contrast to energy relaxation, pure dephasing is not a resonant phenomenon, which means that noise at any frequency can modify the qubit frequency and cause dephasing. Thus, qubit dephasing is subject to broadband noise [88].

Decoherence

Also known as *dephasing* or *transverse decay*, since it includes the aforementioned pure dephasing. It is the decay of off-diagonal elements in the density matrix, i.e., loss of coherence without energy exchange. Given a basis $\{|i\rangle\}$, the coherences decay exponentially as follows:

$$\rho_{ij}(t) \to \rho_{ij}(0)\, e^{-t/T_2}, \quad i \neq j, \tag{3.12}$$

where T_2 is the *decoherence time* [88].

As we will show at the end of Sec. 3.2.1, the timescales above are related by

$$\frac{1}{T_2} = \frac{1}{2T_1} + \frac{1}{T_\phi}, \tag{3.13}$$

indicating that decoherence is a combination of energy relaxation and pure dephasing [see Fig. 3.1(c)]. It is important to note that, while characterizing these rates is of the utmost importance to experimentalists, us theorists tend to neglect many of these loss channels. For instance, the models developed in Papers A, B, C and D do not account for pure dephasing nor non-radiative decay. In Paper E, we add these contributions ad hoc, as we show through the master-equation formalism derived next.

3.2 Master equations

When dealing with open quantum systems, we are interested in how the system dynamics are affected by the environment, but not so much in the dynamical processes taking place in the environment itself. In order to provide a mathematical description of such dynamics, we derive a *master equation* for the system's reduced density matrix, which includes the effects of the interaction

with the bath, but traces out the bath's degrees of freedom. Since the environment consists of infinitely many quantum systems, we need to make several approximations which, fortunately, are well justified in most experiments.

The term master equation originates from classical statistical mechanics, where it refers to equations describing the evolution of probability distributions [119]. In quantum theory, it refers to analogous equations for density matrices. Due to their differential equation form, master equations are sometimes referred to as *equations of motion* [120].

Let us briefly review the progression of relevant quantum dynamical equations (remember that $\hbar = 1$ throughout the thesis).

The *Schrödinger equation* governs the time evolution of state vectors in closed systems:

$$\frac{\mathrm{d}}{\mathrm{d}t}\left|\psi(t)\right\rangle = -iH\left|\psi(t)\right\rangle. \tag{3.14}$$

The equivalent equation generalized for density matrices is the *von Neumann equation*:

$$\frac{\mathrm{d}\rho}{\mathrm{d}t} = -i[H,\rho], \tag{3.15}$$

often called the *Liouville-von Neumann equation*, since it can be derived by canonical quantization of the classical Liouville equation [120].

For open quantum systems, the *Liouvillian superoperator* $\mathcal{L}$ is typically introduced to include both Hamiltonian and dissipative contributions [120]:

$$\frac{\mathrm{d}\rho}{\mathrm{d}t} = -i[H,\rho] + \text{dissipative terms} = \mathcal{L}\rho. \tag{3.16}$$

One of the most common forms of the master equation above in the Markovian regime is given by the *Lindblad equation* [121]:

$$\frac{\mathrm{d}\rho}{\mathrm{d}t} = -i[H,\rho] + \sum_k \mathcal{D}[\mathcal{L}_k]\rho, \tag{3.17}$$

where $\mathcal{D}[X]\rho = X\rho X^\dagger - \frac{1}{2}\{X^\dagger X, \rho\}$, and the $\mathcal{L}_k$ are jump operators characterizing different dissipative processes (e.g., photon loss, dephasing, spontaneous emission)[1]. This equation is also often referred to as the *Gorini-Kossakowski-Sudarshan-Lindblad (GKSL) equation* to acknowledge the concurrent derivation of the equation by the other authors [122].

3.2.1 Lindblad master equation for a qubit coupled to a waveguide

To illustrate the derivation of a master equation, we consider a model where our quantum system is a two-level atom, coupled to a bath of an infinite number

[1] While our notation is fairly established, sometimes $\mathcal{L}$ is used instead to denote the Liouvillian superoperator or the Lindblad operator $\mathcal{D}$. Since we do not use the Liouvillian in this thesis or in the appended papers, we will consistently refer to the dissipative terms by $\mathcal{D}[\mathcal{L}_k]$.

of harmonic oscillators, such as a waveguide. The total Hamiltonian H is then the sum of the atomic Hamiltonian H_a [Eq. (2.9)], the bath Hamiltonian H_b [Eq. (2.1)], and their interaction $H_{\rm int}$, taken from the Rabi Hamiltonian [123]:

$$H = H_a + H_b + H_{\rm int}, \tag{3.18}$$

$$H_a = \frac{\omega_a}{2}\sigma_z, \tag{3.19}$$

$$H_b = \sum_k \omega_k \, a_k^\dagger a_k, \tag{3.20}$$

$$H_{\rm int} = \sum_k g_k (a_k + a_k^\dagger)(\sigma_- + \sigma_+), \tag{3.21}$$

where ω_a is the transition frequency of the atom; σ_z is the Pauli-Z matrix; $\sigma_\pm = (\sigma_x \pm i\sigma_y)/2$ are the ladder operators of the atom, such that $\sigma_+\sigma_- = (1+\sigma_z)/2$; and g_k denotes the coupling strength between the atom and the bath.

Let $\rho_{\rm tot}(t)$ be the density operator of the total system (atom plus bath). Then the von-Neumann equation reads

$$\dot\rho_{\rm tot} = -i[H, \rho_{\rm tot}], \tag{3.22}$$

with H given by Eq. (3.18). In the interaction picture, henceforth denoted by $\sim$, we can write Eq. (3.22) by separating the rapid motion generated by $H_a + H_b$ from the slow motion generated by $H_{\rm int}$. Defining

$$\tilde\rho_{\rm tot}(t) \equiv e^{i(H_a+H_b)t}\rho_{\rm tot}(t)e^{-i(H_a+H_b)t}, \tag{3.23}$$

we obtain

$$\dot{\tilde\rho}_{\rm tot}(t) = -i[\tilde H_{\rm int}(t), \tilde\rho_{\rm tot}(t)], \tag{3.24}$$

the solution of which is

$$\tilde\rho_{\rm tot}(t) = \tilde\rho_{\rm tot}(0) - i\int_0^t d\tau \Big[\tilde H_{\rm int}(\tau), \tilde\rho_{\rm tot}(\tau)\Big]. \tag{3.25}$$

By inserting Eq. (3.25) into Eq. (3.24) and tracing over the the bath degrees of freedom, we obtain an equation for the atomic density matrix ρ_a:

$$\dot{\tilde\rho}_a(t) = {\rm Tr}_b\left\{-i\Big[\tilde H_{\rm int}(t), \tilde\rho_{\rm tot}(0)\Big] - \int_0^t d\tau \Big[\tilde H_{\rm int}(t), \Big[\tilde H_{\rm int}(\tau), \tilde\rho_{\rm tot}(\tau)\Big]\Big]\right\}. \tag{3.26}$$

Note that all steps from Eq. (3.22) to Eq. (3.26) are exact and generalizable to any Hamiltonian of the form Eq. (3.18). To go forward, however, we need to make some approximations.

Born, Markov, and rotating-wave approximations

The *Born approximation* is based on the couplings g_k being weak and the reservoir being large enough to be virtually unaffected by its interaction with the

atom. In this approximation, we first assume that the interaction is turned on at $t = 0$ and that no correlations exist between the system and the bath at this initial time. Therefore, the initial state factorizes as $\rho_{\rm tot}(0) = \rho_a(0) \otimes \rho_b(0)$. At later times, correlations between the system and the bath arise due to their coupling. However, since we assume that the coupling is very weak and $\rho_{\rm tot}(t)$ should only show deviations of order $H_{\rm int}$ from an uncorrelated state, we can neglect higher-order terms, i.e., $\tilde{\rho}_{\rm tot}(t) = \tilde{\rho}_a(t)\rho_b(0) + O(H_{\rm int})$. Then, Eq. (3.26) becomes, under the Born approximation,

$$\dot{\tilde{\rho}}_a(t) = -\int_0^t d\tau \, {\rm Tr}_b \left\{ \left[\tilde{H}_{\rm int}(t), \left[\tilde{H}_{\rm int}(\tau), \tilde{\rho}_a(\tau)\rho_b(0) \right] \right] \right\}. \tag{3.27}$$

The *Markov approximation* states that the bath has no memory, i.e., that any imprint the atom makes on the bath at time t_1 does not affect the dynamics at a later time t_2. It can be understood as follows: if the reservoir is large, we do not expect it to preserve the minor changes caused by its interaction with the atom for very long—at least, not long enough to significantly affect the future evolution of the atom. Therefore, we can replace $\tilde{\rho}_a(\tau)$ in Eq. (3.27) with $\tilde{\rho}_a(t)$ to obtain a master equation in the *Born-Markov approximation*:

$$\dot{\tilde{\rho}}_a(t) = -\int_0^t d\tau \, {\rm Tr}_b \left\{ \left[\tilde{H}_{\rm int}(t), \left[\tilde{H}_{\rm int}(\tau), \tilde{\rho}_a(t)\rho_b(0) \right] \right] \right\}. \tag{3.28}$$

To proceed from here is quite straightforward, so the remaining details of the derivation are left out of the scope of this thesis and we refer the interested reader to Refs. [86, 124].

The only non-trivial step left to take is the *rotating-wave approximation* (RWA), through which we neglect the fast oscillating terms [125]. Explicitly, the RWA is applied in the interaction picture, where terms in the Hamiltonians that oscillate with frequencies $\omega_a + \omega_b$ are neglected, while terms that oscillate with frequencies $\omega_a - \omega_b$ are kept. This is a valid approximation when the bath frequency ω_b is close to the atomic transition ω_a, and the coupling is weak (i.e., when $\omega_a, \omega_b \gg g$), which is a safe assumption to make in the optical and microwave regimes.

Finally, after all approximations have been made and the bath has been traced out, we can transform back from the interaction picture to obtain a master equation in the Lindblad form:

$$\dot{\rho}_a = -i\left[\frac{\omega_a'}{2}\sigma_z, \rho_a \right] + \Gamma_a \mathcal{D}[\sigma_-]\rho_a, \tag{3.29}$$

where $\mathcal{D}[\sigma_-]\rho$ is the Lindblad superoperator[2] defined under Eq. (3.17), Γ_a is the atomic relaxation rate, and ω_a' is the Lamb-shifted transition frequency. In a small atom, the relaxation rate is given by

$$\Gamma_{\rm small} = 2\pi D(\omega_a) g^2(\omega_a), \tag{3.30}$$

[2]Note that, by the definition of the Lindblad superoperator, $\Gamma_a \mathcal{D}[\sigma_-]\rho_a = \mathcal{D}[\sqrt{\Gamma_a}\,\sigma_-]\rho_a$.

where $D(\omega)$ is the bath density of states and $g(\omega_k) = g_k$ is the coupling strength [19]. For a GA, Γ also accounts for the interference between coupling points and it therefore depends on the spacing between the points. As we will see in subsequent examples (see, e.g., Table 4.1), it can take values up to $\Gamma_{\text{giant}} \leq N^2\Gamma_{\text{small}}$, where N is the number of coupling points[3] [19, 86].

It should be noted that we could have made the RWA earlier, for instance, directly on H_{int} in Eq. (3.21), by neglecting the terms $a\sigma_-$ and $a^\dagger\sigma^+$, which would yield the interaction Hamiltonian from the Jaynes-Cummings model [10, 126]. However, while that is a very common practice, it carries the consequence that ω_a' does not accurately capture the Lamb shift of the transition frequency [124, 127, 128]. Thus, only if we are not interested in the exact value of the frequency shift can we apply the RWA directly on the Hamiltonian, which is the case in the appended papers.

A master-equation treatment like the one presented in this section is used in Paper A to study the waveguide-mediated interaction between giant atoms in a chiral setting. While such an approach had been used before for giant atoms [46], variations in the direction of propagation of light had not been considered. Since the setup in Paper A deals with more interconnected systems and a more complex system-bath interaction, an accurate description of it requires some additional formalism beyond the master equation derived here. In particular, we use the SLH formalism, which we introduce in Chapter 4.

Decoherence in the Lindblad equation

In the derivation of the Lindblad equation Eq. (3.29), we have assumed that the atom only couples to the waveguide and no other bath, and we have not considered any noise sources. While this common approach allows us to isolate the atomic dynamics arising from the coupling to the bath, it does not draw a realistic picture. As explained in Sec. 3.1.2, qubits are also susceptible to pure dephasing, which is caused by longitudinal (Z) noise and is modeled in the Lindblad equation by including an additional dissipation term in σ_z [129]:

$$\dot{\rho}_a = -i\left[\frac{\omega_a'}{2}\sigma_z, \rho_a\right] + \Gamma_a\mathcal{D}[\sigma_-]\rho_a + \frac{\Gamma_\phi}{2}\mathcal{D}[\sigma_z]\rho. \tag{3.31}$$

[3]Throughout this thesis and in the appended papers, we distinguish between Γ being the *atomic* or *individual relaxation rate* (including interference effects), γ being the *bare relaxation rate* at each coupling point (no interference effects), and g being the *coupling strength*. Experimentally, the variable that is set by design is g, but the one that is measured to characterize the system is Γ, which may sometimes lead to an abuse of language: calling Γ the coupling strength. Moreover, in Chapter 4 and in Papers A and E, g is used for the exchange interaction between two atoms. There, in order to avoid confusions, we refrain from using g to refer to the coupling strength, and default to using the bare relaxation rates γ in our calculations.

In matrix form, considering $\sigma_z = |0\rangle\langle 0| - |1\rangle\langle 1|$, it reads

$$\begin{aligned}\begin{pmatrix}\dot{\rho}_{00} & \dot{\rho}_{01}\\ \dot{\rho}_{10} & \dot{\rho}_{11}\end{pmatrix} &= i\omega_a'\begin{pmatrix}0 & -\rho_{01}\\ \rho_{10} & 0\end{pmatrix} + \Gamma_a\begin{pmatrix}\rho_{11} & -\rho_{01}/2\\ -\rho_{10}/2 & -\rho_{11}\end{pmatrix} + \Gamma_\phi\begin{pmatrix}0 & -\rho_{01}\\ -\rho_{10} & 0\end{pmatrix}\\ &= \begin{pmatrix}\Gamma_a\rho_{11} & (-i\omega_a' - \Gamma_a/2 - \Gamma_\phi)\rho_{01}\\ (i\omega_a' - \Gamma_a/2 - \Gamma_\phi)\rho_{10} & -\Gamma_a\rho_{11}\end{pmatrix}. \end{aligned} \tag{3.32}$$

With the two expressions above, we can relate the different terms back to the decoherence mechanisms from Sec. 3.1.2 as follows.

First, we see that, as expected, relaxation transfers population from state $|1\rangle$ to $|0\rangle$ at a rate $\Gamma_a = 1/T_1$. Then, the term $\Gamma_a\mathcal{D}[\sigma_-]\rho_a$, together with the fact that $\Gamma_a \propto g^2$ [Eq. (3.30)], indicates that this process is induced by the off-diagonal term of the interaction Hamiltonian $g\sigma_-$. This agrees with our previous intuition that relaxation is caused by transverse (X or Y) noise.

Moreover, we see that relaxation induces a decoherence of the off-diagonal terms at half the relaxation rate $\Gamma_a/2$. If we additionally consider pure dephasing, the coherences decay at a rate $\Gamma_a/2+\Gamma_\phi = 1/T_2$. This leads to the relation presented in Eq. (3.13):

$$\frac{1}{T_2} = \frac{1}{2T_1} + \frac{1}{T_\phi}, \tag{3.33}$$

which illustrates decoherence as a combination of both relaxation and pure dephasing.

Finally, regarding the pure dephasing term, we note that one could more naturally define it as $\Gamma_\phi\mathcal{D}[\sigma_z]\rho$. However, the canonical renormalization with the factor 1/2 is done to match the effect of the relaxation: in the same way that the factor Γ_a in the Lindblad equation leads to a decay of the populations at a rate Γ_a, the factor $\Gamma_\phi/2$ leads to a decay of the coherences at a rate Γ_ϕ.

Note that in the case of a three-level atom, we would normally switch our Pauli matrices for harmonic ladder operators in all the equations above: $\sigma_- \to a$ and $\sigma_z \to a^\dagger a - aa^\dagger$, although the exact form of dephasing and relaxation for higher levels depends a lot on the specific system we consider [129].

4 Cascaded quantum systems

> And when they try to pay you back,
> tell them instead to pay it forward.
>
> Catherine Ryan Hyde (1999)

In this chapter, we introduce the theory of cascaded quantum systems, used in Paper A to model a quantum emitter (or an ensemble of them) chirally coupled to a 1D continuous waveguide. In particular, we discuss the properties and applications of chiral interfaces, and we delve into the SLH formalism [130–132], which we then use in conjunction with the Lindblad equation derived in the previous chapter.

4.1 Chiral interfaces and applications

In general, we say that atoms couple *chirally* to a waveguide when their bare relaxation rate (the relaxation rate before any interference effects are taken into account) is generally different towards the right and left directions, i.e., $\gamma_R \neq \gamma_L$. Consequently, there are two limiting cases: the *bidirectional* or *nonchiral* case, where atoms couple symmetrically to the right and left ($\gamma_R = \gamma_L$), and the *unidirectional* or *cascaded* case, where atoms couple to modes propagating in only one direction (e.g., $\gamma_L = 0$).

While most waveguides are bidirectional, chirality emerges naturally in optical nanofibers when light is strongly transversely confined [133–135]. It is also achievable in atomic waveguides [136] and in microwave waveguides by using circulators [13, 137–140], sawtooth lattices [141], or entangled states between quantum emitters [80, 82, 83]. Even beyond photonic reservoirs [142], other architectures with phononic [143–146] and magnonic waveguides [146–148] have been proposed to realize chiral coupling.

Chiral quantum networks have been increasingly attracting interest in recent years [103, 149–157] since they have immediate applications in quantum information processing. With two-level emitters representing stationary qubits, and photons as 'flying qubits' for distributing quantum information in a quantum network, the chiral light-matter coupling enables photons to be routed between

the nodes. In particular, it has been shown how this coupling can be harnessed to transfer quantum states between qubits and to manipulate stabilizer codes for quantum error correction [79].

As a simple example, consider two small atoms, A and B, coupled to a common waveguide where they can only absorb and emit right-moving excitations (i.e., the setting in Fig. 4.2(a) with all $\gamma_L = 0$). Consider the emitter on the left to be in an arbitrary superposition $c_0 |0\rangle_A + c_1 |1\rangle_A$ (defined by the complex coefficients c_0 and c_1) and the emitter on the right in the ground state $|0\rangle_B$. Then the chiral setting could enable the quantum-state transfer $(c_0 |0\rangle_A + c_1 |1\rangle_A) |0\rangle_B \to |0\rangle_A (c_0 |0\rangle_B + c_1 |1\rangle_B)$, whereby an arbitrary superposition stored in emitter A is mapped to emitter B. Chiral coupling serves here to convert the first qubit to a rightward-propagating photonic qubit, and to increase the chance of reabsorption of this photon by the second qubit.

Let us now take the case of entanglement between emitters. On the one hand, even the slightest directionalities in the couplings have been shown to improve the maximum entanglement achievable as compared to nonchiral systems [150], while on the other hand, chirality can destroy collective emission effects. Consider the spontaneous emission of an ensemble of two-level emitters. Owing to the fact that all emitters are coupled to the same bath, the emission differs strongly from that of independent emitters—an effect referred to as sub- or super-radiance [158] (see more in Sec. 4.4.2). For instance, for bidirectional coupling, two small atoms can share a single excitation that is prevented from decaying by destructive interference between coupling points. This collective behavior, however, is not possible if the atoms are coupled to a unidirectional waveguide, where the symmetry is broken and only one of the atoms "knows" about the presence of the other [153]. Interestingly, we found in Paper A that GAs in the nested configuration [i.e., where the coupling points of atom B are situated between the points of atom A—see Fig. 2.2(b)] preserve the symmetry and thus the entanglement for any chirality of the coupling.

To get around the lack of collective effects for small atoms in chiral waveguides one can coherently drive the system [149, 151]. In such a case, the diatomic ensemble evolves to a dynamic equilibrium between drive and dissipation where the stream of photons scattered from the first atom interferes destructively with the photons scattered from the second [153]. In Paper A, we showed that such a regime not only is accessible for GAs, but the driven-dissipative equilibrium can be reached *faster* than with small atoms. This result prompted the conception of Paper E, where we designed an experiment to generate this driven-dissipative entangled states with separate giant atoms [see Fig. 2.2(a) and Fig. 2.5(b)].

To derive these results, in Paper A we used the SLH formalism, which is explained next.

4.2 SLH framework for quantum networks

The SLH framework [130–132] was developed in 2009 to model *quantum input-output networks*, i.e., quantum optical networks made of local components that interact via itinerant quantum bosonic fields. Its conception was motivated by the need to simplify complicated descriptions of networks containing *cascaded quantum systems* [159, 160], where the output from one system is used as the input for another.

The SLH formalism is a modular framework where each local component is treated as a black box that scatters the propagating fields according to some pre-specified input-output behavior. In addition, it incorporates the quantum nature of the itinerant fields and any quantum dynamics in the localized components. The power of the SLH formalism lies in its ability to compose the propagator for local components according to how they are connected in a network.

4.2.1 SLH formalism

In the SLH formalism, an open quantum system with n input-output ports is described by a triplet $G = (\mathcal{S}, \mathcal{L}, H)$, where $\mathcal{S}$ is an $n \times n$ scattering matrix, $\mathcal{L}$ is an $n \times 1$ vector representing the coupling between the system and the environment at the input-output ports, and H is the Hamiltonian of the system. Let us elucidate why.

Consider two cascaded quantum systems with Hamiltonians H_1 and H_2, such that the output from system 1 becomes the input to system 2. Both systems are coupled via an input-output port to the environment, by jump operators $\mathcal{L}_1$ and $\mathcal{L}_2$, respectively. Through input-output theory and quantum stochastic calculus, it can be shown that the total system behaves as if it had a Hamiltonian $H = H_1 + H_2 + (\mathcal{L}_2^\dagger \mathcal{L}_1 - \mathcal{L}_1^\dagger \mathcal{L}_2)/(2i)$ and was coupled to the environment via an operator $\mathcal{L} = \mathcal{L}_1 + \mathcal{L}_2$ [86, 132, 161]. This suggests that an open quantum system could be assigned a doublet $G = (\mathcal{L}, H)$, and that the doublet corresponding to two quantum systems *in series* would defined as follows:

$$G = G_2 \triangleleft G_1 = (\mathcal{L}_2, H_2) \triangleleft (\mathcal{L}_1, H_1) = \left(\mathcal{L}_1 + \mathcal{L}_2, H_1 + H_2 + \frac{1}{2i}(\mathcal{L}_2^\dagger \mathcal{L}_1 - \mathcal{L}_1^\dagger \mathcal{L}_2) \right) \tag{4.1}$$

Now, the doublet above is still missing the $\mathcal{S}$ in SLH, i.e., the scattering matrix. For a single-channel case, the $\mathcal{S}$ may describe the non-negligible distance between two systems G_1 and G_2 through, for instance, an acquired phase shift ϕ, which is inserted by placing the triplet $G_\phi = (e^{i\phi}, 0, 0)$ between G_1 and G_2. Note that in such a case, the time it takes for an excitation to travel between systems must be small compared to the timescale of the systems' evolution.

On the other hand, the scattering matrix is also essential to describe many-channel systems such as beamsplitters or circulators, which take several inputs and mix them into several outputs.

Finally, another widely used component is the coherent drive. For example, a coherent signal of $|\beta|^2$ photons per second can be represented by the triplet $G_\beta = (1, \beta, 0)$.

4.2.2 SLH composition rules

Now that we have introduced the different components of the SLH triplet, we can compose them to build more complex quantum networks. For that, we need the three fundamental composition rules for the SLH formalism: the series product, the concatenation product, and the feedback operation (see Fig. 4.1).

As shown in Eq. (4.1), the *series product* is denoted by $\triangleleft$ and describes systems which are laid out in a cascaded way. Now accounting for the scattering matrix, the series product is defined as:

$$G_2 \triangleleft G_1 = \left(\mathcal{S}_2\mathcal{S}_1,\ \ \mathcal{S}_2\mathcal{L}_1 + \mathcal{L}_2, H_1 + H_2 + \frac{1}{2i}\left(\mathcal{L}_2^\dagger \mathcal{S}_2 \mathcal{L}_1 - \mathcal{L}_1^\dagger \mathcal{S}_2^\dagger \mathcal{L}_2\right)\right), \quad (4.2)$$

which we note does not commute, i.e., it is not invariant under the permutation of 1 and 2.

The *concatenation product* is denoted by $\boxplus$ and is used in processes that occur in parallel, and there is therefore no need to let one system evolve before calculating the evolution of the other. Mathematically, it is defined as:

$$G_1 \boxplus G_2 = \left(\begin{pmatrix} \mathcal{S}_1 & 0 \\ 0 & \mathcal{S}_2 \end{pmatrix}, \begin{pmatrix} \mathcal{L}_1 \\ \mathcal{L}_2 \end{pmatrix}, H_1 + H_2 \right). \quad (4.3)$$

The concatenation product may also be generalized to consider the case where G_1 is directly coupled to G_2 by some interaction H_{int}. Then, we would just need to replace H_1 by $H_1 + H_{\text{int}}$ in Eq. (4.3).

The *feedback* operation describes the process of feeding the x-th output of a system into the y-th input of the same system, a link denoted by $x \to y$. As shown in Fig. 4.1(c), this interconnection results in a triplet of reduced dimension $G_{x\to y} = (\mathcal{S}_{\text{red}}, \mathcal{L}_{\text{red}}, H_{\text{red}})$, where

$$\begin{aligned} \mathcal{S}_{\text{red}} &= \mathcal{S}_{\cancel{x},\cancel{y}} + \mathcal{S}_{\not{x},y}(1 - \mathcal{S}_{x,y})^{-1}\mathcal{S}_{x,\not{y}} \\ \mathcal{L}_{\text{red}} &= \mathcal{L}_{\not{x}} + \mathcal{S}_{\not{x},y}(1 - \mathcal{S}_{x,y})^{-1}\mathcal{L}_x \\ H_{\text{red}} &= H + \frac{1}{2i}\left(\mathcal{L}^\dagger \mathcal{S}_{:,y}(1 - \mathcal{S}_{x,y})^{-1}\mathcal{L}_x - \text{H.c.}\right), \end{aligned} \quad (4.4)$$

and $\mathcal{S}_{\cancel{x},\cancel{y}}$ is the scattering matrix with row x and column y removed; $\mathcal{S}_{\not{x},y}$ ($\mathcal{S}_{x,\not{y}}$) denotes the column y (row x) of the matrix with the x-th (y-th) element removed; $\mathcal{S}_{:,y}$ is the entire y-th column; $\mathcal{S}_{x,y}$ denotes the element xy; $\mathcal{L}_{\not{x}}$ refers to the coupling vector with the x-th element removed; $\mathcal{L}_x$ is the x-th element of the vector; and H.c. denotes Hermitian conjugate.

These three composition rules are sufficient to describe any arbitrary quantum network that satisfies (i) the Born-Markov approximation, (ii) that the bosonic fields propagate in a linear medium without dispersion, and (iii) that

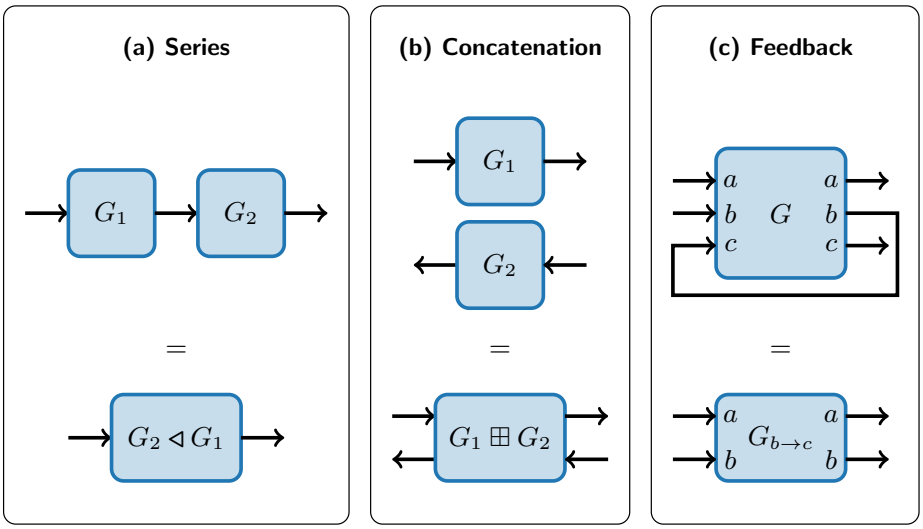

Figure 4.1: The three SLH composition rules: (a) series product, (b) concatenation product, (c) feedback operation.

the travel time between components is negligible compared to the relaxation times of the systems. In fact, once we calculate the triplet $G = (\mathcal{S}, \mathcal{L}, H)$ of the network, we can extract the Lindblad master equation

$$\dot{\rho} = -i[H, \rho] + \sum_{j=1}^{n} \mathcal{D}[\mathcal{L}_j]\rho. \tag{4.5}$$

4.3 Example: two atoms chirally coupled to a continuous waveguide

In this section, we illustrate the SLH formalism for two small atoms [Fig. 4.2(a)] and two giant braided atoms [Fig. 4.2(b)], which are some of the elementary setups studied in Paper A.

Let us consider two atoms A and B with resonant frequencies ω_A and ω_B, respectively[1]. Taking the atoms to be two-level systems, their Hamiltonians can be written as

$$H_A = \frac{\omega_A}{2}\sigma_z^A, \quad H_B = \frac{\omega_B}{2}\sigma_z^B, \tag{4.6}$$

regardless of whether they are small or giant.

The atoms are coupled to the waveguide at connection points identified by their position x_k and their bare relaxation rates γ_k, for $k = 1, 2, 3, 4$. At each

[1]Not to be confused with the subscripts a, b from Sec. 3.2.1 denoting atom and bath.

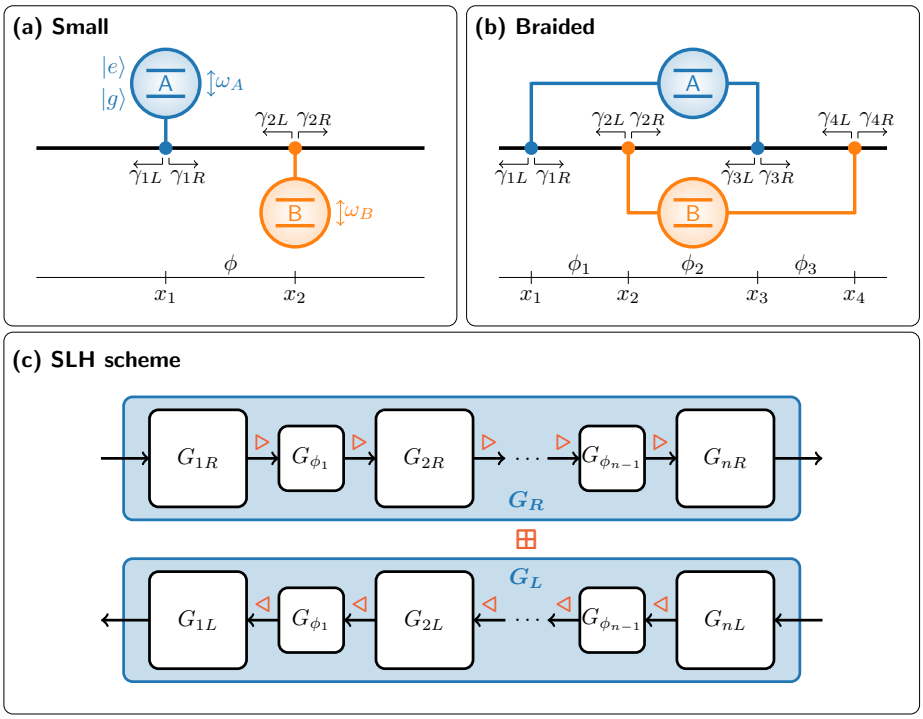

Figure 4.2: Atoms coupled to a 1D continuous open waveguide. (a, b) A sketch for (a) two small atoms, and (b) two giant braided atoms showing the relevant parameters. (c) The SLH scheme that describes the input-output flows from the setups in (a) and (b), and which is also applicable to an arbitrary number of atoms with an arbitrary number of coupling points. All figures are adapted from Paper A.

coupling point, we distinguish the decay rate to the right- and left-propagating modes as γ_{kR} and γ_{kL}, in such a way that $\gamma_{kR}+\gamma_{kL}=\gamma_k$. The phase shifts acquired between neighboring coupling points are denoted by $\phi_k=\omega|x_{k+1}-x_k|/v$ for $k=1,2,3$, where ω and v are the frequency and velocity of the traveling bosons, respectively. Note that in order for the setup to be consistent with the assumptions behind the SLH formalism, we need to assume that the coupling of each atom is weak compared to their transition frequency, and that the travel time between connection points is negligible compared to the relaxation times of all the atoms. Finally, in each propagation direction, we can model the coupling between an atom j and the waveguide at a connection point k with the jump operator $\mathcal{L}$, in such a way that $\mathcal{L}_k=\sqrt{\gamma_k}\sigma_-^j$ (as we did in Sec. 3.2.1).

With all the elements we established, we can now define an SLH triplet at each connection point k:

$$G_k = \begin{cases} \left(1,\, \sqrt{\gamma_k}\sigma_-^j,\, \frac{1}{2}\omega_j\sigma_z^j\right) & \text{if } k \text{ is the first coupling point of atom } j \\ \left(1,\, \sqrt{\gamma_k}\sigma_-^j,\, 0\right) & \text{otherwise.} \end{cases} \tag{4.7}$$

To account for the phase shift acquired between connection points k and $k+1$, we define

$$G_{\phi_k} = (e^{i\phi_k},\, 0,\, 0). \tag{4.8}$$

We then take each propagation direction (right and left) separately and apply a series product between all the triplets, as if the system was cascaded [see Eq. (4.2)]. In particular, for two *small* atoms, that is

$$\begin{aligned} G_R\Big|_{\text{sma}} &= G_{2R} \triangleleft G_\phi \triangleleft G_{1R} = \\ &= \left(1,\, \sqrt{\gamma_{2R}}\,\sigma_-^B,\, \frac{1}{2}\omega_B\sigma_z^B\right) \triangleleft (e^{i\phi},\, 0,\, 0) \triangleleft \left(1,\, \sqrt{\gamma_{1R}}\,\sigma_-^A,\, \frac{1}{2}\omega_A\sigma_z^A\right) = \\ &= \Bigg(e^{i\phi},\, e^{i\phi}\sqrt{\gamma_{1R}}\,\sigma_-^A + \sqrt{\gamma_{2R}}\,\sigma_-^B, \\ &\qquad \frac{\omega_A}{2}\sigma_z^A + \frac{\omega_B}{2}\sigma_z^B + \frac{\sqrt{\gamma_{1R}\gamma_{2R}}}{2i}[e^{i\phi}\sigma_-^A\sigma_+^B - \text{H.c.}]\Bigg), \end{aligned} \tag{4.9}$$

$$\begin{aligned} G_L\Big|_{\text{sma}} &= G_{1L} \triangleleft G_\phi \triangleleft G_{2L} = \\ &= \left(1,\, \sqrt{\gamma_{1L}}\,\sigma_-^A,\, \frac{1}{2}\omega_A\sigma_z^A\right) \triangleleft (e^{i\phi},\, 0,\, 0) \triangleleft \left(1,\, \sqrt{\gamma_{2L}}\,\sigma_-^B,\, \frac{1}{2}\omega_B\sigma_z^B\right) = \\ &= \Bigg(e^{i\phi},\, \sqrt{\gamma_{1L}}\,\sigma_-^A + e^{i\phi}\sqrt{\gamma_{2L}}\,\sigma_-^B, \\ &\qquad \frac{\omega_A}{2}\sigma_z^A + \frac{\omega_B}{2}\sigma_z^B + \frac{\sqrt{\gamma_{1L}\gamma_{2L}}}{2i}[e^{i\phi}\sigma_-^B\sigma_+^A - \text{H.c.}]\Bigg). \end{aligned} \tag{4.10}$$

Similarly, for two *giant braided* atoms, the triplets are

$$\begin{aligned} G_R\Big|_{\text{bra}} &= G_{4R} \triangleleft G_{\phi_3} \triangleleft G_{3R} \triangleleft G_{\phi_2} \triangleleft G_{2R} \triangleleft G_{\phi_1} \triangleleft G_{1R} = \\ &= \left(1,\, \sqrt{\gamma_{4R}}\,\sigma_-^B,\, 0\right) \triangleleft (e^{i\phi_3},\, 0,\, 0) \triangleleft \left(1,\, \sqrt{\gamma_{3R}}\,\sigma_-^B,\, 0\right) \triangleleft (e^{i\phi_2},\, 0,\, 0) \\ &\quad \triangleleft \left(1,\, \sqrt{\gamma_{2R}}\,\sigma_-^B,\, \frac{\omega_B}{2}\sigma_z^B\right) \triangleleft (e^{i\phi_1},\, 0,\, 0) \triangleleft \left(1,\, \sqrt{\gamma_{1R}}\,\sigma_-^B,\, \frac{\omega_A}{2}\sigma_z^A\right), \end{aligned} \tag{4.11}$$

$$
\begin{aligned}
G_L\Big|_{\text{bra}} &= G_{1L} \lhd G_{\phi_1} \lhd G_{2L} \lhd G_{\phi_2} \lhd G_{3L} \lhd G_{\phi_3} \lhd G_{4L} = \\
&= \Big(1,\, \sqrt{\gamma_{1L}}\,\sigma_-^B,\, \frac{\omega_A}{2}\sigma_z^A\Big) \lhd (e^{i\phi_1},\, 0,\, 0) \lhd \Big(1,\, \sqrt{\gamma_{2L}}\,\sigma_-^B,\, \frac{\omega_B}{2}\sigma_z^B\Big) \\
&\quad \lhd (e^{i\phi_2},\, 0,\, 0) \lhd \big(1,\, \sqrt{\gamma_{3L}}\,\sigma_-^B,\, 0\big) \lhd (e^{i\phi_3},\, 0,\, 0) \lhd \big(1,\, \sqrt{\gamma_{4L}}\,\sigma_-^B,\, 0\big)\,,
\end{aligned}
\tag{4.12}
$$

which results in the components

$$
\begin{aligned}
\mathcal{S}_R\Big|_{\text{bra}} &= e^{i(\phi_1+\phi_2+\phi_3)}, \\
\mathcal{L}_R\Big|_{\text{bra}} &= \Big(e^{i(\phi_1+\phi_2+\phi_3)}\sqrt{\gamma_{1R}} + e^{i\phi_3}\sqrt{\gamma_{3R}}\Big)\,\sigma_-^A + \Big(e^{i(\phi_2+\phi_3)}\sqrt{\gamma_{2R}} + \sqrt{\gamma_{4R}}\Big)\,\sigma_-^B, \\
H_R\Big|_{\text{bra}} &= \frac{1}{2}(\omega_A + \sin(\phi_1+\phi_2)\sqrt{\gamma_{1R}\gamma_{3R}})\sigma_z^A \\
&\quad + \frac{1}{2}(\omega_B + \sin(\phi_2+\phi_3)\sqrt{\gamma_{2R}\gamma_{4R}})\sigma_z^B \\
&\quad + \frac{1}{2i}\Big[\Big(e^{i\phi_1}\sqrt{\gamma_{1R}\gamma_{2R}} + e^{i(\phi_1+\phi_2+\phi_3)}\sqrt{\gamma_{1R}\gamma_{4R}} - e^{-i\phi_2}\sqrt{\gamma_{2R}\gamma_{3R}} \\
&\qquad + e^{i\phi_3}\sqrt{\gamma_{3R}\gamma_{4R}}\Big)\sigma_-^A\sigma_+^B - \text{H.c.}\Big],
\end{aligned}
\tag{4.13}
$$

$$
\begin{aligned}
\mathcal{S}_L\Big|_{\text{bra}} &= e^{i(\phi_1+\phi_2+\phi_3)}, \\
\mathcal{L}_L\Big|_{\text{bra}} &= \Big(\sqrt{\gamma_{1L}} + e^{i(\phi_1+\phi_2)}\sqrt{\gamma_{3L}}\Big)\,\sigma_-^A + \Big(e^{i\phi_1}\sqrt{\gamma_{2L}} + e^{i(\phi_1+\phi_2+\phi_3)}\sqrt{\gamma_{4L}}\Big)\,\sigma_-^B, \\
H_L\Big|_{\text{bra}} &= \frac{1}{2}(\omega_A + \sin(\phi_1+\phi_2)\sqrt{\gamma_{1L}\gamma_{3L}})\sigma_z^A \\
&\quad + \frac{1}{2}(\omega_B + \sin(\phi_2+\phi_3)\sqrt{\gamma_{2L}\gamma_{4L}})\sigma_z^B \\
&\quad + \frac{1}{2i}\Big[\Big(-e^{-i\phi_1}\sqrt{\gamma_{1L}\gamma_{2L}} - e^{-i(\phi_1+\phi_2+\phi_3)}\sqrt{\gamma_{1L}\gamma_{4L}} \\
&\qquad + e^{i\phi_2}\sqrt{\gamma_{2L}\gamma_{3L}} - e^{-i\phi_3}\sqrt{\gamma_{3L}\gamma_{4L}}\Big)\sigma_-^A\sigma_+^B - \text{H.c.}\Big].
\end{aligned}
\tag{4.14}
$$

Now, since propagation to the right and left directions occurs simultaneously, we can concatenate the two triplets G_R and G_L according to SLH practice, such that $G = G_R \boxplus G_L$ [see Eq. (4.3)]. This yields the components

$$
\begin{aligned}
\mathcal{S}\Big|_{\text{sma}} &= \begin{pmatrix} e^{i\phi} & 0 \\ 0 & e^{i\phi} \end{pmatrix} \\
\mathcal{L}\Big|_{\text{sma}} &= \begin{pmatrix} e^{i\phi}\sqrt{\gamma_{1R}}\,\sigma_-^A + \sqrt{\gamma_{2R}}\,\sigma_-^B \\ \sqrt{\gamma_{1L}}\,\sigma_-^A + e^{i\phi}\sqrt{\gamma_{2L}}\,\sigma_+^B \end{pmatrix} \\
H\Big|_{\text{sma}} &= \frac{\omega_A}{2}\sigma_z^A + \frac{\omega_B}{2}\sigma_z^B + \frac{1}{2i}\Big[\Big(e^{i\phi}\sqrt{\gamma_{1R}\gamma_{2R}} - e^{-i\phi}\sqrt{\gamma_{1L}\gamma_{2L}}\Big)\sigma_-^A\sigma_+^B - \text{H.c.}\Big],
\end{aligned}
\tag{4.15}
$$

$$
\begin{aligned}
\mathcal{S}\Big|_{\text{bra}} =& \begin{pmatrix} e^{i(\phi_1+\phi_2+\phi_3)} & 0 \\ 0 & e^{i(\phi_1+\phi_2+\phi_3)} \end{pmatrix} \\
\mathcal{L}\Big|_{\text{bra}} =& \begin{pmatrix} \left(e^{i(\phi_1+\phi_2+\phi_3)}\sqrt{\gamma_{1R}} + e^{i\phi_3}\sqrt{\gamma_{3R}}\right)\sigma_-^A + \left(e^{i(\phi_2+\phi_3)}\sqrt{\gamma_{2R}} + \sqrt{\gamma_{4R}}\right)\sigma_-^B \\ \left(\sqrt{\gamma_{1L}} + e^{i(\phi_1+\phi_2)}\sqrt{\gamma_{3L}}\right)\sigma_-^A + \left(e^{i\phi_1}\sqrt{\gamma_{2L}} + e^{i(\phi_1+\phi_2+\phi_3)}\sqrt{\gamma_{4L}}\right)\sigma_-^B \end{pmatrix} \\
H\Big|_{\text{bra}} =& \frac{1}{2}(\omega_A + \sin(\phi_1+\phi_2)(\sqrt{\gamma_{1R}\gamma_{3R}} + \sqrt{\gamma_{1L}\gamma_{3L}}))\sigma_z^A \\
&+ \frac{1}{2}(\omega_B + \sin(\phi_2+\phi_3)(\sqrt{\gamma_{2R}\gamma_{4R}} + \sqrt{\gamma_{2L}\gamma_{4L}}))\sigma_z^B \\
&+ \frac{1}{2i}\Big[\Big(e^{i\phi_1}\sqrt{\gamma_{1R}\gamma_{2R}} + e^{i(\phi_1+\phi_2+\phi_3)}\sqrt{\gamma_{1R}\gamma_{4R}} - e^{-i\phi_2}\sqrt{\gamma_{2R}\gamma_{3R}} \\
&\quad + e^{i\phi_3}\sqrt{\gamma_{3R}\gamma_{4R}} - e^{-i\phi_1}\sqrt{\gamma_{1L}\gamma_{2L}} - e^{-i(\phi_1+\phi_2+\phi_3)}\sqrt{\gamma_{1L}\gamma_{4L}} \\
&\quad + e^{i\phi_2}\sqrt{\gamma_{2L}\gamma_{3L}} - e^{-i\phi_3}\sqrt{\gamma_{3L}\gamma_{4L}}\Big)\sigma_-^A\sigma_+^B - \text{H.c.}\Big],
\end{aligned}
\tag{4.16}
$$

for small and braided atoms, respectively.

Finally, with the triplets above, we can compute the time evolution of the density matrix according to the master equation in Eq. (4.5), which results in an expression of the form

$$
\begin{aligned}
\dot{\rho} =& -i[H,\rho] + \sum_{j=1}^{n}\mathcal{D}[\mathcal{L}_j]\rho = \\
=& -i\left[\omega_A'\frac{\sigma_z^A}{2} + \omega_B'\frac{\sigma_z^B}{2} + \left(g\sigma_-^A\sigma_+^B + \text{H.c.}\right), \rho\right] \\
&+ \Gamma_A\mathcal{D}[\sigma_-^A]\rho + \Gamma_B\mathcal{D}[\sigma_-^B]\rho \\
&+ \left[\Gamma_{\text{coll}}\left(\sigma_-^A\rho\sigma_+^B - \frac{1}{2}\left\{\sigma_-^A\sigma_+^B, \rho\right\}\right) + \text{H.c.}\right],
\end{aligned}
\tag{4.17}
$$

where $\omega_j' = \omega_j + \delta\omega_j$ is the Lamb-shifted frequency of atom $j \in \{A, B\}$, g is the *exchange interaction* between atoms, Γ_j is the *individual relaxation rate* of atom j, and Γ_{coll} is the *collective relaxation rate* for the atoms. The exact expressions for these parameters are shown in Table 4.1.

On the one hand, the exchange interaction[2] g is set by emission from connection points of one atom being absorbed at connection points of the other atom, and it is the complex term in the Hamiltonians from Eqs. (4.15)–(4.16).

On the other hand, the relaxation rates $\Gamma_j, \Gamma_{\text{coll}}$ are set by interference between emission from connection points belonging to the same atom (Γ_j), and

[2]The exchange interaction g used in this chapter, in Papers A and E, and in other related papers [20, 46] should not be confused with the coupling strength g used in Chapter 3, Chapter 5, and Papers B, C, and D. It should also not be confused with the atomic ground state $|g\rangle$. To avoid mix-ups, in Papers A and E, we use the bare relaxation rates γ instead of the coupling strengths at each connection point. Other common nomenclature for the exchange interaction in the literature is J [62], but we instead use J for the hopping rate between the cavities of a structured waveguide, as described in Sec. 2.2.2.

Table 4.1: Frequency shifts, exchange interaction, individual and collective decays [$\delta\omega_j, g, \Gamma_j, \Gamma_{\rm coll}$ in Eq. (4.17)] for small and braided giant atoms chirally coupled to a 1D open waveguide. We assume arbitrary phase shifts ϕ_1, ϕ_2, ϕ_3 and arbitrary bare relaxation rates γ_{kR}, γ_{kL} at each coupling point $k = 1, 2, 3, 4$.

Parameter	Topology	Expression for two atoms, A and B
Frequency shifts, $\delta\omega_A$, $\delta\omega_B$	Small	0 0
	Braided	$\sin(\phi_1+\phi_2)(\sqrt{\gamma_{1R}\gamma_{3R}}+\sqrt{\gamma_{1L}\gamma_{3L}})$ $\sin(\phi_2+\phi_3)(\sqrt{\gamma_{2R}\gamma_{4R}}+\sqrt{\gamma_{2L}\gamma_{4L}})$
Individual decays, Γ_A, Γ_B	Small	$\gamma_{1R}+\gamma_{1L}$ $\gamma_{2R}+\gamma_{2L}$
	Braided	$\gamma_{1R}+\gamma_{1L}+\gamma_{3R}+\gamma_{3L}$ $+2\cos(\phi_1+\phi_2)(\sqrt{\gamma_{1R}\gamma_{3R}}+\sqrt{\gamma_{1L}\gamma_{3L}})$ $\gamma_{2R}+\gamma_{2L}+\gamma_{4R}+\gamma_{4L}$ $+2\cos(\phi_2+\phi_3)(\sqrt{\gamma_{2R}\gamma_{4R}}+\sqrt{\gamma_{2L}\gamma_{4L}})$
Collective decay, $\Gamma_{\rm coll}$	Small	$e^{i\phi}\sqrt{\gamma_{1R}\gamma_{2R}}+e^{-i\phi}\sqrt{\gamma_{1L}\gamma_{2L}}$
	Braided	$e^{i\phi_1}\sqrt{\gamma_{1R}\gamma_{2R}}+e^{i(\phi_1+\phi_2+\phi_3)}\sqrt{\gamma_{1R}\gamma_{4R}}$ $+e^{-i\phi_2}\sqrt{\gamma_{2R}\gamma_{3R}}+e^{i\phi_3}\sqrt{\gamma_{3R}\gamma_{4R}}$ $+e^{-i\phi_1}\sqrt{\gamma_{1L}\gamma_{2L}}+e^{-i(\phi_1+\phi_2+\phi_3)}\sqrt{\gamma_{1L}\gamma_{4L}}$ $+e^{i\phi_2}\sqrt{\gamma_{2L}\gamma_{3L}}+e^{-i\phi_3}\sqrt{\gamma_{3L}\gamma_{4L}}$
Exchange interaction, g	Small	$[e^{i\phi}\sqrt{\gamma_{1R}\gamma_{2R}}-e^{-i\phi}\sqrt{\gamma_{1L}\gamma_{2L}}]/2i$
	Braided	$[e^{i\phi_1}\sqrt{\gamma_{1R}\gamma_{2R}}+e^{i(\phi_1+\phi_2+\phi_3)}\sqrt{\gamma_{1R}\gamma_{4R}}$ $-e^{-i\phi_2}\sqrt{\gamma_{2R}\gamma_{3R}}+e^{i\phi_3}\sqrt{\gamma_{3R}\gamma_{4R}}$ $-e^{-i\phi_1}\sqrt{\gamma_{1L}\gamma_{2L}}-e^{-i(\phi_1+\phi_2+\phi_3)}\sqrt{\gamma_{1L}\gamma_{4L}}$ $+e^{i\phi_2}\sqrt{\gamma_{2L}\gamma_{3L}}-e^{-i\phi_3}\sqrt{\gamma_{3L}\gamma_{4L}}]/2i$

different atoms ($\Gamma_{\rm coll}$). They relate to the right (R) and left (L) collapse operators from Eqs. (4.15)–(4.16) as follows:

$$\mathcal{L}_{R/L} = \sqrt{\Gamma_{A,R/L}}\,\sigma_-^A + \sqrt{\Gamma_{B,R/L}}\,\sigma_-^B, \tag{4.18}$$

with

$$\Gamma_j = \Gamma_{jR} + \Gamma_{jL}, \qquad \text{for } j = A, B \tag{4.19}$$

$$\Gamma_{\text{coll}} = \sqrt{\Gamma_{A,R}\Gamma^*_{B,R}} + \sqrt{\Gamma_{A,L}\Gamma^*_{B,L}}, \tag{4.20}$$

where * denotes complex conjugate.

The procedure used in these examples follows the SLH scheme depicted in Fig. 4.2(c), and it is the same used in Paper A, where we generalize it to a setup of an arbitrary number of atoms with an arbitrary number of coupling points to the waveguide, and for any chirality of the coupling.

4.4 Interference effects

As we can see from the expressions in Table 4.1, for both small and giant atoms, the phase shifts acquired in the waveguide determine the interference effects between different atoms; for GAs, they also determine the self-interference effects. We explain these effects below.

4.4.1 Self-interference

Frequency-dependent relaxation rates

As introduced in Sec. 2.2.1, while a small atom coupled to a waveguide will always relax, the relaxation rate of a GA can be tuned during an experiment. This tunability is determined by the phase ϕ_k between coupling points k and $k+1$, which is, in turn, dictated by the atomic frequency ω, since $\phi_k = \omega|x_{k+1} - x_k|/v$, with v being the speed of the traveling excitation in the waveguide.

We see this effect in Table 4.1, where taking all bare relaxation rates to be equal (i.e., $\gamma_{kR} = \gamma_{kL} = \gamma/2$ for all k) leads to $\Gamma_j\big|_{\text{sma}} = \gamma$, but $\Gamma_j\big|_{\text{bra}} \in [0,\ 4\gamma]$ depending on the phases. In particular, the total suppression of the relaxation $\Gamma_j\big|_{\text{bra}} = 0$ occurs when an excitation acquires a phase $\pi \pmod{2\pi}$ between the coupling points of atom j (e.g., $\phi_1 + \phi_2 = \phi_2 + \phi_3 = \pi$), thus leading to destructive interference. Equivalently, this occurs when the coupling points are separated by half the excitation's wavelength, $\lambda/2 \pmod{\lambda}$. We refer to this as that the atom is *perfectly subradiant* or *decoherence free*, or is set to a *decoherence-free frequency/point*.

Although recalling the decoherence mechanisms introduced in Sec. 3.1.2 bares the question: does $\Gamma = 0$ truly mean decoherence free? The answer is no, at least not for experimentalists. For us theorists, who do not typically consider other loss channels other than relaxation to the waveguide, then yes, total suppression of relaxation means total suppression of decoherence. However, dephasing and non-radiative decay will not be suppressed, as demonstrated in Ref. [20], although these are typically orders of magnitude smaller than relaxation.

4.4.2 Collective interference

Subradiance

Let us now delve into the aforementioned phenomenon of subradiance [158, 162–164], which is the suppression of spontaneous emission by collective interference. We typically label a many-atom state as *subradiant* whenever it decays slower than the relaxation of each individual atom. A *perfectly subradiant* state—that which does not decay—is known as a *dark* state. In an atomic ensemble, dark states $|D\rangle$ are non-radiative pure states which are annihilated by all collapse operators and are eigenstates of the multiatom Hamiltonian [149, 151, 152, 163, 165], i.e., they satisfy

$$\begin{aligned} \mathcal{L}_R |D\rangle &= \mathcal{L}_L |D\rangle = 0 \\ H |D\rangle &= \mu |D\rangle , \ \ \mu \in \mathbb{R}. \end{aligned} \tag{4.21}$$

By applying Eq. (4.21) to the examples in Sec. 4.3 we find that, under certain conditions for γ_k, ϕ_k and ω_j, the possible dark states are the Bell states $|\Psi^+\rangle$ and $|\Psi^-\rangle$, which are maximally entangled states with one atom being excited and the other being in the ground state[3]:

$$\left|\Psi^{\pm}\right\rangle \equiv |T/S\rangle \equiv |\pm\rangle \equiv \frac{1}{\sqrt{2}}(|01\rangle \pm |10\rangle) = \frac{1}{\sqrt{2}}(|ge\rangle \pm |eg\rangle). \tag{4.22}$$

These conditions for the existence of dark states, which are well known for small atoms and have been studied since the discovery of superradiance [158], had not been derived before for GAs, until we did in Paper A. In fact, it was by applying the conditions from Eq. (4.21) that we found that, while most diatomic configurations (including small atoms) require the coupling to be bidirectional for dark states to exist, i.e., $\gamma_R = \gamma_L$, the nested configuration does not.

By coherently driving the system, and applying the same conditions from Eq. (4.21), in Paper A we found that the system evolves into an equilibrium between drive and dissipation, where the dark steady state reads[4]

$$\left|D_{S/T}\right\rangle = \frac{1}{\sqrt{1+|\alpha|^2}}(\alpha |S/T\rangle + |gg\rangle). \tag{4.23}$$

Here, α is a function of the bare relaxation rates, the coherent drive, and the detuning of the atoms from the drive; and $\left|D_{S/T}\right\rangle$ approaches $|S/T\rangle$ for strong drives[5]. This state has the same form for small [149, 151] and giant atoms, but

[3] There is no universal nomenclature for these states, but rather common naming practice differs between fields. The Bell state $\left|\Psi^+\right\rangle \equiv |\beta_{01}\rangle$ is also commonly referred to as the *plus* state $|+\rangle$, the *triplet* $|T\rangle$, or the *symmetric* state $|s\rangle$; whereas the Bell state $\left|\Psi^-\right\rangle \equiv |\beta_{11}\rangle$ is also known as the *minus* state $|-\rangle$, the *singlet* $|S\rangle$, or the *antisymmetric* state $|a\rangle$. In Paper A, we follow the notation $|T/S\rangle$, but we use $|\pm\rangle$ in Paper B.

[4] We note an erratum in Table III of Paper A, where the conditions for the existence of driven-dissipative dark states are collected. For separate atoms, the phase shifts that lead to the existence of $|D_S\rangle$ are $\phi_1 = \phi_2 = \phi_3 = 0 \pmod{2\pi}$ — not $\phi_2 = \pi$.

[5] This factor α should not be confused with the anharmonicity introduced in Eq. (2.8).

can be reached faster for certain configurations of GAs—a feature that we use for the design of the experiment in Paper E.

While collective emission phenomena have always been of interest to the quantum-optics community, subradiance is receiving a recently renewed interest in the context of quantum technologies: being able to access and harness dark states is a key ingredient in the development of quantum memories [166–168] and in the robust distribution of information in scalable quantum networks with quantum repeaters [169, 170].

Finally, it is important to remark that, in Papers B and C, we talk about (perfect) subradiance not as the collective interference effect between two atoms described here, but as the destructive interference between two coupling points of the *same* atom—i.e., as the decoherence-free effect explained in Sec. 4.4.1. While that may very well be abuse of language, we believe it is justified since, in the single-excitation regime, the subradiance that takes place between two small atoms is identical to that of a GA with two coupling points.

Decoherence-free interaction

Perfect subradiance offers a way of protecting atoms against decoherence only when the atoms are in the dark state. A much more robust way of protecting the atoms is achieved by braided GAs through the so-called *decoherence-free interaction* (DFI), which is independent of the states of the GAs, meaning that the entire Hilbert space of the atomic ensemble is protected from decoherence.

As mentioned in Sec. 2.2.1, this is one of the most promising properties of GAs and a feature of great potential in quantum computing applications, a field which is currently largely limited by quantum decoherence and dissipation.

Waveguide-mediated DFI between two atoms A and B takes place when the interference from their coupling points suppresses both the individual and collective relaxation rates ($\Gamma_j, \Gamma_{\text{coll}} = 0 \ \forall j \in \{A, B\}$) while maintaining their exchange interaction ($g \neq 0$). Let us see when that happens.

As explained before, the individual decay rate of each atom $\Gamma_j = 0$ is zero when the coupling points of each atom are separated by a phase $\pi \pmod{2\pi}$ [see Fig. 4.3(a)]. For this particular distance, the emission from each atom's connection points interferes destructively, making the sum over all atoms zero and thus preventing collective decay ($\Gamma_{\text{coll}} = 0$). In separate and nested atoms, the connection points of atom B are consecutive, so the emission between them cancels the interaction ($g = 0$) when $\Gamma_B = 0$. Unlike these topologies, braided atoms have the particularity that no consecutive points belong to the same atom, allowing a non-zero exchange interaction (see Table 4.1). As depicted in Fig. 4.3(b), this implies that an excitation can be released from atom A to be reabsorbed by atom B and vice versa, in a perpetual loop. What is more, one can braid more than two GAs to achieve decoherence-free chains and all-to-all decoherence-free interaction [46].

DFI was first described in 2018 [46] and demonstrated experimentally in 2020 [20]. Later, we showed that it holds in continuous waveguides of any chirality (Paper A), as well as in 1D and 2D structured baths (Papers B and

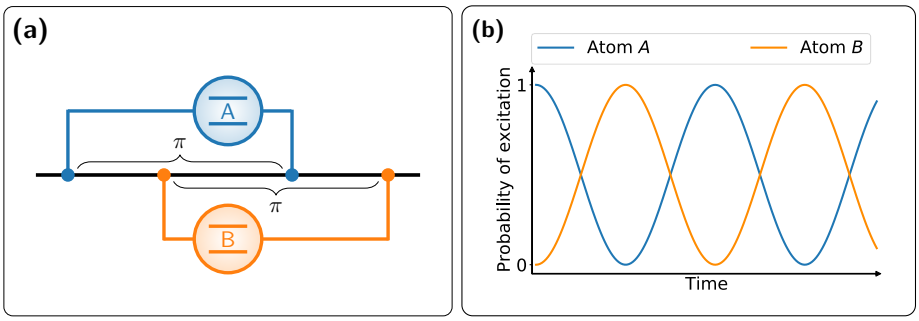

Figure 4.3: (a) Two braided giant atoms with the coupling points of each atom separated by a phase shift of $\pi \pmod{2\pi}$, which is the distance that allows them to interact without decohering. (b) Excitation exchange between two atoms arranged in the setup from (a), showing a decoherence-free interaction.

C, respectively). In Papers B and C, we also studied how DFI is affected by non-Markovianities, which requires the formalism explained in the next chapter.

4.5 Quantum logic gates

The interference effects explained above can be harnessed to implement two-qubit quantum gates (i.e., unitary operations performed on two interacting qubits) without the help of additional resources such as couplers. This is an important application, because access to an entangling two-qubit gate such as the iSWAP or the CZ, together with a complete set of single-qubit gates, is sufficient to achieve a universal gate set for a quantum computer [171]. That means that it is sufficient to approximate any unitary transformation on any number of qubits to any desired precision.

4.5.1 iSWAP

An iSWAP gate leaves the states $|00\rangle$ and $|11\rangle$ unchanged, while the states $|01\rangle$ and $|10\rangle$ are swapped and acquire a phase factor $e^{i\pi/2} = i$ [88]. In matrix form, it reads

$$\text{iSWAP} = \begin{array}{c} \begin{matrix} |00\rangle & |01\rangle & |10\rangle & |11\rangle \end{matrix} \\ \begin{pmatrix} 1 & 0 & 0 & 0 \\ 0 & 0 & i & 0 \\ 0 & i & 0 & 0 \\ 0 & 0 & 0 & 1 \end{pmatrix} \end{array}. \tag{4.24}$$

In GAs, the iSWAP gate is the operation performed after half a period of the DFI oscillations from Fig. 4.3(b). Experimentally [20], it usually requires the atoms to have three coupling points each, so that they have two decoherence-free

frequencies. In this way, the gate is started by tuning atom A to a decoherence-free frequency ω_{DF1} and atom B to ω_{DF2}. Then, atom A is tuned to ω_{DF2}, resonantly with atom B, so that they interact. Finally, after one population swap, atom A is detuned back to ω_{DF1} for readout or further operations.

The same procedure can be followed to perform a $\sqrt{\mathrm{iSWAP}}$ gate by cutting the interaction time in half. In this case, instead of starting in the state $|10\rangle$ and ending in $|01\rangle$, we end in the entangled state $(|01\rangle - i\,|10\rangle)/\sqrt{2}$, as was achieved in Ref. [20] with 94% fidelity.

4.5.2 CZ

A controlled-Z gate, or CZ gate, leaves all the states unchanged except for $|11\rangle$, which accumulates a phase $e^{i\pi} = -1$ [3, 88]. In matrix form, this is

$$\mathrm{CZ} = \begin{array}{c} \begin{array}{cccc} |00\rangle & |01\rangle & |10\rangle & |11\rangle \end{array} \\ \begin{pmatrix} 1 & 0 & 0 & 0 \\ 0 & 1 & 0 & 0 \\ 0 & 0 & 1 & 0 \\ 0 & 0 & 0 & -1 \end{pmatrix} \end{array}. \tag{4.25}$$

A common way to implement the CZ gate is to bring the population of the $|11\rangle$ state to the $|20\rangle$ (or $|02\rangle$) state and back [87]. In three-level GAs, this can be done [172] by tuning resonantly the transitions ω_{12} of atom A and ω_{01} of atom B, which leads to DFI between the states $|11\rangle$ and $|20\rangle$. For the population exchanges to be fully protected, the transition ω_{01} of atom A should also be decoherence-free, but detuned away from the DFI frequency. This requires the atom to have an additional coupling point to the waveguide, with respect to the layout described for the iSWAP gate.

The CZ gate with GAs has been demonstrated theoretically in a continuous waveguide [172]; and in Paper D, we study how to perform it in a structured waveguide under non-Markovian effects.

5 Resolvent formalism

> I passed Complex Analysis! Unbelievable! Now I can throw away the notes and never see this again...
>
> Ariadna Soro (2016)

In this chapter, we present the resolvent formalism used in Papers B and C to model GAs coupled to 1D and 2D structured environments (see Sec. 2.2.2). This theory, which is more general and requires fewer assumptions than the Lindblad master equation (Sec. 3.2.1) or the SLH formalism (Sec. 4.2), allows us study exact atomic dynamics and non-Markovian effects.

Let us start by considering a system with a total Hamiltonian $H = H_0 + H_{\text{int}}$, where H_0 is the "unperturbed" Hamiltonian for which the eigenstates and eigenenergies are known, and H_{int} represents the coupling between subspaces spanned by some of the unperturbed eigenstates. This could be the case of the Hamiltonian used in Chapter 3 [in Eq. (3.18)], where $H_0 = H_a + H_b$, i.e., the sum of the bare atom and bath Hamiltonians. There, we made many simplifications to be able to describe the atomic dynamics: we made the Born-Markov approximation, and we assumed a linear dispersionless bath with negligible travel time between components. With fewer simplifications, in many cases, we could take a perturbative approach to solve the dynamics. However, sometimes, a deeper understanding of certain physical phenomena requires going beyond perturbation theory and taking into account some effects of H_{int} to all orders.

For this type of problem, we resort to the so-called *resolvent formalism*, based on the definition of the *resolvent* $G(z) = 1/(z - H)$ of the Hamiltonian H, with $z \in \mathbb{C}$. The relation between the resolvent $G(z)$ and the unperturbed resolvent $G_0(z) = 1/(z - H_0)$ is an *algebraic* equation, much simpler to manipulate than the *integral* equation connecting the evolution operators $U(t) = \exp\{-iHt\}$ and $U_0(t) = \exp\{-iH_0t\}$. The matrix elements of $U(t)$ are then calculated from the matrix elements of $G(z)$ via a contour integral. Moreover, the analytical properties of $G(z)$ provide information about the different contributions to the dynamics.

5.1 From resolvent to evolution operator

The time-evolution operator $U(t,t')$ of the Hamiltonian $H = H_0 + H_{\text{int}}$ is the solution to the Schrödinger equation

$$i\frac{\mathrm{d}}{\mathrm{d}t}U(t,t') = (H_0 + H_{\text{int}})U(t,t'), \tag{5.1}$$

with the initial condition $U(t',t') = 1$. In fact, the solution can be written as

$$U(t,t') = U_0(t,t') - i\int_{t'}^{t} d\tau U_0(t,\tau)H_{\text{int}}U(\tau,t'), \tag{5.2}$$

where $U_0(t,t') = \exp\{-iH_0(t-t')\}$. Note that this expression is close to a convolution product, but not quite, since τ varies between t' and t. Fortunately, by introducing new operators, we can convert it to a true convolution product, which will transform into a simple product by Fourier transformation. We define

$$K_+(t,t') = U(t,t')\theta(t-t'); \qquad K_{0+}(t,t') = U_0(t,t')\theta(t-t'), \tag{5.3}$$

where $\theta(t-t')$ is the Heaviside function, equal to 1 for $t > t'$ and to 0 otherwise. With these operators, we can rewrite Eq. (5.2) as a true convolution:

$$K_+(t,t') = K_{0+}(t,t') - i\int_{-\infty}^{\infty} d\tau K_{0+}(t,\tau)H_{\text{int}}K_+(\tau,t'). \tag{5.4}$$

We note that $K_+(t,t')$ satisfies the equation

$$\left(i\frac{\mathrm{d}}{\mathrm{d}t} - H\right)K_+(t,t') = \delta(t-t'), \tag{5.5}$$

which is why the operator $K_+(t,t')$ is sometimes called the *Green's function*. In fact, it is a *retarded* Green's function because it is non-zero only for $t > t'$. Conversely, we can define the *advanced* Green's function

$$K_-(t,t') = -U(t,t')\theta(t'-t), \tag{5.6}$$

which obeys the same evolution equation as K_+ but satisfies different boundary conditions.

It is now convenient to introduce the Fourier transform of $K_+(t,t')$, which depends only on $t-t'$, so by redefining $t := t-t'$, we can write

$$K_+(t) = -\frac{1}{2\pi i}\int_{-\infty}^{\infty} dE\, e^{-iEt}G_+(E), \tag{5.7}$$

or, inversely,

$$\begin{aligned} G_+(E) &= -i\int_{-\infty}^{\infty} dt\, e^{iEt}\overbrace{K_+(t)}^{\exp\{-iHt\}\theta(t)} = -i\int_0^{\infty} dt\, e^{i(E-H)t} = \\ &= \lim_{\eta\to 0_+} -i\int_0^{\infty} dt\, e^{i(E-H+i\eta)t} = \lim_{\eta\to 0_+}\frac{1}{E-H+i\eta}, \end{aligned} \tag{5.8}$$

were η is a positive real number that tends to zero, and $G_+(E)$ is called *retarded propagator*[1]. Similarly, the advanced Green's function and propagator satisfy

$$K_-(t) = -\frac{1}{2\pi i}\int_{-\infty}^{\infty} dE\, e^{-iEt} G_-(E), \tag{5.9}$$

$$G_-(E) = \lim_{\eta\to 0_+} \frac{1}{E - H - i\eta}. \tag{5.10}$$

Notice that, now, the integral from Eq. (5.4) becomes a simple product by Fourier transform, thus resulting in the algebraic equation

$$G_+(E) = G_{0+}(E) + G_{0+}(E) H_{\rm int} G_+(E), \tag{5.11}$$

where G_{0+} is the retarded propagator associated with H_0.

The simple form of $G_\pm(E)$ suggests the introduction of the *resolvent* operator of the Hamiltonian H,

$$G(z) = \frac{1}{z - H}, \tag{5.12}$$

as a function of the complex variable z. Then, the retarded (advanced) propagator $G_+(E)$ $[G_-(E)]$ is simply the limit of $G(z)$ when z tends to the point E on the real axis, with a positive (negative) value of its imaginary part:

$$G_\pm(E) = \lim_{\eta\to 0_+} G(E \pm i\eta). \tag{5.13}$$

Finally, the time-evolution operator $U(t) = K_+(t) - K_-(t)$ is expressed by a contour integral of G(z):

$$\begin{aligned} U(t) &= \frac{1}{2\pi i}\int_{-\infty}^{\infty} dE\, e^{-iEt}[G_-(E) - G_+(E)] = \\ &= \frac{1}{2\pi i}\int_{\gamma_+ + \gamma_-} dz\, e^{-izt} G(z), \end{aligned} \tag{5.14}$$

where γ_+ (γ_-) is a line situated infinitesimally above (below) the real axis and followed from right (left) to left (right), and the contribution of C_- (C_+) is zero for $t > 0$ ($t < 0$). Later, to compute this integral, we will use the residue theorem (Sec. 5.4), which requires the contour to be a closed curve. Conveniently, Jordan's lemma [173] allows us to extend $\gamma_\pm$ without changing the value of the integral, by integrating around a semicircle of infinite radius in the upper half-plane for $t < 0$ and in the lower half-plane for $t > 0$. Thus, for $t > 0$, as is the case in most physical scenarios, the contour in Eq. (5.14) reduces to a counter-clockwise path around the closed lower half-plane (i.e., the lower half-plane and the real axis)—as depicted in the example of Fig. 5.2(a).

[1] Since K_+ and G_+ are interchangeable by Fourier transform, sometimes, it is K_+ which is referred to as the retarded propagator, and G_+ receives instead the name of retarded Green's function.

5.2 Singularities of the resolvent

It becomes patent from Eq. (5.14) that we can determine properties of $U(t)$ from the analytical properties of $G(z)$. In fact, the matrix elements of $G(z)$ are analytic functions of z in the whole complex plane except for the real axis, where they have two types of singularities:

- **Real poles**, located at the discrete eigenvalues of the Hamiltonian H, and
- **Branch cuts**, extending over the intervals corresponding to the continuous spectrum of H. A cut appears when the matrix elements of $G(z)$ do not tend to the same value when z tends from below or from above toward a point on the real axis, located on the cut.

Now, it is possible to analytically continue $G(z)$ from, e.g., the upper half-plane towards the lower half-plane, into the so-called *second Riemann sheet*. In this case, the continued function is not necessarily analytic outside the real axis and may have

- **Complex poles**, which describe *unstable* states of the system, i.e., states having a complex energy and characterized by exponential damping.

5.3 From level-shift operator to resolvent

The identity Eq. (5.11) can be applied to give the perturbative expansion of $G(z)$ in powers of V, and iterated to yield

$$\begin{aligned} G(z) &= G_0(z) + G_0(z) H_{\text{int}} G(z) = \\ &= G_0(z) + G_0(z) H_{\text{int}} G_0(z) + G_0(z) H_{\text{int}} G_0(z) H_{\text{int}} G_0(z) + \dots \end{aligned} \tag{5.15}$$

Then, the matrix elements of $G(z)$ between two eigenstates $\langle l|$ and $|m\rangle$ of H_0, with unperturbed energies E_l and E_m, read

$$\begin{aligned} G_{lm}(z) = \frac{1}{z-E_l}\delta_{lm} + \frac{1}{z-E_l} H^{\text{int}}_{lm} \frac{1}{z-E_m} \\ + \sum_i \frac{1}{z-E_l} H^{\text{int}}_{li} \frac{1}{z-E_i} H^{\text{int}}_{im} \frac{1}{z-E_m} + \dots, \end{aligned} \tag{5.16}$$

where $|i\rangle$ are eigenstates of H_0, $G_{lm}(z) = \langle l|G(z)|m\rangle$, and $H^{\text{int}}_{im} = \langle i|H_{\text{int}}|m\rangle$. Note that this expression is quite simple, consisting only of products of matrix elements of H_{int} and of unperturbed energy denominators. In this way, we can regroup the terms where a denominator $1/(z-E_e)$ involving a particular unperturbed state $|e\rangle$ appears x times, and then formally sum the perturbation series. Let us take $l = m = e$. Then, the zero-order term in H_{int} of Eq. (5.16) is just $1/(z-E_e)$ and thus contains this denominator once. Meanwhile, the next

terms in the expansion contain the denominator at least twice. If we require them to contain the denominator *only* twice, then we can express the sum as

$$\Sigma_e(z) = H_e^{\text{int}} + \sum_{i\neq e} \frac{1}{z-E_i} H_{ie}^{\text{int}} + \sum_{i\neq e}\sum_{j\neq e} H_{ei}^{\text{int}} \frac{1}{z-E_i} H_{ij}^{\text{int}} \frac{1}{z-E_j} H_{je}^{\text{int}} + \dots, \tag{5.17}$$

but we can generalize it to contain the denominator x times. In fact, it is sufficient to sum the contributions corresponding to different values of x to obtain

$$G_e(z) = \sum_{x=1}^{\infty} \frac{[\Sigma_e(z)]^{x-1}}{(z-E_e)^x} = \frac{1}{z-E_e} \sum_{x=0}^{\infty} \left[\frac{\Sigma_e(z)}{z-E_e}\right]^x = \frac{1}{z-E_e-\Sigma_e(z)}, \tag{5.18}$$

which is an exact expression for $G_e(z) = \langle e|G(z)|e\rangle$.

5.3.1 Projection of the resolvent

Equation (5.18) can also be derived using projection operators. Consider the subspace spanned by some eigenvectors $\{|a\rangle, |b\rangle, \dots, |l\rangle\}$ of the unperturbed Hamiltonian H_0. If they are orthonormal, the projector onto the subspace is

$$P = |a\rangle\langle a| + |b\rangle\langle b| + \dots + |l\rangle\langle l|. \tag{5.19}$$

The projector onto the complementary subspace is then $Q = 1 - P$. Since the subspaces are orthogonal, then $PQ = QP = 0$, and since the states $|a\rangle, |b\rangle, \dots, |l\rangle$ are eigenstates of H_0, then $[P, H_0] = [Q, H_0] = 0$. From these two relations, we derive that

$$PH_0Q = QH_0P = 0. \tag{5.20}$$

Let us now take the definition of resolvent and manipulate it by multiplying on the right by P and on the left by P or Q:

$$\begin{aligned}
&G(z) = \frac{1}{z-H} \implies (z-H)G(z) = 1 \\
&\implies \begin{cases} P(z-H)\underbrace{(P+Q)}_{1} G(z)P = \underbrace{P^2}_{P} \\ Q(z-H)\overbrace{(P+Q)} G(z)P = \underbrace{QP}_{0} \end{cases} \\
&\implies \begin{cases} P(z-H)[PG(z)P + QG(z)P] = P \\ Q(z-H)[PG(z)P + QG(z)P] = 0 \end{cases} \\
&\implies \begin{cases} P(z-H)\underbrace{PP}_{P} G(z)P + P(z\underbrace{-H_0-H_{\text{int}}}_{-H})\underbrace{QQ}_{Q} G(z)P = P \\ Q(z\underbrace{-H_0-H_{\text{int}}}_{-H})\underbrace{PP}_{P} G(z)P + Q(z-H)\underbrace{QQ}_{Q} G(z)P = 0 \end{cases}
\end{aligned}$$

$$\Longrightarrow \begin{cases} P(z-H)P[PG(z)P] + \cancelto{0}{PQz} - \cancelto{0}{PH_0Q} - PH_{\text{int}}Q[QG(z)P] = P \\ \cancelto{0}{QPz} - \cancelto{0}{QH_0P} - QH_{\text{int}}P[PG(z)P] + Q(z-H)Q[QG(z)P] = 0 \end{cases} \tag{5.21}$$

We can solve the system of equations above for $PG(z)P$ by substitution of $QG(z)P$ to obtain

$$P\left[z - H_0 - H_{\text{int}} - H_{\text{int}}\frac{Q}{z - QH_0Q - QH_{\text{int}}Q}H_{\text{int}}\right]PG(z)P = P. \tag{5.22}$$

For this expression, we define the *level-shift operator* $\Sigma(z)$ as follows:

$$\Sigma(z) = H_{\text{int}} + H_{\text{int}}\frac{Q}{z - QH_0Q - QH_{\text{int}}Q}H_{\text{int}}, \tag{5.23}$$

whose perturbative expansion in powers of H_{int} reads

$$\Sigma(z) = H_{\text{int}} + H_{\text{int}}\frac{Q}{z - H_0}H_{\text{int}} + H_{\text{int}}\frac{Q}{z - H_0}H_{\text{int}}\frac{Q}{z - H_0}H_{\text{int}} + \dots. \tag{5.24}$$

Rewriting Eq. (5.22) in terms of the level-shift operator [Eq. (5.23)] yields

$$PG(z)P = \frac{P}{z - PH_0P - P\Sigma(z)P}, \tag{5.25}$$

which generalizes equation Eq. (5.18). The form of Eq. (5.25) suggests that $P\Sigma P$ can be considered as a "Hamiltonian" (ignoring the dependence on z) in the subspace spanned by $\{|a\rangle, |b\rangle, \dots, |l\rangle\}$ being added to PH_0P and allowing us to determine the shifts of the perturbed levels relative to unperturbed levels. This is why $\Sigma(z)$ is called the *level-shift operator*.

5.4 Residue theorem

Before we move on to applying the resolvent formalism to a physical scenario, let us review one last concept from complex analysis: the residue theorem.

Consider a function $f(z)$ that has a pole of order m at $z = a$. Then, by the definition of a pole,

$$f(z) = \frac{A_{-m}}{(z-a)^m} + \frac{A_{-m+1}}{(z-a)^{m-1}} + \dots + \frac{A_{-1}}{(z-a)} + g(z), \tag{5.26}$$

where $g(z)$ is analytic near and at a, and the coefficient A_{-1} is called the *residue* $\text{Res}(f, a)$ of the function $f(z)$ relative to the pole a [174]. Formally,

$$\text{Res}(f, a) = A_{-1} = \lim_{z \to a}\left(\frac{1}{(m-1)!}\left(\frac{\mathrm{d}}{\mathrm{d}z}\right)^{m-1}\left[(z-a)^m f(z)\right]\right). \tag{5.27}$$

It follows from the above definition that, if a is a *simple* pole of $f(z)$, the residue of $f(z)$ at that pole is $\lim_{z\to a}[(z-a)f(z)]$.

The *residue theorem* states that if $f(z)$ is analytic throughout a contour γ and its interior except at a number of poles $a_1, \ldots, a_n$ inside the contour, then

$$\frac{1}{2\pi i}\int_\gamma f(z)dz = \sum_{j=1}^{n} \mathrm{Res}(f, a_j)\,\mathrm{wind}(\gamma, a_j), \tag{5.28}$$

where $\mathrm{wind}(\gamma, a_j)$ is the winding number of γ around a_j [174]. Note that $\mathrm{wind}(\gamma, a_j) = 0$ if a_j falls outside the contour.

5.5 Example: a giant atom in a 1D structured waveguide

Consider the simplest setup from Paper B, shown in Fig. 5.1: a single giant atom with two connection points coupled to a 1D structured waveguide, and suppose we want to find the time evolution of the atomic population. We can start by writing the total Hamiltonian as the sum $H = H_0 + H_{\mathrm{int}}$, with

$$H_0 = \Delta\sigma^+\sigma^- + \sum_k \omega(k) a_k^\dagger a_k, \tag{5.29}$$

$$H_{\mathrm{int}} = \frac{g}{\sqrt{N}}\sum_k \left[\left(e^{ikn_1} + e^{ikn_2}\right) a_k\sigma^+ + \mathrm{H.c.}\right], \tag{5.30}$$

where Δ is the detuning of the atom with respect to the bath frequency, $\sigma^\pm$ denote the atomic ladder operators, $a_k^\dagger, a_k$ are the creation and annihilation operators of the cavity modes, $\omega(k)$ is given by the dispersion relation from Eq. (2.3), g is the coupling strength at each connection point, N is the number of coupled cavities conforming the bath, and n_p denotes the position of the p-th coupling point.

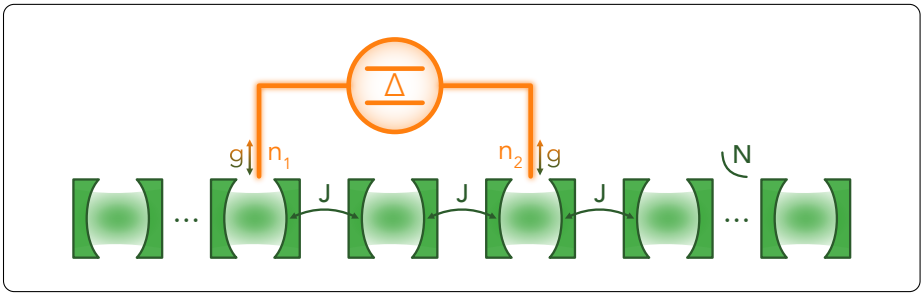

Figure 5.1: A giant atom with two connection points coupled to a 1D structured waveguide. Figure adapted from Paper B.

Note that we have applied the RWA directly on the Hamiltonian, which requires that the atomic and bath resonant frequencies are much larger than the coupling strength g, and, as explained in Sec. 3.2.1, will not yield an accurate value of the Lamb shifts.

In the single-excitation subspace, the eigenstates of the unperturbed Hamiltonian H_0 consist of an atomic excitation $|e\rangle := |e,0\rangle$, and a photonic excitation in mode $k \in [-\pi, \ldots, \pi - \frac{2\pi}{N}]$, $|k\rangle := |g,k\rangle$. It is the interaction term H_{int} that couples the subspace $\{|e\rangle\}$ with $\{|k\rangle\}$. We can then define the projector $P = |e\rangle\langle e|$ and its complement $Q = \sum_k |k\rangle\langle k|$, and use the techniques described in the previous section, but in inverse order: we will first derive the matrix elements of the level-shift operator and, from there, we will deduce the resolvent and the time-evolution operator.

Let us start with the perturbative expansion of the level-shift operator in powers of H_{int} shown in Eq. (5.24), truncated to second order:

$$\Sigma(z) = H_{\text{int}} + H_{\text{int}} \frac{Q}{z - QH_0Q - QH_{\text{int}}Q} H_{\text{int}} \approx H_{\text{int}} + H_{\text{int}} \frac{Q}{z - H_0} H_{\text{int}}. \quad (5.31)$$

It is nontrivial to see why this truncation is justified, so let us elucidate. Assume the eigenstate $|e\rangle$ of H_0 is well isolated from all the other discrete eigenstates of H_0. Let us examine Eq. (5.17) near $z = E_e$, which is where $G_e(z)$ [see Eq. (5.18)] takes on the most important values. All the energy denominators involved in the expansion of $\Sigma_e(z)$ are large because the other discrete energies of H_0 are assumed to be far from E_e. Nevertheless, even if E_e falls within the continuous spectrum of H_0, the sums over the intermediate states associated with this continuous spectrum involve delta functions and principal parts which do not lead to any divergence. Thus, if H_{int} is small compared to H_0, the perturbative series in Eq. (5.17) is rapidly convergent and it is completely valid to approximate $\Sigma_e(z)$ by retaining only a finite number of terms.

It is important to remark that a perturbative approximation for $\Sigma_e(z)$ does *not* correspond to a perturbative approximation for $G_e(z)$, since $G_e(z)$ obtained by truncation of $\Sigma_e(z)$ still contains arbitrarily high powers of H_{int}. In other words, the truncation in Eq. (5.31) is equivalent to making a partial resummation of the perturbation theory.

Now, we can go back to the level-shift operator in Eq. (5.31) and calculate the matrix element $\Sigma_e(z) = \langle e|\Sigma(z)|e\rangle$, known as the *self-energy* of the atom:

$$\begin{aligned}
\Sigma_e(z) &= \cancelto{0}{\langle e|H_{\text{int}}|e\rangle} + \sum_k \langle e|\, H_{\text{int}} \frac{|k\rangle\langle k|}{z - H_0} H_{\text{int}}\, |e\rangle = \\
&= \frac{g^2}{N} \sum_k \frac{(e^{ikn_1} + e^{ikn_2})(e^{-ikn_1} + e^{-ikn_2})}{z - \omega(k)} = \\
&= \frac{2g^2}{N} \sum_k \frac{1 + \cos(k(n_2 - n_1))}{z - \omega(k)}. \qquad (5.32)
\end{aligned}$$

Henceforth, we use the dispersion relation $\omega(k) = -2J\cos(k)$ introduced in Eq. (2.3), and that the distance between coupling points is $d = n_2 - n_1$. In

the continuum limit, i.e., when $N \to \infty$, the sum over k becomes an integral: $\sum_k \frac{2\pi}{N} \to \int_k dk$. Therefore, we can write the self-energy as

$$\begin{aligned}\Sigma_e(z) &= \frac{g^2}{\pi}\int_{-\pi}^{\pi}\frac{1+\cos(kd)}{z+2J\cos(k)}dk = \\ &= \frac{g^2}{\pi}\int_{-\pi}^{\pi}\frac{dk}{z+2J\cos(k)} + \frac{g^2}{\pi}\int_{-\pi}^{\pi}\frac{e^{ikd}}{z+2J\cos(k)}dk,\end{aligned} \tag{5.33}$$

where, in the second integral, we have substituted the cosine for an exponential because odd functions do not contribute to the integral. Now, we can introduce the change of variable $\tilde{z} = e^{ik}$ such that $2\cos(k) = \tilde{z} + \tilde{z}^{-1}$ and $dk = -i\tilde{z}^{-1}d\tilde{z}$, and integrate over the unit circle:

$$\begin{aligned}\Sigma_e(z) &= -\frac{ig^2}{\pi}\oint\frac{d\tilde{z}}{z\tilde{z}+J\tilde{z}^2+1} - \frac{ig^2}{\pi}\oint\frac{\tilde{z}^d d\tilde{z}}{z\tilde{z}+J\tilde{z}^2+1} = \\ &= -\frac{ig^2}{\pi J}\oint\frac{(1+\tilde{z}^d)d\tilde{z}}{(\tilde{z}-f_+)(\tilde{z}-f_-)},\end{aligned} \tag{5.34}$$

where the function $(1+\tilde{z}^d)$ is an entire function, i.e., it does not have singularities in the complex plane, and the poles of the denominator are

$$f_\pm(z) = \frac{-z \pm \sqrt{z^2-4J^2}}{2J}. \tag{5.35}$$

Applying the residue theorem [Eq. (5.28)], we obtain that

$$\oint \underbrace{\frac{(1+\tilde{z}^d)}{(\tilde{z}-f_+)(\tilde{z}-f_-)}}_{F(\tilde{z})} d\tilde{z} = 2\pi i \sum_{\pm}\mathrm{Res}(F, f_\pm)\,\mathrm{wind}(S^1, f_\pm) \tag{5.36}$$

where the residues are

$$\begin{aligned}\mathrm{Res}(F, f_\pm) &= \lim_{\tilde{z}\to f_\pm}(\tilde{z}-f_\pm)F(\tilde{z}) = \frac{1+f_\pm^d}{f_\pm - f_\mp} = \\ &= \frac{\pm J}{\sqrt{z^2-4J^2}}\left[1+\left(\frac{-z\pm\sqrt{z^2-4J^2}}{2J}\right)^d\right],\end{aligned} \tag{5.37}$$

and the winding number is zero for the poles that fall outside of the unit circle S^1, i.e.,

$$\mathrm{wind}(S^1, f_+) = \begin{cases}1 & \mathrm{Re}\{z\} > 0 \\ 0 & \mathrm{Re}\{z\} < 0\end{cases}, \qquad \mathrm{wind}(S^1, f_-) = \begin{cases}0 & \mathrm{Re}\{z\} > 0 \\ 1 & \mathrm{Re}\{z\} < 0.\end{cases} \tag{5.38}$$

Therefore, we can insert the results of the residue theorem into Eq. (5.34) to obtain the final expression of the self-energy:

$$\Sigma_e(z) = \mathrm{sgn}(\mathrm{Re}\{z\})\frac{2g^2}{\sqrt{z^2-4J^2}}\left[1+\left(\frac{-z+\mathrm{sgn}(\mathrm{Re}\{z\})\sqrt{z^2-4J^2}}{2J}\right)^d\right]. \tag{5.39}$$

According to Eq. (5.18), the resolvent matrix element corresponding to the excited state of the atom is then

$$G_e(z) = \frac{1}{z - \Delta - \Sigma_e(z)}, \tag{5.40}$$

with Δ being the atom-cavity detuning. Lastly, we can express the probability amplitude of an initially excited GA, for $t > 0$, as follows from Eq. (5.14):

$$C_e(t) = -\frac{1}{2\pi i} \int_\gamma G_e(z) e^{-izt}\, dz, \tag{5.41}$$

where the contour γ is shown in Fig. 5.2.

The derivation presented here is used in Paper B for a single giant atom. For two atoms, the procedure is similar, but a bit trickier, since the $G(z)$ is not diagonal in the basis $\{|eg\rangle, |ge\rangle\}$ (where one atom is excited and the other one is in the ground state), thus making it harder to calculate the matrix elements. An outline of the procedure to follow in such a case is presented in the appendix of Paper B.

5.6 Contributions to the probability amplitude

In Fig. 5.2, we illustrate the different singularities of the resolvent that we introduced in Sec. 5.2, applied to the example of a giant atom coupled to a structured waveguide. Below, we show how the singularities relate to physical phenomena.

5.6.1 Real poles

Real poles are isolated poles of the resolvent [Eq. (5.40)] that fall on the real axis outside the continuum of propagating modes, i.e., they satisfy $z - \Delta - \Sigma_e(z) = 0$ and $|z| > 2J$.

Atom-photon bound states outside the continuum

These poles correspond to the energies of states that are *bound* (not propagating), and exponentially localized in the vicinity of the atoms. In particular, they are often called *bound states outside the continuum* (BOCs) [175–177], or *atom-photon bound states* [49, 52, 105–107] since, in these dressed states, the excitation lives partly in the atom and partly in the bath. Depending on the detuning and the coupling strength of the atom, the bound states can have a more atomic nature, localized and isolated from the continuum; or a more photonic nature, delocalized and hybridized with the continuum. A common measure of localization is the *inverse participation ratio* (IPR), defined as [178]

$$\mathrm{IPR} = \sum_n |\psi(n)|^4, \tag{5.42}$$

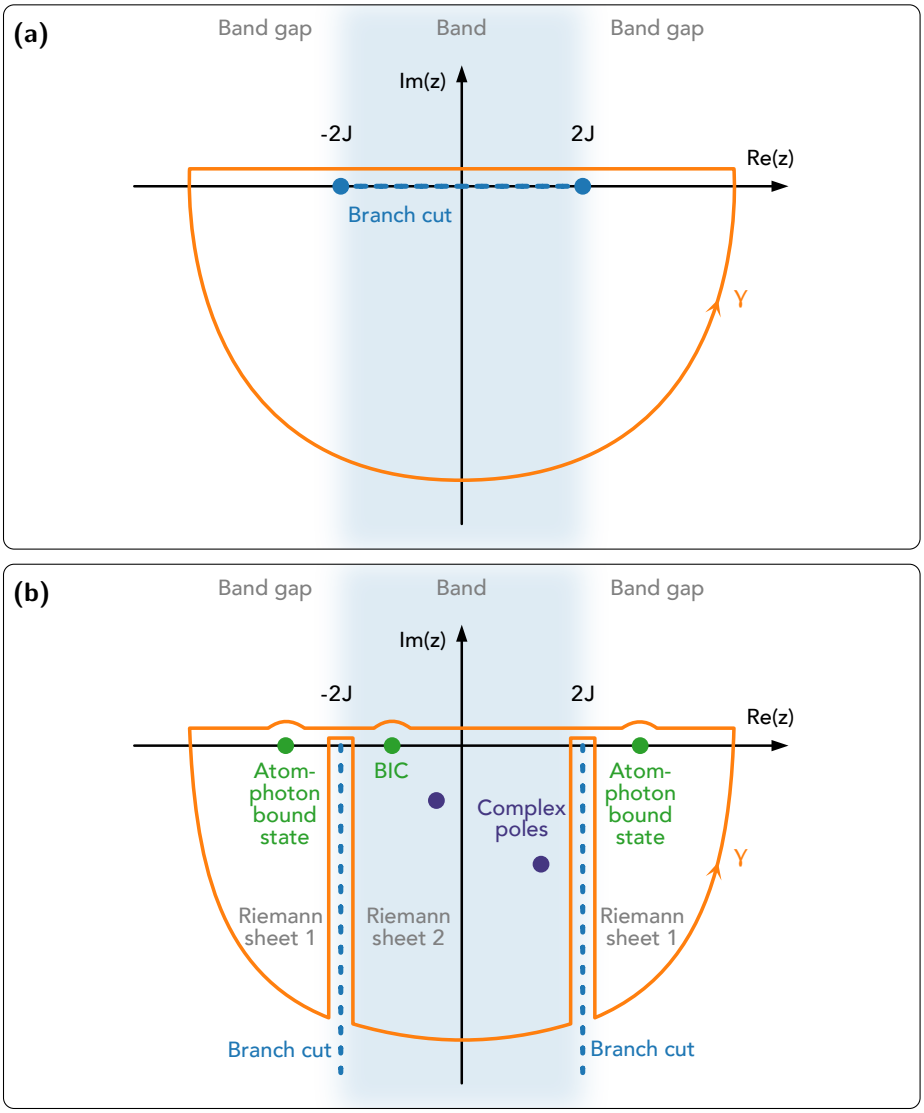

Figure 5.2: (a) Contour γ of the integral in Eq. (5.41). A branch cut arises along the real axis and across the continuous energy band, i.e., at $\mathrm{Re}(z) \in [-2J, 2J]$, and therefore the residue theorem cannot be applied using this contour. Figure adapted with permission from Ref. [179]. (b) Contour γ modified from (a) to include the energy band but exclude the branch cuts and branch points. This is achieved by defining the branch cuts along the band edges ($|\mathrm{Re}(z)/J| = 2$), and contouring around them into the second Riemann sheet. In this way, the probability amplitude gets contributions from both the poles of the resolvent [Eq. (5.40)] and the detours around the branch cuts. Figure adapted from Paper B and inspired by Ref. [62].

where $\psi(n)$ is the real-space wavefunction at cavity site n. The IPR can takes values from $1/N$ for fully delocalized states, to 1 for perfectly localized, which means that for 1D baths, the IPR is inversely proportional to the localization length.

As mentioned in Sec. 2.2.2, multiple atoms coupled to the band gap of the same reservoir can interact through the overlap of their bound-state photonic wavefunctions [57–59], without losing their excitations to the environment. This is similar to the DFI explained in Sec. 4.4.2, although the latter occurs inside the continuum, and it requires more than an overlap of the photonic part of the wavefunctions (see Sec. 5.6.3).

5.6.2 Branch cuts

Contrary to the real poles, a branch cut extends over the interval corresponding to the *continuous* energy spectrum [see Fig. 5.2(a)]. It arises due to the square root in the self-energy [Eq. (5.39)], which is in turn introduced by the dispersion relation. The presence of this branch cut implies that $G_e(z)$ is not analytic within the contour γ, and we cannot therefore apply the residue theorem to compute the probability amplitude $C_e(t)$ in Eq. (5.41). We circumvent this problem by taking the branch cuts at the band edges instead, and contouring around them, thus including the energy band and excluding the branch cuts and points [see Fig. 5.2(b)]. In this case, the detour around the branch cuts will add a contribution to the probability amplitude $C_e(t)$, as shown in Eq. (5.45).

5.6.3 Complex poles

While the branch cuts no longer fall inside the contour, the function $G(z)$ is still not analytical within the contour. We tackle this by analytically continuing the function into the second Riemann sheet, i.e., the surface contained between the branch cuts; which can be done by replacing $\sqrt{\dots}$ with $-\sqrt{\dots}$ in $\Sigma_e(z)$ [Eq. (5.39)]. This gives rise to the appearance of complex poles within the energy band (i.e., poles with $|\mathrm{Re}\{z\}| < 2J$ and $\mathrm{Im}\{z\} \leq 0$), which are responsible for the spontaneous emission of the atom into the bath when $\Delta \in [-2J, 2J]$.

Bound states in the continuum

As found in Paper B, certain configurations of GAs suppress the imaginary part of these poles, thus suppressing the spontaneous emission into the bath. While complex poles lead to unstable states that relax into the bath, these real poles lead to the so-called *bound states in the continuum*[2] (BICs) [180–183], where

[2]We did not actually use the term *bound state in the continuum* in Paper B, as we were not aware of the concept at the time. It took further studies of giant atoms in structured environments to realize, in retrospect, that what we had referred to as *real poles* and *trapped excitation* where the cause and consequence of BICs. The terminology was introduced in Paper C.

excitations get trapped by the atom and by the cavities between the coupling points. In structured environments, this is a feature unique to GAs caused by destructive interference between their coupling points, and we refer to the geometries that allow it as *decoherence-free* or *perfectly subradiant*.

We remark that, while it may be tempting to refer to the BICs as "dark states" (or "perfectly subradiant states"), we have refrained from doing so in this thesis and the appended papers. Certainly, a dark state is, by definition, perfectly subradiant (see Sec. 4.4.2) and this is an established nomenclature in the quantum-optics literature; but the terminology becomes more intricate in the case of GAs. While dark states for small (and giant) atoms are specific states that decouple from the bath for a certain arrangement of the coupling points, decoherence-free geometries make *all* states dark. Now, one could argue that the limited definition of a dark state is as such because, in quantum optics, we have historically considered all atoms to be small, and that the definition should also be extended to non-radiative giant atoms. But for the sake of avoiding confusions, we refrain from using the term "dark" in this context, and only allude to the fact that the atoms do not radiate to the bath by using the term *decoherence-free* or *perfectly subradiant GA / configuration / geometry* (not state).

Now, by chaining two (or more) braided GAs in these decoherence-free geometries we can engineer DFI, as described in Sec. 4.4.2. We noted before that this interaction bears some resemblance to the interaction through overlapping BOCs, however, the interaction mechanism in the continuum is not quite the same. For DFI to take place, each of the GAs need to be perfectly subradiant and have at least one of their coupling points in a cavity populated by a BIC associated with the other atom—this is only achieved in the braided configuration. What is more, in this case, we can understand DFI as the two-atom analogue of *oscillating BICs* [184–189]. The latter have been shown to appear in GAs with three or more coupling points to a the waveguide, where multiple BIC solutions coexist and give rise to dynamic oscillations. Here, the multiplicity of BICs does not come from the multiplicity of coupling points, but instead, from the multiplicity of atoms.

5.6.4 Sum of contributions

With the modifications to the integration contour γ and the analytic continuation of $G_e(z)$ into the second Riemann sheet, we can use the residue theorem to calculate the probability amplitude $C_e(t)$ [Eq. (5.41)] as a sum of the different contributions [62]:

$$C_e(t) = \sum_{\alpha \in \substack{\text{branch} \\ \text{cuts}}} C_e(t)\Big|_\alpha + \sum_{\beta \in \text{poles}} \text{Res}(G_e, z_\beta) e^{-iz_\beta t}, \tag{5.43}$$

where $C_e(t)\big|_\alpha$ has the form of Eq. (5.41) and $\text{Res}(G_e, z_\beta)$ is the residue of the real and unstable poles that we obtain through the residue theorem and that

gives the overlap of the initial wavefunction with the poles, i.e.,

$$\mathrm{Res}(G_e, z_\beta) = \left.\frac{1}{1-\partial_z \Sigma_e(z)}\right|_{z=z_\beta}. \tag{5.44}$$

In particular, the contribution of the detour around the branch cuts to Eq. (5.43) can be written as

$$\begin{aligned}
C_e(t)\Big|_{\mathrm{UBC}} &= -\frac{1}{2\pi i}\int_{-\infty}^{0} G_e(2J+iy)e^{-i(2J+iy)t}\,dy \\
&\quad -\frac{1}{2\pi i}\int_{0}^{-\infty} G_e^{\mathrm{2RS}}(2J+iy)e^{-i(2J+iy)t}\,dy, \\
C_e(t)\Big|_{\mathrm{LBC}} &= -\frac{1}{2\pi i}\int_{-\infty}^{0} G_e^{\mathrm{2RS}}(-2J+iy)e^{-i(-2J+iy)t}\,dy \\
&\quad -\frac{1}{2\pi i}\int_{0}^{-\infty} G_e(-2J+iy)e^{-i(-2J+iy)t}\,dy,
\end{aligned} \tag{5.45}$$

where UBC and LBC denote upper and lower branch cut, respectively, and the superscript 2RS stands for second Riemann sheet.

Finally, we note that the poles and the branch-cut integrals can be solved numerically, thus allowing us to simulate the exact dynamics of the atom through Eq. (5.43).

5.7 Example: a giant atom coupled to a 2D structured lattice

Let us now reproduce the previous example for the simplest setup in Paper C, shown in Fig. 5.3: a giant atom with four connection points coupled to a 2D square lattice. We model the total Hamiltonian of the setup as the sum of the bare and interaction Hamiltonians, $H = H_0 + H_{\mathrm{int}}$, with

$$H_0 = \Delta\sigma^+\sigma^- + \sum_{\vec{k}} \omega(\vec{k}) a_{\vec{k}}^\dagger a_{\vec{k}}, \tag{5.46}$$

$$H_{\mathrm{int}} = \sum_{p=1}^{4} \frac{g_p}{N} \sum_{\vec{k}} \left(e^{-i\vec{k}\cdot\vec{n}_p} a_{\vec{k}}\sigma^+ + \mathrm{H.c.} \right), \tag{5.47}$$

where Δ is the detuning of the atom with respect to the bath frequency, $\sigma^\pm$ denote the atomic ladder operators, $a_{\vec{k}}^\dagger, a_{\vec{k}}$ are the creation and annihilation operators of the cavity modes, $\omega(\vec{k})$ is given by the dispersion relation from Eq. (2.5), g_p is the coupling strength at the p-th connection point, $N \times N$ is the number of coupled cavities forming the bath, and $\vec{n}_p = (n_x, n_y)_p$ with $n_x, n_y \in [0, N-1]$ denotes the position of the p-th coupling point. In the same

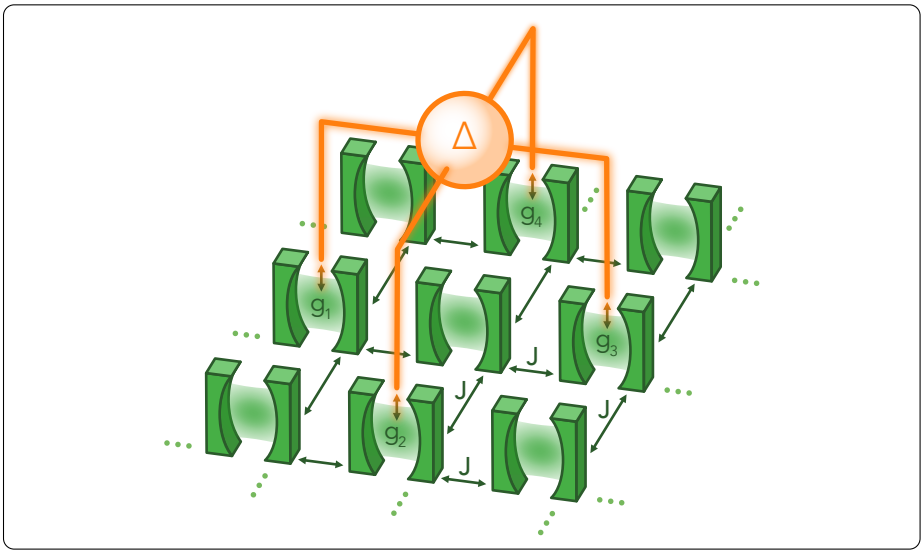

Figure 5.3: A giant atom with four connection points coupled to a 2D square lattice. Figure adapted from Paper C.

way as we did in the 1D example, we have applied the RWA directly on the Hamiltonian, which requires that the atomic and bath resonant frequencies are much larger than the coupling strength, and, as explained in Sec. 3.2.1, will not yield an accurate value of the Lamb shifts.

In the single-excitation subspace, the eigenstates of the bare Hamiltonian H_0 are $|e\rangle := |e,0\rangle$ and $|\vec{k}\rangle := |g,\vec{k}\rangle$, for $\vec{k} = (k_x, k_y)$ and $k_x, k_y \in \{-\pi, \ldots, \pi - \frac{2\pi}{N}\}$. The interaction term H_{int} couples these atomic and photonic subspaces $\{|e\rangle\}$ and $\{|\vec{k}\rangle\}$ to one another. This means that we can define $P = |e\rangle\langle e|$ and its complement $Q = \sum_{\vec{k}} |\vec{k}\rangle\langle\vec{k}|$, and write [similarly to Eq. (5.32)] the self-energy of the atom $\Sigma_e(z) = \langle e|\Sigma(z)|e\rangle$ as follows:

$$\begin{aligned}\Sigma_e(z) =& \cancelto{0}{\langle e|H_{\text{int}}|e\rangle} + \sum_{\vec{k}} \langle e|\, H_{\text{int}} \frac{|\vec{k}\rangle\langle\vec{k}|}{z - H_0} H_{\text{int}}\, |e\rangle \\ =& \frac{1}{N^2} \sum_{\vec{k}} \frac{\left(\sum_p^4 g_p e^{-i\vec{k}\cdot\vec{n_p}}\right)\left(\sum_q^4 g_q^* e^{i\vec{k}\cdot\vec{n_q}}\right)}{z - \omega(\vec{k})}. \end{aligned} \tag{5.48}$$

Henceforth, we use the dispersion relation $\omega(\vec{k}) = -2J[\cos(k_x) + \cos(k_y)]$ introduced in Eq. (2.5), and that the distance vector between two different coupling

points is $\Delta\vec{n}$. For simplicity, let us also assume that $g_p = g_q = g \in \mathbb{R}$. Then,

$$\Sigma_e(z) = \frac{g^2}{N^2} \sum_{\vec{k}} \frac{4 + 2\sum_{\Delta\vec{n}} \cos\left(\vec{k}\cdot\Delta\vec{n}\right)}{z + 2J[\cos(k_x) + \cos(k_y)]}. \tag{5.49}$$

In the continuum limit, i.e., when $N \to \infty$, the sum over $\vec{k}$ becomes a double integral: $\sum_{\vec{k}} \left(\frac{2\pi}{N}\right)^2 \to \iint_{\vec{k}} \mathrm{d}^2\vec{k}$. Therefore, we can write the self-energy as

$$\Sigma_e(z) \to \frac{g^2}{(2\pi)^2} \iint_{-\pi}^{\pi} \mathrm{d}^2\vec{k}\, \frac{4 + 2\sum_{\Delta\vec{n}} \cos\left(\vec{k}\cdot\Delta\vec{n}\right)}{z + 2J[\cos(k_x) + \cos(k_y)]} \tag{5.50}$$

$$= 4 \underbrace{\frac{g^2}{(2\pi)^2} \iint_{-\pi}^{\pi} \mathrm{d}^2\vec{k}\, \frac{1}{z + 2J[\cos(k_x) + \cos(k_y)]}}_{\Sigma_{\mathrm{SA}}(z)}$$

$$+ 2\sum_{\Delta\vec{n}} \underbrace{\frac{g^2}{(2\pi)^2} \iint_{-\pi}^{\pi} \mathrm{d}^2\vec{k}\, \frac{\cos\left(\vec{k}\cdot\Delta\vec{n}\right)}{z + 2J[\cos(k_x) + \cos(k_y)]}}_{\Sigma_{\Delta\vec{n}}(z)}, \tag{5.51}$$

where the self-energy of a small atom $\Sigma_{\mathrm{SA}}(z)$ is calculated from the particular case of a GA [Eq. (5.50)] with only one coupling point (and therefore $\Delta\vec{n} = 0$); and $\Sigma_{\Delta\vec{n}}(z)$ denotes the contribution to the self-energy from the interference between coupling points that are spaced by $\Delta\vec{n}$.

For example, let us consider that our GA is centered at some arbitrary point in the lattice that we take as the origin $\left[\begin{smallmatrix}0\\0\end{smallmatrix}\right]$, and that its four coupling points draw a diamond around it, i.e., they are placed at coordinates $\left[\begin{smallmatrix}0\\1\end{smallmatrix}\right]$, $\left[\begin{smallmatrix}0\\-1\end{smallmatrix}\right]$, $\left[\begin{smallmatrix}1\\0\end{smallmatrix}\right]$, $\left[\begin{smallmatrix}-1\\0\end{smallmatrix}\right]$—as is the case in Fig. 5.3. Because there are four pairs of points spaced by $\Delta\vec{n} = \left[\begin{smallmatrix}1\\1\end{smallmatrix}\right]$ and two pairs spaced by $\Delta\vec{n} = \left[\begin{smallmatrix}2\\0\end{smallmatrix}\right]$ (disregarding rotations), the self-energy of the atom in such a case, according to Eq. (5.51), is

$$\Sigma_{\diamondsuit}(z) = 4\Sigma_{\mathrm{SA}}(z) + 2\left[4\Sigma_{\left[\begin{smallmatrix}1\\1\end{smallmatrix}\right]}(z) + 2\Sigma_{\left[\begin{smallmatrix}2\\0\end{smallmatrix}\right]}(z)\right]. \tag{5.52}$$

As shown in Ref. [190], it is convenient to rewrite Σ_{SA} and $\Sigma_{\Delta\vec{n}}$ in a different basis, such that instead of integrating in the $k_{x,y}$ horizontal and vertical directions, we integrate in the $q_\pm$ diagonal directions. For that, we apply the following change of variables:

$$q_\pm = \frac{1}{2}(k_x \pm k_y), \tag{5.53}$$

$$\Delta n_\pm = \Delta n_x \pm \Delta n_y. \tag{5.54}$$

Note that this implies $\mathrm{d}^2\vec{q} = \frac{1}{2}\mathrm{d}^2\vec{k}$ and that the integration area in the $k_{x,y}$ direction is twice the area of that in the $q_\pm$ direction. Using the trigonometric

expressions $\cos(\alpha \pm \beta) = \cos(\alpha)\cos(\beta) \mp \sin(\alpha)\sin(\beta)$ and $\cos(2\alpha) = 2\cos^2(\alpha) - 1 = 1 - 2\sin^2(\alpha)$, we can show that

$$\begin{aligned}\Sigma_{\mathrm{SA}}(z) &= \frac{g^2}{(2\pi)^2}\iint_{-\pi}^{\pi} \mathrm{d}^2\vec{k}\,\frac{1}{z + 2J[\cos(k_x) + \cos(k_y)]} \\ &= \frac{g^2}{(2\pi)^2}\iint_{-\pi}^{\pi} \mathrm{d}^2\vec{q}\,\frac{1}{z + 4J\cos(q_+)\cos(q_-)}, \end{aligned} \tag{5.55}$$

$$\begin{aligned}\Sigma_{\Delta\vec{n}}(z) &= \frac{g^2}{(2\pi)^2}\iint_{-\pi}^{\pi} \mathrm{d}^2\vec{k}\,\frac{\cos\left(\vec{k}\Delta\vec{n}\right)}{z + 2J[\cos(k_x) + \cos(k_y)]} \\ &= \frac{g^2}{(2\pi)^2}\iint_{-\pi}^{\pi} \mathrm{d}^2\vec{q}\,\frac{\cos(q_+\Delta n_+)\cos(q_-\Delta n_-)}{z + 4J\cos(q_+)\cos(q_-)}. \end{aligned} \tag{5.56}$$

In this basis, the expressions above can be integrated by parts and rewritten in a compact way in terms of elliptic integrals [190]. For instance, from Ref. [62]:

$$\Sigma_{\mathrm{SA}}(z) = \frac{2g^2}{\pi z}K[m(z)], \tag{5.57}$$

$$\Sigma_{\left[\begin{smallmatrix}1\\1\end{smallmatrix}\right]}(z) = \frac{2g^2}{\pi z}\left\{\left[\frac{2}{m(z)} - 1\right]K[m(z)] - \frac{2}{m(z)}E[m(z)]\right\}, \tag{5.58}$$

$$\Sigma_{\left[\begin{smallmatrix}1\\0\end{smallmatrix}\right]}(z) = \frac{g^2}{4J} - \frac{g^2}{2\pi J}K[m(z)], \tag{5.59}$$

where

$$m(z) = \left(\frac{4J}{z}\right)^2, \tag{5.60}$$

and K and E are the complete elliptical integrals of the first and second kind, respectively:

$$K(m) = \int_0^{\pi/2}\frac{\mathrm{d}\phi}{\sqrt{1 - m\sin^2(\phi)}}, \tag{5.61}$$

$$E(m) = \int_0^{\pi/2}\mathrm{d}\phi\sqrt{1 - m\sin^2(\phi)}. \tag{5.62}$$

Finally, using the recursive formulas in Ref. [190], we can obtain the self-energy at any arbitrary site. For example, using

$$\Sigma_{\left[\begin{smallmatrix}m+1\\0\end{smallmatrix}\right]}(z) = -\frac{1}{2J}\left[2z\,\Sigma_{\left[\begin{smallmatrix}m\\0\end{smallmatrix}\right]}(z) + 2J\,\Sigma_{\left[\begin{smallmatrix}m-1\\0\end{smallmatrix}\right]}(z) + 4J\,\Sigma_{\left[\begin{smallmatrix}m\\1\end{smallmatrix}\right]}(z)\right], \tag{5.63}$$

together with Eqs. (5.57)–(5.58), we can show that

$$\begin{aligned}\Sigma_{\left[\begin{smallmatrix}2\\0\end{smallmatrix}\right]}(z) &= -\frac{z}{J}\Sigma_{\left[\begin{smallmatrix}1\\0\end{smallmatrix}\right]}(z) - \underbrace{\Sigma_{\left[\begin{smallmatrix}0\\0\end{smallmatrix}\right]}(z)}_{\Sigma_{\mathrm{SA}}(z)} - 2\Sigma_{\left[\begin{smallmatrix}1\\1\end{smallmatrix}\right]}(z) \\ &= \frac{2g^2}{\pi z}\left(K[m(z)] + \frac{4}{m(z)}\left\{E[m(z)] - \frac{\pi}{2}\right\}\right). \end{aligned} \tag{5.64}$$

Going back to the diamond configuration [Eq. (5.52)], we have now derived an expression for the self-energy that is integrable in the first Riemann sheet, i.e., for $|z| > 4J$. Then, according to Eq. (5.18), the resolvent-operator element corresponding to the excited state of the atom is

$$G_e(z) = \frac{1}{z - \Delta - \Sigma_e(z)}, \tag{5.65}$$

with Δ the atom-cavity detuning. Lastly, we can express the probability amplitude of an initially excited GA, for $t > 0$, as follows:

$$C_e(t) = -\frac{1}{2\pi i} \int_{-\infty}^{\infty} G_e(E + i0^+) e^{-iEt}\, dE, \tag{5.66}$$

i.e., as the Fourier transform of the retarded Green's function G_e.

5.7.1 Contributions to the probability amplitude

Similarly to the example in the 1D coupled-cavity array, the contour in Eq. (5.66) can be extended to the closed lower-half plane and modified to exclude branch points, as shown in Fig. 5.4. In the same way as in 1D, the energy dispersion of the 2D square lattice introduces branch cuts that we can place at the band edges, making the contour detour around them. However, an additional branch point

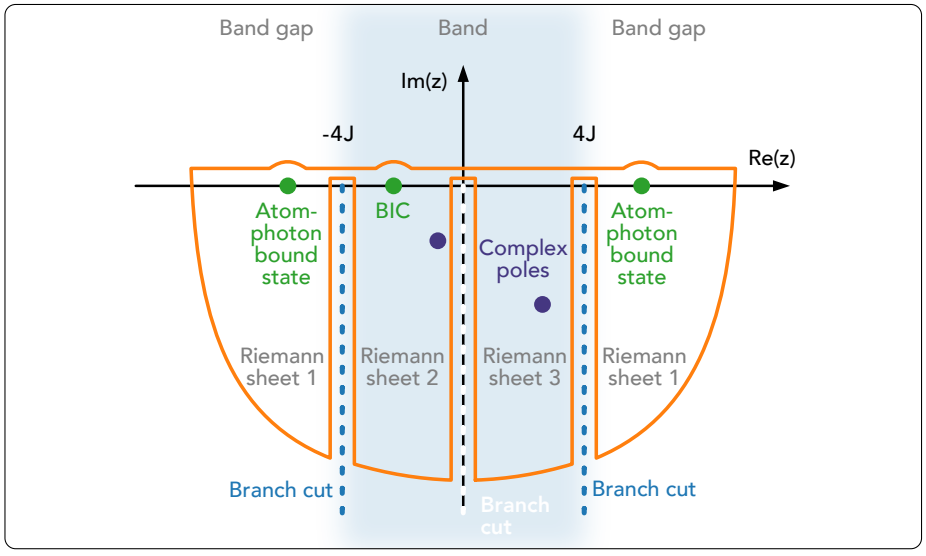

Figure 5.4: Contour of the integral in Eq. (5.66), with contributions from the poles of the Green's function [Eq. (5.65)], as well as the branch cuts at the band edges and at the middle of the band.

that is not present in the 1D case arises in the middle of the band due to the additional van Hove singularity described in Sec. 2.2.2. In this way, the branch cuts divide the surface enclosed by the contour into three Riemann sheets: the first Riemann sheet corresponds to the energy values outside the band ($|z| > 4J$) and contains real poles of the Green's function [Eq. (5.65)], which are associated to the atom-photon bound states; while the second ($-4J < z < 0$) and third ($0 < z < 4J$) Riemann sheets extend over the band and contain the complex poles of the Green's function, which are responsible for the spontaneous emission into the bath. As mentioned in the 1D example, the poles in the second and third Riemann sheets that are real—which only occurs for GAs—are responsible for the existence of the BICs.

Note that the singularities that give rise to the branch cuts not only affect the contour of the probability-amplitude integral, but also limit the domain of definition of the self-energy. In fact, the analytical continuation of the expressions in Eqs. (5.57)–(5.59) and Eq. (5.64) into the second [II] and third [III] Riemann sheets can be obtained by transforming the elliptic integrals in the following way [62]:

$$K^{\mathrm{II[III]}}(m) = K(m) \pm 2iK(1-m), \tag{5.67}$$

$$E^{\mathrm{II[III]}}(m) = E(m) \pm 2i[K(1-m) - E(1-m)]. \tag{5.68}$$

Finally, we have all the ingredients to calculate the probability amplitude $C_e(t)$ as a sum of the different contributions.

Comparing the 1D and 2D cases, we note the increasing analytical complexity of the formalism with the dimensionality of the bath. Similarly, the complexity increases when going beyond the single-excitation regime and the two-level approximation. This is the reason why, in Paper D, where we consider three-level GAs coupled to a 1D structured waveguide in the two-photon subspace, we resort to numerical simulations over analytical methods.

5.8 Non-Markovian effects

Unlike in Chapter 3 and Chapter 4 for continuous waveguides, here we have not made the Markovian approximation at any point in our derivation, thus allowing us to discern non-Markovian behaviors when computing the time evolution of the atoms.

5.8.1 Unstable poles and branch cuts

In the previous section, we mentioned that the unstable poles of the resolvent are responsible for the spontaneous emission of the atoms into the bath when the atoms are tuned to the band.

Within the Markovian approximation, we assume that the coupling g is sufficiently weak such that $\Sigma_e(E + i0^+) \approx \Sigma_e(\Delta)$ [62]. Then, $C_e(t)$ can be easily

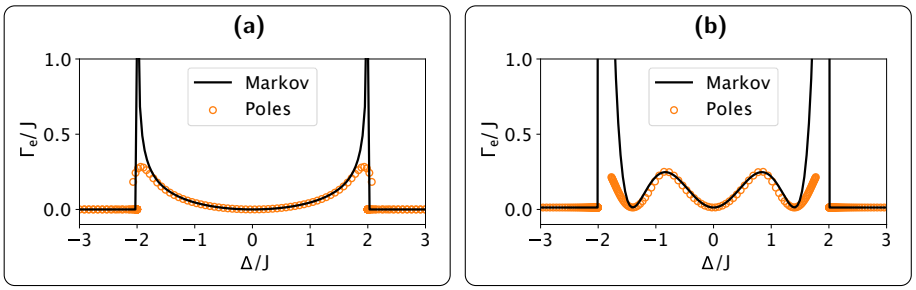

Figure 5.5: Atomic decay rate as a function of detuning for (a) a GA with two coupling points, of coupling strength $g/J = 0.2$ each, and spaced by $d = 2$ cavities; and (b) a GA with four coupling points, of coupling strength $g/J = 0.4$ each, and spaced by $d = 2$ cavities. The black solid line corresponds to the Markov prediction from Eq. (5.69), while the orange markers are the poles of the Green's function [Eq. (5.40)]. Within the band ($\Delta/J \in [-2, 2]$), we find as many decoherence-free points as the number of coupling points minus one. Figures adapted from Paper B.

solved by applying the residue theorem around the pole $z = \Delta + \Sigma_e(\Delta)$ to yield $C_e(t) \approx \exp\{-i[\Delta + \Sigma_e(\Delta)]t\}$. It then follows that we can split $\Sigma_e(\Delta)$ into its real and imaginary parts, and identify the frequency-dependent Lamb shift $\delta_e(\Delta) = \mathrm{Re}\{\Sigma_e(\Delta)\}$ and the decay rate $\Gamma_e(\Delta) = -2\,\mathrm{Im}\{\Sigma_e(\Delta)\}$ as follows [191]:

$$\Sigma_e(\Delta) = \delta_e(\Delta) - i\frac{\Gamma_e(\Delta)}{2}. \tag{5.69}$$

Moreover, using the same approximation for $C_k(t)$ shows that the modes dominating the emission will be those satisfying $\omega(k) \approx \Delta$ [62].

Now, solving the exact pole equation of the resolvent as we outlined in Sec. 5.5 for 1D [Eq. (5.40)] and Sec. 5.7 for 2D [Eq. (5.65)] allows us to go beyond the Markov approximation and obtain a more accurate profile of the decay rate $\Gamma_e(\Delta)$. In fact, we can depict such a profile by plotting both $\Gamma_e(\Delta) = -2\,\mathrm{Im}\{\Sigma_e(\Delta)\}$ (Markov) and $\Gamma_e(\Delta) = -2\,\mathrm{Im}\{z\}$ with z being the poles (beyond Markov), and clearly illustrate where the Markovian approximation breaks down. This is what we did in Paper B, and we showed that, as expected, the middle of the band falls in the Markovian regime, whereas the approximation breaks down close to the band edges (see Fig. 5.5).

Around the band edges, the branch-cut contributions to the probability amplitude are also more prominent than at the band center [62, 192]. However, they never take prevalence over the contributions from the poles, and they are only relevant at the initial time of decay (small t), quickly decaying due to the exponential in Eq. (5.45). Therefore, although we include these contributions in both analytical and numerical results of Papers B and C, the branch cuts are not responsible for any of the main phenomena studied in those manuscripts.

5.8.2 Time delay

Another consequence of solving the atomic dynamics exactly is that we observe time-delay effects, which arise from the time it takes an excitation to travel between two points through the bath. These become relevant in processes governed by interference effects, such as subradiance and DFI (see Sec. 4.4).

For instance, in Papers B and C, we show that perfect subradiance is deteriorated by relaxation to the bath during the time it takes for the interference to build up, i.e., the time it takes for the excitation to travel between coupling points. The deterioration grows exponentially with increasing distance between coupling points. Similarly, DFI between two braided giant atoms is also worsened by the delay of the interference, in addition to an exponential deterioration over time caused by the small imaginary part of the unstable poles that sustain the interaction (i.e., the BICs that give rise to DFI become quasi-BICs).

Interestingly, one could think about a giant atom with non-negligible time delay between its coupling points as a new regime in atomic size. We could then distinguish between a small atom with $r \ll \lambda$, a Markovian giant atom with $r \simeq \lambda$, and a non-Markovian giant atom with $r \gg \lambda$. In fact, in the first-ever conference on giant emitters held in Zurich in 2023, the question was posed: how should we call the latter regime? A *gigantic* atom? A *supergiant* atom? Or maybe *giant* should be demoted to *large* instead[3]? Since it is probably a decade too late to rename a giant atom, the Markovian / non-Markovian denomination seems here to stay.

5.8.3 Fractional and other anomalous decay

As mentioned in Sec. 2.2.2, atom-photon bound states (real poles of the resolvent) cause fractional decay at the band edges [53–56]. This occurs because the spontaneous emission of the atom is counteracted by the hybridization with the bound state, prompting an initial exponential decay with a few beatings that stabilizes to a nonzero value of the population ($|C_e(t \to \infty)|^2 \neq 0$).

Similarly, other anomalous decay takes place due to the existence of other poles. As we described in Sec. 5.8.1, in the Markovian regime, the atomic population of each atom is dominated by a single pole. However, with increasing distance between coupling points and increasing detuning from the middle of the band, more poles appear and, as their contributions become relevant, the population exhibits beatings and other anomalous behavior. This can be understood through Eq. (5.43), where the atomic probability amplitudes become a sum of exponential functions with different frequencies and weights. In fact, this is the very reason why DFI is destroyed close to the band edges, as we showed in Paper B.

[3]Actually, in Swedish (the native language of the majority of authors in the original giant-atom papers [14, 19]), a giant atom is called *stor atom*, which literally translates to "large atom". While less flashy, the name fits perfectly within the modest Swedish culture. Although if you ask me, an even better alternative would have been *lagom atom*, which roughly translates to "an atom that is not too little and not too large—it is just the right size".

6 Paper overview

In this chapter, we give an overview of the five papers (three of them appended) upon which this thesis is based.

6.1 Paper A – Chiral quantum optics with giant atoms

In Paper A, we studied the interaction between atoms chirally coupled to a continuous open waveguide (see Sec. 4.1 for more on chiral interfaces). We began by considering simple setups: two small atoms and two giant atoms with two coupling points each, in all the possible configurations of coupling points (separate, nested, and braided—see Fig. 2.2). For simplicity, we first assumed all points had the same coupling strength γ, but that it was different in each propagation direction, i.e., $\gamma_R \neq \gamma_L$.

By using the SLH formalism, we derived a master equation to model the atomic dynamics in the same way as we exemplified in Sec. 4.3.

We showed that braided giant atoms can interact without decohering regardless of the chirality of their coupling to the waveguide, and we derived the phase-shift conditions for that to occur, as explained in Sec. 4.4.2. With this, we demonstrated that the most robust way we know of protecting against decoherence was also robust against variations in directionality.

In the spirit of searching for ways to protect the atoms against decoherence, we also investigated dark states. We derived conditions for the existence of such states in undriven atomic ensembles, as outlined in Sec. 4.4.2. We showed that, unlike small atoms, nested giant atoms allow for perfect subradiance regardless of the chirality of their coupling.

We also went further and looked at the effects of coherently driving the system, since it is known [149, 151] that this is a way to get around the absence of dark states for small atoms in chiral settings. We showed that, when a drive is considered, two giant atoms evolve to a dynamic equilibrium between drive and dissipation, where the scattered photons from the first atom interfere destructively with those from the second atom. This is the same behavior as for two small atoms, except that we showed giant atoms can populate these

driven-dissipative dark states faster—a feature that prompted us to design the experiment in Paper E.

Finally, we generalized all results to an arbitrary number of atoms with an arbitrary number of coupling points, and presented interesting configurations that could be used to harness DFI and dark states.

6.2 Paper B – Interaction between giant atoms in a one-dimensional structured environment

In Paper B, we studied two-level giant atoms coupled to a 1D structured waveguide, modeled as an array of evenly spaced coupled cavities with nearest-neighbor interaction, and with the dispersion relation introduced in Sec. 2.2.2 [Eq. (2.3)].

First, we considered a single giant atom, and from the system-bath Hamiltonian, we characterized the energy spectrum of the total system and the wavefunction of the atom-photon bound states. Then, we looked into the dynamics of the atom, both through numerical simulations and through complex-analysis techniques, as detailed in Sec. 5.5. In particular, we showed how the interference between coupling points of the atom affects its relaxation, and how, as depicted in Fig. 5.5, the poles of the resolvent provide a much more accurate description of the decay rate than the Markovian prediction does close to the band edges. We related those results to the time evolution of the atomic population, when the atom is tuned to different regions of the band structure.

With a single atom fully characterized, we modeled the interaction between two giant atoms and analyzed the differences between tuning the atoms to the continuum and to the band gap. Within the band, we showed that DFI is best in the continuous-waveguide case, i.e., in the middle of the band, but also possible for other detunings. We also demonstrated, through different metrics, how DFI deteriorates exponentially with increasing distance between the coupling points. By mapping the DFI mechanism to the singularities of the resolvent introduced in Sec. 5.2, we dissected the dynamics into different contributions and showed the significance of time delay and other non-Markovian effects. Lastly, we identified DFI as the multiple-giant-atom analogue of subradiance.

In the band gap, we showed that GAs can interact through the overlap of bound states in the same way small atoms do. That raised the question: what kind of interaction is best—giant atoms inside the band (DFI), giant atoms outside the band (bound-state overlap), or small atoms outside the band (bound-state overlap)? We concluded that the answer depends on three parameters: the coupling strength, the distance between coupling points, and the detuning of the atoms from the cavities. In particular, giant atoms can provide an advantage over small atoms in some regions of the parameter space, for instance, when restricting the maximum coupling strength achievable per coupling point. We

also found that there is a trade-off between good population exchanges and high interaction rates. All in all, while for some parameters giant atoms can interact more strongly and over longer distances than small atoms, the preference of a giant-atom design over a small-atom design should depend on the experimental constraints and the intended application.

6.3 Paper C – Avoiding decoherence with giant atoms in a two-dimensional structured environment

In Paper C, we conducted a detailed theoretical study of GAs in a 2D structured environment. We focused on the case when this environment is a square lattice of cavities which, as explained in Sec. 2.2.2, leads to band gaps and an energy band that comes with an anisotropic energy dispersion at its center. In this setting, we showed how GAs can avoid relaxing into the environment.

For a single GA with a transition frequency in the center of the band, we found that it can display perfect subradiance, i.e., completely suppressed emission of energy into the environment, if the atom couples to the bath through at least four cavities. This suppression is because the propagation of excitations in the environment is restricted to be diagonal at the band center: with four coupling points it becomes possible to cancel emission along these four propagation directions through destructive interference between the emissions from pairs of coupling points. We also showed how such perfect subradiance can be achieved with more coupling points.

For multiple GAs, we showed that DFI, previously only demonstrated in 1D environments, can also be realized in 2D. More specifically, we showed that this DFI can take place if the individual atoms have their coupling points arranged to be subradiant and each atom has some (but not all) of its coupling points enclosed by coupling points from the other atom. This setup constitutes a generalization of the braided configuration required for GAs in 1D. We further showed how this DFI for GAs in 2D can be extended to more atoms, forming effective high-connectivity (even all-to-all coupling) lattices of atoms connected through DFI.

As explained in Sec. 5.6.3, the results we found for both single and multiple GAs can be understood as manifestations of bound states in the continuum (BICs). For a single GA in a subradiant configuration, an initial excitation in the atom mostly remains there. A small amount of energy leaks into the environment outside the atom before the destructive interference between emissions from the different coupling points kicks in, but about half that energy remains in the photonic part of a BIC formed in-between the coupling points of the atom. For multiple GAs, DFI between pairs of them is only possible when some coupling point(s) of each atom in the pair are placed in locations that contain a part of the BIC associated with the other atom.

We note that these results were enabled by nontrivial extensions of the resolvent formalism (see Sec. 5.7) and numerical methods previously employed to study small atoms in 2D structured environments [62]. Through these extensions, we were able to obtain analytical expressions for the steady-state populations of GAs and their BICs, and perform numerical simulations of how the atomic and photonic populations evolve in time for both single and multiple GAs. For DFI between a pair of GAs, we observed that both the atomic populations and the photonic parts of the BIC populations undergo Rabi oscillations when one of the atoms is initialized in its excited state and the rest of the system is initialized in its ground state.

6.4 Paper D – Two-photon quantum gates with giant atoms in structured waveguides

In Paper D, we extended the setup from Paper B (GAs coupled to a 1D structured waveguide) to the two-photon subspace with three-level GAs. Taking a more applied approach than in Paper B, we looked at how to engineer DFI to perform two-qubit entangling gates such as the iSWAP and the CZ (see Sec. 4.5). Compared to previous works on continuous waveguides [20, 172], the structured-waveguide platform allowed us to study how non-Markovianities degrade the gates, and how to avoid these undesired effects.

Because this work builds on the existing knowledge from Papers B and C, where the interference and interaction mechanisms were well studied, we deemed it was not necessary to use the resolvent formalism from Chapter 5. Instead, we used exact numerical simulations involving the spectral decomposition of the Hamiltonian to compute the system's dynamics. This method is not free of hurdles, since it becomes computationally more expensive with the increasing dimension of the Hilbert space which, in turn, increases with the number of photons, atoms, and cavities.

Compared to the CZ gate in continuous waveguides, we found that we can create a CZ gate with one less coupling point, by engineering the decoherence-free frequencies not involved in DFI to fall in the band gap. However, this makes the DFI frequency fall close to the band edges, where non-Markovian effects are most prominent (see Fig. 5.5), which leads to a very poor interaction. To circumvent these effects, an additional coupling point is needed, which makes all decoherence-free frequencies fall in the continuum, and away from the band edges. By increasing the coupling strength of the middle point, the decoherence-free frequencies may be tuned even further away from the band edges.

6.5 Paper E – Driven-dissipative entanglement with separate giant atoms

Paper E is the experimental demonstration of one of the results from Paper A: that GAs can populate driven-dissipative dark states faster than small atoms. In the experiment, the atoms are realized by transmon qubits capacitively coupled to a meandering transmission line, as shown in Fig. 2.5(b). While in Paper A we considered the atom-waveguide coupling to be generally chiral, in Paper E, we took it to be bidirectional ($\gamma_R = \gamma_L$ for all coupling points), which is significantly easier to fabricate.

The setup is formed by two separate giant atoms with two coupling points each, with phase shifts $\phi_1 = \phi_3 = 4\pi$ between the coupling points of the same atom, and a phase $\phi_2 = \pi$ between the atoms. In this configuration, there exists a driven-dissipative dark state $|D_T\rangle$ [Eq. (4.23)] that approaches the maximally entangled triplet state $|T\rangle$ [Eq. (4.22)] for strong drives. In fact, we choose the design parameters to maximize the entanglement between the qubits, which is done by calculating both the fidelity to the triplet state and the concurrence, as described in Sec. 3.1.1. Note that, because the drive required to maximize entanglement is quite strong, the two-level approximation breaks down, and the third level needs to be considered [Eq. (2.8)].

Once the dark state has been populated, we measure the entanglement by detuning the atoms to their decoherence-free frequencies (which corresponds to $\phi_1 = \phi_3 = 3\pi$) and performing quantum state tomography through the readout resonators coupled to the giant atoms [see Fig. 2.5(b)]. This is a major advantage of the giant-atom setup with respect to similar experiments done with small atoms [193], where the qubits do not have a decoherence-free frequency, and thus readout needs to be done at the end of the waveguide, through field emission tomography.

Such methods for easily and quickly generating entanglement between distant qubits are much sought after for quantum communication and distributed quantum computing, since these applications can use the entanglement to transfer quantum information or perform operations involving several modules of a quantum computer.

7 Conclusion and outlook

That's all folks!

Porky Pig

In this thesis, we have explored giant atoms as potential resources for preventing decoherence in quantum-technology applications. A key insight of this work has been establishing the relation between the concepts of subradiance, dark states, decoherence-free interaction, and bound states in and out of the continuum.

We did so by considering the coupling of giant atoms to environments that had not been explored in depth before (continuous waveguides with chiral coupling and structured baths), starting from a more idealistic and fundamental perspective on light-matter interactions and advancing towards more realistic setups and applications. For instance, in the first articles, we mostly worked in the single-photon subspace (Papers B and C) and considered the giant atoms to be two-level systems (Papers A, B, and C); while in later projects (Papers D and E), we went beyond those approximations into the two- and many-photon subspace, and considered the third level of the atoms. Moreover, throughout the different works, we transitioned from a more analytical approach (Papers A, B, C), to relying on numerical simulations (Papers C and D), to bringing the ideas to experiment (Paper E). In the latter, we went beyond the assumption that atoms couple exclusively to the environment we study, and added other sources of decoherence to our model, such as the effects of qubit dephasing and non-radiative decay.

This evolution, which unfolded very organically, could be further developed in the future by modeling, for example, the effect of losses in the waveguide, longer-range interactions between atoms (cross-talk) and cavities (beyond nearest-neighbor [105]), or richer band structures of the photonic baths [89, 103, 106, 194]. Another interesting avenue to explore could be to use giant atoms for the quantum simulation of more complex open quantum systems [195]. This pathway is attractive not only because giant atoms offer more possibilities for design, control, and tunability than small atoms do, but also because their interference effects can find parallels in a myriad of systems.

We highlight that, because this thesis—and more generally, all giant-atom

research—sits at the intersection of quantum optics, photonics, quantum electrodynamics (QED) and quantum computing, some parameters and physical phenomena receive different names in different fields (as evidenced by the countless footnotes in the dissertation), which hinders establishing links to related concepts. For this reason, further efforts to contextualize the physics presented here are necessary. For instance, bound states in the continuum are ubiquitous in different physical systems, and classified into several categories according to their nature [196, 197], but they are an emerging concept in the context of waveguide QED. Thus, to not reinvent the wheel, a relation should be drawn to the established nomenclature.

Bibliography

[1] J. P. Dowling and G. J. Milburn, "Quantum technology: The second quantum revolution", Philosophical Transactions of the Royal Society A: Mathematical, Physical and Engineering Sciences **361**, 1655–1674 (2003).

[2] I. Georgescu and F. Nori, "Quantum technologies: an old new story", Physics World **25**, 16–17 (2012).

[3] M. A. Nielsen and I. L. Chuang, *Quantum Computation and Quantum Information* (Cambridge University Press, 2010).

[4] I. M. Georgescu, S. Ashhab, and F. Nori, "Quantum simulation", Reviews of Modern Physics **86**, 153 (2014).

[5] N. Gisin and R. Thew, "Quantum Communication", Nature Photonics **1**, 165–171 (2007).

[6] C. L. Degen, F. Reinhard, and P. Cappellaro, "Quantum sensing", Reviews of Modern Physics **89**, 035002 (2017).

[7] A. S. Sheremet, M. I. Petrov, I. V. Iorsh, A. V. Poshakinskiy, and A. N. Poddubny, "Waveguide quantum electrodynamics: Collective radiance and photon-photon correlations", Rev. Mod. Phys. **95**, 015002 (2023).

[8] D. Leibfried, R. Blatt, C. Monroe, and D. Wineland, "Quantum dynamics of single trapped ions", Reviews of Modern Physics **75**, 281–324 (2003).

[9] S. Haroche, "Nobel lecture: Controlling photons in a box and exploring the quantum to classical boundary", Reviews of Modern Physics **85**, 1083–1102 (2013).

[10] D. Walls and G. J. Milburn, *Quantum Optics* (Springer Berlin, Heidelberg, 2008).

[11] R. Hanson, L. P. Kouwenhoven, J. R. Petta, S. Tarucha, and L. M. K. Vandersypen, "Spins in few-electron quantum dots", Reviews of Modern Physics **79**, 1217–1265 (2007).

[12] J. Q. You and F. Nori, "Atomic physics and quantum optics using superconducting circuits", Nature **474**, 589-597 (2011).

[13] X. Gu, A. F. Kockum, A. Miranowicz, Y.-X. Liu, and F. Nori, "Microwave photonics with superconducting quantum circuits", Physics Reports **718-719**, 1–102 (2017).

[14] M. V. Gustafsson, T. Aref, A. F. Kockum, M. K. Ekström, G. Johansson, and P. Delsing, "Propagating phonons coupled to an artificial atom", Science **346**, 207–211 (2014).

[15] J. Maurer and U. Keller, "Ionization in intense laser fields beyond the electric dipole approximation: concepts, methods, achievements and future directions", Journal of Physics B: Atomic, Molecular and Optical Physics **54**, 094001 (2021).

[16] N. H. List, J. Kauczor, T. Saue, H. J. A. Jensen, and P. Norman, "Beyond the electric-dipole approximation: A formulation and implementation of molecular response theory for the description of absorption of electromagnetic field radiation", The Journal of Chemical Physics **142**, 244111 (2015).

[17] J. Koch, T. M. Yu, J. Gambetta, A. A. Houck, D. I. Schuster, J. Majer, A. Blais, M. H. Devoret, S. M. Girvin, and R. J. Schoelkopf, "Charge-insensitive qubit design derived from the Cooper pair box", Physical Review A **76**, 042319 (2007).

[18] S. Datta, *Surface Acoustic Wave Devices* (Prentice-Hall, 1986).

[19] A. Frisk Kockum, P. Delsing, and G. Johansson, "Designing frequency-dependent relaxation rates and Lamb shifts for a giant artificial atom", Physical Review A **90**, 013837 (2014).

[20] B. Kannan, M. J. Ruckriegel, D. L. Campbell, A. Frisk Kockum, J. Braumüller, D. K. Kim, M. Kjaergaard, P. Krantz, A. Melville, B. M. Niedzielski, A. Vepsäläinen, R. Winik, J. L. Yoder, F. Nori, T. P. Orlando, S. Gustavsson, and W. D. Oliver, "Waveguide quantum electrodynamics with superconducting artificial giant atoms", Nature **583**, 775–779 (2020).

[21] D. Meschede, W. Jhe, and E. A. Hinds, "Radiative properties of atoms near a conducting plane: An old problem in a new light", Physical Review A **41**, 1587–1596 (1990).

[22] J. Eschner, C. Raab, F. Schmidt-Kaler, and R. Blatt, "Light interference from single atoms and their mirror images", Nature **413**, 495-498 (2001).

[23] U. Dorner and P. Zoller, "Laser-driven atoms in half-cavities", Physical Review A **66**, 023816 (2002).

[24] A. Beige, J. Pachos, and H. Walther, "Spontaneous emission of an atom in front of a mirror", Physical Review A **66**, 063801 (2002).

[25] M. A. Wilson, P. Bushev, J. Eschner, F. Schmidt-Kaler, C. Becher, R. Blatt, and U. Dorner, "Vacuum-field level shifts in a single trapped ion mediated by a single distant mirror", Physical Review Letters **91**, 213602 (2003).

[26] F. Dubin, D. Rotter, M. Mukherjee, C. Russo, J. Eschner, and R. Blatt, "Photon correlation versus interference of single-atom fluorescence in a half-cavity", Physical Review Letters **98**, 183003 (2007).

[27] H. Dong, Z. R. Gong, H. Ian, L. Zhou, and C. P. Sun, "Intrinsic cavity qed and emergent quasinormal modes for a single photon", Physical Review A **79**, 063847 (2009).

[28] K. Koshino and Y. Nakamura, "Control of the radiative level shift and linewidth of a superconducting artificial atom through a variable boundary condition", New Journal of Physics **14**, 043005 (2012).

[29] Y. Wang, J. Minář, G. Hétet, and V. Scarani, "Quantum memory with a single two-level atom in a half cavity", Physical Review A **85**, 013823 (2012).

[30] T. Tufarelli, F. Ciccarello, and M. S. Kim, "Dynamics of spontaneous emission in a single-end photonic waveguide", Physical Review A **87**, 013820 (2013).

[31] T. Shi, D. E. Chang, and J. I. Cirac, "Multiphoton-scattering theory and generalized master equations", Physical Review A **92**, 053834 (2015).

[32] I.-C. Hoi, A. F. Kockum, L. Tornberg, A. Pourkabirian, G. Johansson, P. Delsing, and C. M. Wilson, "Probing the quantum vacuum with an artificial atom in front of a mirror", Nature Physics **11**, 1045-1049 (2015).

[33] H. Pichler and P. Zoller, "Photonic circuits with time delays and quantum feedback", Physical Review Letters **116**, 093601 (2016).

[34] P. Y. Wen, A. F. Kockum, H. Ian, J. C. Chen, F. Nori, and I.-C. Hoi, "Reflective amplification without population inversion from a strongly driven superconducting qubit", Physical Review Letters **120**, 063603 (2018).

[35] E. Wiegand, B. Rousseaux, and G. Johansson, "Transmon in a semi-infinite high-impedance transmission line: Appearance of cavity modes and rabi oscillations", Physical Review Research **3**, 023003 (2021).

[36] E. Wiegand, P.-Y. Wen, P. Delsing, I.-C. Hoi, and A. F. Kockum, "Ultimate quantum limit for amplification: a single atom in front of a mirror", New Journal of Physics **23**, 043048 (2021).

[37] A. J. Daley, I. Bloch, C. Kokail, S. Flannigan, N. Pearson, M. Troyer, and P. Zoller, "Practical quantum advantage in quantum simulation", Nature **607**, 667–676 (2022).

[38] J. T. Shen and S. Fan, "Coherent photon transport from spontaneous emission in one-dimensional waveguides", Optics Letters **30**, 2001–2003 (2005).

[39] J. T. Shen and S. Fan, "Coherent Single Photon Transport in a One-Dimensional Waveguide Coupled with Superconducting Quantum Bits", Physical Review Letters **95**, 213001 (2005).

[40] I. De Vega and D. Alonso, "Dynamics of non-Markovian open quantum systems", Reviews of Modern Physics **89**, 015001 (2017).

[41] D. Roy, C. M. Wilson, and O. Firstenberg, "Colloquium: Strongly interacting photons in one-dimensional continuum", Reviews of Modern Physics **89**, 021001 (2017).

[42] C. Cohen-Tannoudji, B. Diu, and F. Laloë, *Quantum Mechanics, Vol. II* (Wiley, New York, 1977).

[43] A. M. Vadiraj, A. Ask, T. G. McConkey, I. Nsanzineza, C. W. S. Chang, A. F. Kockum, and C. M. Wilson, "Engineering the level structure of a giant artificial atom in waveguide quantum electrodynamics", Physical Review A **103**, 023710 (2021).

[44] Z. Q. Wang, Y. P. Wang, J. Yao, R. C. Shen, W. J. Wu, J. Qian, J. Li, S. Y. Zhu, and J. Q. You, "Giant spin ensembles in waveguide magnonics", Nature communications **13**, 7580 (2022).

[45] G. Andersson, M. K. Ekström, and P. Delsing, "Electromagnetically Induced Acoustic Transparency with a Superconducting Circuit", Physical Review Letters **124**, 240402 (2020).

[46] A. Frisk Kockum, G. Johansson, and F. Nori, "Decoherence-Free Interaction between Giant Atoms in Waveguide Quantum Electrodynamics", Physical Review Letters **120**, 140404 (2018).

[47] T. M. Karg, B. Gouraud, P. Treutlein, and K. Hammerer, "Remote Hamiltonian interactions mediated by light", Physical Review A **99**, 063829 (2019).

[48] A. Carollo, D. Cilluffo, and F. Ciccarello, "Mechanism of decoherence-free coupling between giant atoms", Physical Review Research **2**, 043184 (2020).

[49] G. Calajó, F. Ciccarello, D. Chang, and P. Rabl, "Atom-field dressed states in slow-light waveguide QED", Physical Review A **93**, 033833 (2016).

[50] J. S. Douglas, H. Habibian, C. L. Hung, A. V. Gorshkov, H. J. Kimble, and D. E. Chang, "Quantum many-body models with cold atoms coupled to photonic crystals", Nature Photonics **9**, 326–331 (2015).

[51] A. González-Tudela, C. L. Hung, D. E. Chang, J. I. Cirac, and H. J. Kimble, "Subwavelength vacuum lattices and atom-atom interactions in two-dimensional photonic crystals", Nature Photonics **9**, 320–325 (2015).

[52] D. E. Chang, J. S. Douglas, A. González-Tudela, C. L. Hung, and H. J. Kimble, "Colloquium: Quantum matter built from nanoscopic lattices of atoms and photons", Reviews of Modern Physics **90**, 31002 (2018).

[53] V. P. Bykov, "Spontaneous Emission From a Medium With a Band Spectrum.", Soviet Journal of Quantum Electronics **4**, 861 (1975).

[54] S. John and J. Wang, "Quantum electrodynamics near a photonic band gap: Photon bound states and dressed atoms", Physical Review Letters **64**, 2418–2421 (1990).

[55] S. John and T. Quang, "Spontaneous emission near the edge of a photonic band gap", Physical Review A **50**, 1764 (1994).

[56] A. G. Kofman, G. Kurizki, and B. Sherman, "Spontaneous and induced atomic decay in photonic band structures", Journal of Modern Optics **41**, 353–384 (1994).

[57] S. Bay, P. Lambropoulos, and K. Mølmer, "Atom-atom interaction in strongly modified reservoirs", Physical Review A **55**, 1485 (1997).

[58] P. Lambropoulos, G. M. Nikolopoulos, T. R. Nielsen, and S. Bay, "Fundamental quantum optics in structured reservoirs", Reports on Progress in Physics **63**, 455 (2000).

[59] E. Shahmoon and G. Kurizki, "Nonradiative interaction and entanglement between distant atoms", Physical Review A **87**, 033831 (2013).

[60] X. Zhang, E. Kim, D. K. Mark, S. Choi, and O. Painter, "A superconducting quantum simulator based on a photonic-bandgap metamaterial", Science **379**, 278–283 (2023).

[61] C. Tabares, A. Muñoz de las Heras, L. Tagliacozzo, D. Porras, and A. González-Tudela, "Variational quantum simulators based on waveguide qed", Physical Review Letters **131**, 073602 (2023).

[62] A. González-Tudela and J. I. Cirac, "Markovian and non-Markovian dynamics of quantum emitters coupled to two-dimensional structured reservoirs", Physical Review A **96**, 043811 (2017).

[63] A. González-Tudela and J. I. Cirac, "Quantum Emitters in Two-Dimensional Structured Reservoirs in the Nonperturbative Regime", Physical Review Letters **119**, 143602 (2017).

[64] T. Aref, P. Delsing, M. K. Ekström, A. F. Kockum, M. V. Gustafsson, G. Johansson, P. J. Leek, E. Magnusson, and R. Manenti, in *Superconducting Devices in Quantum Optics*, edited by R. H. Hadfield and G. Johansson (Springer, 2016).

[65] R. Manenti, A. F. Kockum, A. Patterson, T. Behrle, J. Rahamim, G. Tancredi, F. Nori, and P. J. Leek, "Circuit quantum acoustodynamics with surface acoustic waves", Nature Communications **8**, 975 (2017).

[66] A. Noguchi, R. Yamazaki, Y. Tabuchi, and Y. Nakamura, "Qubit-Assisted Transduction for a Detection of Surface Acoustic Waves near the Quantum Limit", Physical Review Letters **119**, 180505 (2017).

[67] K. J. Satzinger, Y. P. Zhong, H.-S. Chang, G. A. Peairs, A. Bienfait, M.-H. Chou, A. Y. Cleland, C. R. Conner, É. Dumur, J. Grebel, I. Gutierrez, B. H. November, R. G. Povey, S. J. Whiteley, D. D. Awschalom, D. I. Schuster, and A. N. Cleland, "Quantum control of surface acoustic-wave phonons", Nature **563**, 661 (2018).

[68] B. A. Moores, L. R. Sletten, J. J. Viennot, and K. W. Lehnert, "Cavity Quantum Acoustic Device in the Multimode Strong Coupling Regime", Physical Review Letters **120**, 227701 (2018).

[69] A. N. Bolgar, J. I. Zotova, D. D. Kirichenko, I. S. Besedin, A. V. Semenov, R. S. Shaikhaidarov, and O. V. Astafiev, "Quantum Regime of a Two-Dimensional Phonon Cavity", Physical Review Letters **120**, 223603 (2018).

[70] L. R. Sletten, B. A. Moores, J. J. Viennot, and K. W. Lehnert, "Resolving Phonon Fock States in a Multimode Cavity with a Double-Slit Qubit", Physical Review X **9**, 021056 (2019).

[71] A. Bienfait, K. J. Satzinger, Y. P. Zhong, H.-S. Chang, M.-H. Chou, C. R. Conner, É. Dumur, J. Grebel, G. A. Peairs, R. G. Povey, and A. N. Cleland, "Phonon-mediated quantum state transfer and remote qubit entanglement", Science **364**, 368 (2019).

[72] G. Andersson, B. Suri, L. Guo, T. Aref, and P. Delsing, "Non-exponential decay of a giant artificial atom", Nature Physics **15**, 1123–1127 (2019).

[73] A. Bienfait, Y. P. Zhong, H.-S. Chang, M.-H. Chou, C. R. Conner, É. Dumur, J. Grebel, G. A. Peairs, R. G. Povey, K. J. Satzinger, and A. N. Cleland, "Quantum Erasure Using Entangled Surface Acoustic Phonons", Physical Review X **10**, 021055 (2020).

[74] C. Joshi, F. Yang, and M. Mirhosseini, "Resonance fluorescence of a chiral artificial atom", Physical Review X **13**, 021039 (2023).

[75] A. González-Tudela, C. S. Muñoz, and J. I. Cirac, "Engineering and Harnessing Giant Atoms in High-Dimensional Baths: A Proposal for Implementation with Cold Atoms", Physical Review Letters **122**, 203603 (2019).

[76] L. Du, Y. Zhang, J. H. Wu, A. F. Kockum, and Y. Li, "Giant Atoms in a Synthetic Frequency Dimension", Physical Review Letters **128**, 223602 (2022).

[77] Y.-T. Chen, L. Du, Y. Zhang, L. Guo, J.-H. Wu, M. Artoni, and G. C. La Rocca, "Giant-atom effects on population and entanglement dynamics of rydberg atoms in the optical regime", Physical Review Research **5**, 043135 (2023).

[78] Y.-T. Chen, L. Du, Z. Wang, M. Artoni, G. C. La Rocca, and J.-H. Wu, "Single-photon manipulations based on optically controlled chiral couplings in waveguide structures of rydberg giant atoms", Physical Review A **109**, 063710 (2024).

[79] P. O. Guimond, B. Vermersch, M. L. Juan, A. Sharafiev, G. Kirchmair, and P. Zoller, "A unidirectional on-chip photonic interface for superconducting circuits", npj Quantum Information **6**, 32 (2020).

[80] N. Gheeraert, S. Kono, and Y. Nakamura, "Programmable directional emitter and receiver of itinerant microwave photons in a waveguide", Physical Review A **102**, 053720 (2020).

[81] Y. X. Zhang, C. R. I Carceller, M. Kjaergaard, and A. S. Sørensen, "Charge-Noise Insensitive Chiral Photonic Interface for Waveguide Circuit QED", Physical Review Letters **127**, 233601 (2021).

[82] B. Kannan, A. Almanakly, Y. Sung, A. Di Paolo, D. A. Rower, J. Braumüller, A. Melville, B. M. Niedzielski, A. Karamlou, K. Serniak, A. Vepsäläinen, M. E. Schwartz, J. L. Yoder, R. Winik, J. I. Wang, T. P. Orlando, S. Gustavsson, J. A. Grover, and W. D. Oliver, "On-demand directional microwave photon emission using waveguide quantum electrodynamics", Nature Physics **19**, 394-400 (2023).

[83] A. Almanakly, B. Yankelevich, M. Hays, B. Kannan, R. Assouly, A. Greene, M. Gingras, B. M. Niedzielski, H. Stickler, M. E. Schwartz, K. Serniak, J. Î.-j. Wang, T. P. Orlando, S. Gustavsson, J. A. Grover, and W. D. Oliver, "Deterministic remote entanglement using a chiral quantum interconnect", Nature Physics **21**, 825–830 (2025).

[84] T. M. Karg, B. Gouraud, C. T. Ngai, G.-L. Schmid, K. Hammerer, and P. Treutlein, "Light-mediated strong coupling between a mechanical oscillator and atomic spins 1 meter apart", Science **369**, 174-179 (2020).

[85] L. Du, X. Wang, A. F. Kockum, and J. Splettstoesser, "Dressed interference in giant superatoms: Entanglement generation and transfer", arXiv:2504.12942 [quant-ph] (2025).

[86] A. Frisk Kockum, *Quantum Optics with Semiconducting Artificial Atoms*, Ph.D. thesis, Chalmers University of Technology (2014).

[87] F. W. Strauch, P. R. Johnson, A. J. Dragt, C. J. Lobb, J. R. Anderson, and F. C. Wellstood, "Quantum logic gates for coupled superconducting phase qubits", Physical Review Letters **91**, 167005 (2003).

[88] P. Krantz, M. Kjaergaard, F. Yan, T. P. Orlando, S. Gustavsson, and W. D. Oliver, "A quantum engineer's guide to superconducting qubits", Applied Physics Reviews **6**, 021318 (2019).

[89] I. Carusotto, A. A. Houck, A. J. Kollár, P. Roushan, D. I. Schuster, and J. Simon, "Photonic materials in circuit quantum electrodynamics", Nature Physics **16**, 268–279 (2020).

[90] S.-P. Yu, J. D. Hood, J. A. Muniz, M. J. Martin, R. Norte, C.-L. Hung, S. M. Meenehan, J. D. Cohen, O. Painter, and H. J. Kimble, "Nanowire photonic crystal waveguides for single-atom trapping and strong light-matter interactions", Applied Physics Letters **104**, 111103 (2014).

[91] A. Goban, C.-L. Hung, S.-P. Yu, J. D. Hood, J. A. Muniz, J. H. Lee, M. J. Martin, A. C. McClung, K. S. Choi, D. E. Chang, O. Painter, and H. J. Kimble, "Atom–light interactions in photonic crystals", Nature Communications **5**, 3808 (2014).

[92] A. Goban, C.-L. Hung, J. D. Hood, S.-P. Yu, J. A. Muniz, O. Painter, and H. J. Kimble, "Superradiance for atoms trapped along a photonic crystal waveguide", Physical Review Letters **115**, 063601 (2015).

[93] J. D. Hood, A. Goban, A. Asenjo-Garcia, M. Lu, S. P. Yu, D. E. Chang, and H. J. Kimble, "Atom-atom interactions around the band edge of a photonic crystal waveguide", Proceedings of the National Academy of Sciences of the United States of America **113**, 10507–10512 (2016).

[94] L. Krinner, M. Stewart, A. Pazmiño, J. Kwon, and D. Schneble, "Spontaneous emission of matter waves from a tunable open quantum system", Nature **559**, 589–592 (2018).

[95] M. Stewart, J. Kwon, A. Lanuza, and D. Schneble, "Dynamics of matter-wave quantum emitters in a structured vacuum", Physical Review Research **2**, 043307 (2020).

[96] T. Lund-Hansen, S. Stobbe, B. Julsgaard, H. Thyrrestrup, T. Sünner, M. Kamp, A. Forchel, and P. Lodahl, "Experimental realization of highly efficient broadband coupling of single quantum dots to a photonic crystal waveguide", Physical Review Letters **101**, 113903 (2008).

[97] A. B. Young, A. C. T. Thijssen, D. M. Beggs, P. Androvitsaneas, L. Kuipers, J. G. Rarity, S. Hughes, and R. Oulton, "Polarization engineering in photonic crystal waveguides for spin-photon entanglers", Physical Review Letters **115**, 153901 (2015).

[98] Y. Liu and A. A. Houck, "Quantum electrodynamics near a photonic bandgap", Nature Physics **13**, 48–52 (2017).

[99] N. M. Sundaresan, R. Lundgren, G. Zhu, A. V. Gorshkov, and A. A. Houck, "Interacting Qubit-Photon Bound States with Superconducting Circuits", Physical Review X **9**, 011021 (2019).

[100] P. M. Harrington, M. Naghiloo, D. Tan, and K. W. Murch, "Bath engineering of a fluorescing artificial atom with a photonic crystal", Physical Review A **99**, 052126 (2019).

[101] M. Mirhosseini, E. Kim, V. S. Ferreira, M. Kalaee, A. Sipahigil, A. J. Keller, and O. Painter, "Superconducting metamaterials for waveguide quantum electrodynamics", Nature Communications **9**, 3706 (2018).

[102] S. Indrajeet, H. Wang, M. D. Hutchings, B. G. Taketani, F. K. Wilhelm, M. D. Lahaye, and B. L. Plourde, "Coupling a Superconducting Qubit to a Left-Handed Metamaterial Resonator", Physical Review Applied **14**, 064033 (2020).

[103] E. Kim, X. Zhang, V. S. Ferreira, J. Banker, J. K. Iverson, A. Sipahigil, M. Bello, A. González-Tudela, M. Mirhosseini, and O. Painter, "Quantum Electrodynamics in a Topological Waveguide", Physical Review X **11**, 011015 (2021).

[104] V. S. Ferreira, J. Banker, A. Sipahigil, M. H. Matheny, A. J. Keller, E. Kim, M. Mirhosseini, and O. Painter, "Collapse and Revival of an Artificial Atom Coupled to a Structured Photonic Reservoir", Physical Review X **11**, 41043 (2021).

[105] M. Scigliuzzo, G. Calajò, F. Ciccarello, D. Perez Lozano, A. Bengtsson, P. Scarlino, A. Wallraff, D. Chang, P. Delsing, and S. Gasparinetti, "Controlling Atom-Photon Bound States in an Array of Josephson-Junction Resonators", Physical Review X **12**, 31036 (2022).

[106] V. Jouanny, S. Frasca, V. J. Weibel, l. Peyruchat, M. Scigliuzzo, F. Oppliger, F. De Palma, D. Sbroggiò, G. Beaulieu, O. Zilberberg, and P. Scarlino, "High kinetic inductance cavity arrays for compact band engineering and topology-based disorder meters", Nature Communications **16**, 3396 (2025).

[107] C. Castillo-Moreno, K. R. Amin, I. Strandberg, M. Kervinen, A. Osman, and S. Gasparinetti, "Dynamical excitation control and multimode emission of an atom-photon bound state", Physical Review Letters **134**, 133601 (2025).

[108] D. Rosenberg, D. Kim, R. Das, D. Yost, S. Gustavsson, D. Hover, P. Krantz, A. Melville, L. Racz, G. O. Samach, S. J. Weber, F. Yan, J. L. Yoder, A. J. Kerman, and W. D. Oliver, "3D integrated superconducting qubits", npj Quantum Information **3**, 42 (2017).

[109] J. Rahamim, T. Behrle, M. J. Peterer, A. Patterson, P. A. Spring, T. Tsunoda, R. Manenti, G. Tancredi, and P. J. Leek, "Double-sided coaxial circuit QED with out-of-plane wiring", Applied Physics Letters **110**, 222602 (2017).

[110] S. Kosen, H.-X. Li, M. Rommel, D. Shiri, C. Warren, L. Grönberg, J. Salonen, T. Abad, J. Biznárová, M. Caputo, L. Chen, K. Grigoras, G. Johansson, A. F. Kockum, C. Križan, D. P. Lozano, G. J. Norris, A. Osman, J. Fernández-Pendás, A. Ronzani, A. F. Roudsari, S. Simbierowicz, G. Tancredi, A. Wallraff, C. Eichler, J. Govenius, and J. Bylander, "Building blocks of a flip-chip integrated superconducting quantum processor", Quantum Science and Technology **7**, 035018 (2022).

[111] G. Jaeger, *Quantum Information: An Overview* (Springer Science + Business Media, 2007).

[112] W. K. Wootters, "Entanglement of formation of an arbitrary state of two qubits", Physical Review Letters **80**, 2245–2248 (1998).

[113] A. Uhlmann, "The "transition probability" in the state space of a *-algebra", Reports on Mathematical Physics **9**, 273-279 (1976).

[114] R. Jozsa, "Fidelity for mixed quantum states", Journal of Modern Optics **41**, 2315–2323 (1994).

[115] J. R. Johansson, P. D. Nation, and F. Nori, "QuTiP 2: A Python framework for the dynamics of open quantum systems", Computer Physics Communications **184**, 1234 (2013).

[116] J. Biznárová, *Development of high-coherence superconducting devices for quantum computing: Fabrication process development, materials analysis, and device characterization*, Ph.D. thesis, Chalmers University of Technology (2024).

[117] D. Brand, I. Sinayskiy, and F. Petruccione, "Markovian noise modelling and parameter extraction framework for quantum devices", Science Reports **14**, 4769 (2024).

[118] Y. Lu, A. Bengtsson, J. J. Burnett, E. Wiegand, B. Suri, P. Krantz, A. F. Roudsari, A. F. Kockum, S. Gasparinetti, G. Johansson, and P. Delsing, "Characterizing decoherence rates of a superconducting qubit by direct microwave scattering", npj Quantum Information **7**, 35 (2021).

[119] A. Nordsieck, W. Lamb, and G. Uhlenbeck, "On the theory of cosmic-ray showers i the furry model and the fluctuation problem", Physica **7**, 344-360 (1940).

[120] H. P. Breuer and F. Petruccione, *The theory of open quantum systems* (Oxford University Press, 2002).

[121] G. Lindblad, "On the generators of quantum dynamical semigroups", Communications in Mathematical Physics **48**, 119-130 (1976).

[122] V. Gorini, A. Kossakowski, and E. C. G. Sudarshan, "Completely positive dynamical semigroups of n-level systems", Journal of Mathematical Physics **17**, 821-825 (1976).

[123] I. I. Rabi, "Space quantization in a gyrating magnetic field", Physical Review **51**, 652–654 (1937).

[124] H. J. Carmichael, *Statistical Methods in Quantum Optics 1* (Springer-Verlag Berlin Heidelberg, 1999).

[125] F. Bloch and A. Siegert, "Magnetic Resonance for Nonrotating Fields", Physical Review **57**, 522 (1940).

[126] E. Jaynes and F. Cummings, "Comparison of quantum and semiclassical radiation theories with application to the beam maser", Proceedings of the IEEE **51**, 89-109 (1963).

[127] G. S. Agarwal, "Rotating-Wave Approximation and Spontaneous Emission", Physical Review A **7**, 1195 (1973).

[128] G. S. Agarwal, "Quantum statistical theories of spontaneous emission and their relation to other approaches", in *Quantum Optics*, edited by G. Höhler (Springer Berlin Heidelberg, Berlin, Heidelberg, 1974) pp. 1–128.

[129] L. S. Bishop, *Circuit Quantum Electrodynamics*, Ph.D. thesis, Yale University (2010).

[130] J. Gough and M. R. James, "Quantum Feedback Networks: Hamiltonian Formulation", Communications in Mathematical Physics **287**, 1109–1132 (2009).

[131] J. Gough and M. R. James, "The Series Product and Its Application to Quantum Feedforward and Feedback Networks", IEEE Transactions on Automatic Control **54**, 2530–2544 (2009).

[132] J. Combes, J. Kerckhoff, and M. Sarovar, "The SLH framework for modeling quantum input-output networks", Advances in Physics: X **2**, 784–888 (2017).

[133] R. Mitsch, C. Sayrin, B. Albrecht, P. Schneeweiss, and A. Rauschenbeutel, "Quantum state-controlled directional spontaneous emission of photons into a nanophotonic waveguide", Nature Communications **5**, 5713 (2014).

[134] J. Petersen, J. Volz, and A. Rauschenbeutel, "Chiral nanophotonic waveguide interface based on spin-orbit interaction of light", Science **346**, 67–71 (2014).

[135] K. Y. Bliokh and F. Nori, "Transverse and longitudinal angular momenta of light", Physics Reports **592**, 1–38 (2015).

[136] S. J. Masson and A. Asenjo-Garcia, "Atomic-waveguide quantum electrodynamics", Physical Review Research **2**, 043213 (2020).

[137] S. R. Sathyamoorthy, L. Tornberg, A. F. Kockum, B. Q. Baragiola, J. Combes, C. M. Wilson, T. M. Stace, and G. Johansson, "Quantum Nondemolition Detection of a Propagating Microwave Photon", Physical Review Letters **112**, 093601 (2014).

[138] K. M. Sliwa, M. Hatridge, A. Narla, S. Shankar, L. Frunzio, R. J. Schoelkopf, and M. H. Devoret, "Reconfigurable Josephson Circulator/Directional Amplifier", Physical Review X **5**, 041020 (2015).

[139] B. J. Chapman, E. I. Rosenthal, J. Kerckhoff, B. A. Moores, L. R. Vale, J. A. B. Mates, G. C. Hilton, K. Lalumière, A. Blais, and K. W. Lehnert, "Widely Tunable On-Chip Microwave Circulator for Superconducting Quantum Circuits", Physical Review X **7**, 041043 (2017).

[140] C. Müller, S. Guan, N. Vogt, J. H. Cole, and T. M. Stace, "Passive On-Chip Superconducting Circulator Using a Ring of Tunnel Junctions", Physical Review Letters **120**, 213602 (2018).

[141] E. Sánchez-Burillo, C. Wan, D. Zueco, and A. González-Tudela, "Chiral quantum optics in photonic sawtooth lattices", Physical Review Research **2**, 023003 (2020).

[142] D. Suárez-Forero, M. Jalali Mehrabad, C. Vega, A. González-Tudela, and M. Hafezi, "Chiral quantum optics: Recent developments and future directions", PRX Quantum **6**, 020101 (2025).

[143] Y.-J. Lin, K. Jiménez-García, and I. B. Spielman, "Spin–orbit-coupled Bose–Einstein condensates", Nature **471**, 83–86 (2011).

[144] V. Galitski and I. B. Spielman, "Spin–orbit coupling in quantum gases", Nature **494**, 49–54 (2013).

[145] T. Ramos, H. Pichler, A. J. Daley, and P. Zoller, "Quantum Spin Dimers from Chiral Dissipation in Cold-Atom Chains", Physical Review Letters **113**, 237203 (2014).

[146] B. Vermersch, T. Ramos, P. Hauke, and P. Zoller, "Implementation of chiral quantum optics with Rydberg and trapped-ion setups", Physical Review A **93**, 063830 (2016).

[147] A. F. van Loo, R. G. E. Morris, and A. D. Karenowska, "Time-Resolved Measurements of Surface Spin-Wave Pulses at Millikelvin Temperatures", Physical Review Applied **10**, 044070 (2018).

[148] T. Ramos, B. Vermersch, P. Hauke, H. Pichler, and P. Zoller, "Non-Markovian dynamics in chiral quantum networks with spins and photons", Physical Review A **93**, 062104 (2016).

[149] K. Stannigel, P. Rabl, and P. Zoller, "Driven-dissipative preparation of entangled states in cascaded quantum-optical networks", New Journal of Physics **14**, 063014 (2012).

[150] C. Gonzalez-Ballestero, A. Gonzalez-Tudela, F. J. Garcia-Vidal, and E. Moreno, "Chiral route to spontaneous entanglement generation", Physical Review B **92**, 155304 (2015).

[151] H. Pichler, T. Ramos, A. J. Daley, and P. Zoller, "Quantum optics of chiral spin networks", Physical Review A **91**, 42116 (2015).

[152] P.-O. Guimond, H. Pichler, A. Rauschenbeutel, and P. Zoller, "Chiral quantum optics with V-level atoms and coherent quantum feedback", Physical Review A **94**, 033829 (2016).

[153] P. Lodahl, S. Mahmoodian, S. Stobbe, A. Rauschenbeutel, P. Schneeweiss, J. Volz, H. Pichler, and P. Zoller, "Chiral quantum optics", Nature **541**, 473–480 (2017).

[154] M. Bello, G. Platero, J. I. Cirac, and A. González-Tudela, "Unconventional quantum optics in topological waveguide QED", Science Advances **5**, eaaw0297 (2019).

[155] T. Ozawa, H. M. Price, A. Amo, N. Goldman, M. Hafezi, L. Lu, M. C. Rechtsman, D. Schuster, J. Simon, O. Zilberberg, and I. Carusotto, "Topological photonics", Reviews of Modern Physics **91**, 015006 (2019).

[156] M. Scheucher, J. Volz, and A. Rauschenbeutel, in *Ultra-High-Q Optical Microcavities*, edited by Y.-F. Xiao, C.-L. Zou, Q. Gong, and L. Yang (World Scientific, 2020) Chap. 5, pp. 159–201.

[157] S. Mahmoodian, G. Calajó, D. E. Chang, K. Hammerer, and A. S. Sørensen, "Dynamics of Many-Body Photon Bound States in Chiral Waveguide QED", Physical Review X **10**, 031011 (2020).

[158] R. H. Dicke, "Coherence in Spontaneous Radiation Processes", Physical Review **93**, 99 (1954).

[159] C. W. Gardiner, "Driving a quantum system with the output field from another driven quantum system", Physical Review Letters **70**, 2269 (1993).

[160] H. J. Carmichael, "Quantum trajectory theory for cascaded open systems", Physical Review Letters **70**, 2273 (1993).

[161] J. Kerckhoff, *Quantum Engineering with Quantum Optics*, Ph.D. thesis, Standford University (2011).

[162] R. H. Lehmberg, "Radiation from an N-Atom System. II. Spontaneous Emission from a Pair of Atoms", Physical Review A **2**, 889 (1970).

[163] G. Lenz and P. Meystre, "Resonance fluorescence from two identical atoms in a standing-wave field", Physical Review A **48**, 3365 (1993).

[164] F. Le Kien, S. D. Gupta, K. P. Nayak, and K. Hakuta, "Nanofiber-mediated radiative transfer between two distant atoms", Physical Review A **72**, 063815 (2005).

[165] K. Lalumière, B. C. Sanders, A. F. van Loo, A. Fedorov, A. Wallraff, and A. Blais, "Input-output theory for waveguide QED with an ensemble of inhomogeneous atoms", Physical Review A **88**, 043806 (2013).

[166] M. Fleischhauer and M. D. Lukin, "Quantum memory for photons: Dark-state polaritons", Physical Review A **65**, 022314 (2002).

[167] A. I. Lvovsky, B. C. Sanders, and W. Tittel, "Optical quantum memory", Nature Photonics **3**, 706–714 (2009).

[168] K. Heshami, D. G. England, P. C. Humphreys, P. J. Bustard, V. M. Acosta, J. Nunn, and B. J. Sussman, "Quantum memories: emerging applications and recent advances", Journal of Modern Optics **63**, 2005–2028 (2016).

[169] H. J. Kimble, "The quantum internet", Nature **453**, 1023–1030 (2008).

[170] S. Wehner, D. Elkouss, and R. Hanson, "Quantum internet: A vision for the road ahead", Science **362**, eaam9288 (2018).

[171] A. Barenco, C. H. Bennett, R. Cleve, D. P. DiVincenzo, N. Margolus, P. Shor, T. Sleator, J. A. Smolin, and H. Weinfurter, "Elementary gates for quantum computation", Physical Review A **52**, 3457 (1995).

[172] G. Chen and A. F. Kockum, "Scalable quantum simulator with an extended gate set in giant atoms", arXiv:2503.04537 [quant-ph] (2025).

[173] J. W. Brown and R. V. Churchill, *Complex Variables and Applications*, 8th ed. (McGraw-Hill, 2009).

[174] E. T. Whittaker and G. N. Watson, *A Course of Modern Analysis* (Cambridge University Press, 1996).

[175] X. Zhang, C. Liu, Z. Gong, and Z. Wang, "Quantum interference and controllable magic cavity QED via a giant atom in a coupled resonator waveguide", Physical Review A **108**, 013704 (2023).

[176] M. Weng, H. Yu, and Z. Wang, "High-fidelity generation of bell and w states in a giant-atom system via bound states in the continuum", Phys. Rev. A **111**, 053711 (2025).

[177] Y. Zhao, H. Wu, X. Li, L. Li, J. Xiao, Z.-Y. Zeng, Y. Chen, and X. Luo, "Generation and stabilization of bound states in the continuum in dissipative floquet optical lattices", arXiv:2505.06931 [quant-ph] (2025).

[178] B. Kramer and A. MacKinnon, "Localization: theory and experiment", Reports on Progress in Physics **56**, 1469 (1993).

[179] E. R. Ingelsten, *Quantum optics with giant atoms in 2D structured environments*, Master's thesis, Chalmers University of Technology (2023).

[180] J. von Neumann and E. P. Wigner, "Über merkwürdige diskrete Eigenwerte", Physikalische Zeitschrift **30**, 467 (1929).

[181] C. W. Hsu, B. Zhen, A. D. Stone, J. D. Joannopoulos, and M. Soljačić, "Bound states in the continuum", Nature Reviews Materials **1**, 16048 (2016).

[182] M. Kang, T. Liu, C. T. Chan, and M. Xiao, "Applications of bound states in the continuum in photonics", Nature Reviews Physics **5**, 659–678 (2023).

[183] G. Xu, H. Xing, Z. Xue, D. Lu, J. Fan, J. Fan, P. P. Shum, and L. Cong, "Recent Advances and Perspective of Photonic Bound States in the Continuum", Ultrafast Science **3**, 0033 (2023).

[184] L. Guo, A. F. Kockum, F. Marquardt, and G. Johansson, "Oscillating bound states for a giant atom", Physical Review Research **2**, 043014 (2020).

[185] S. Guo, Y. Wang, T. Purdy, and J. Taylor, "Beyond spontaneous emission: Giant atom bounded in the continuum", Physical Review A **102**, 033706 (2020).

[186] S. Longhi, "Rabi oscillations of bound states in the continuum", Optics Letters **46**, 2091 (2021).

[187] S. Terradas-Briansó, C. A. González-Gutiérrez, F. Nori, L. Martín-Moreno, and D. Zueco, "Ultrastrong waveguide QED with giant atoms", Physical Review A **106**, 063717 (2022).

[188] D. D. Noachtar, J. Knörzer, and R. H. Jonsson, "Nonperturbative treatment of giant atoms using chain transformations", Physical Review A **106**, 013702 (2022).

[189] K. H. Lim, W. K. Mok, and L. C. Kwek, "Oscillating bound states in non-Markovian photonic lattices", Physical Review A **107**, 023716 (2023).

[190] T. Morita, "Useful Procedure for Computing the Lattice Green's Function-Square, Tetragonal, and bcc Lattices", Journal of Mathematical Physics **12**, 1744-1747 (1971).

[191] C. Cohen-Tannoudji, J. Dupont-Roc, and G. Grynberg, "Nonperturbative Calculation of Transition Amplitudes", in *Atom—Photon Interactions* (John Wiley & Sons, Ltd, 1998) Chap. 3, pp. 165–255.

[192] X. Wang and H.-r. Li, "Chiral quantum network with giant atoms", Quantum Science and Technology **7**, 035007 (2022).

[193] P. S. Shah, F. Yang, C. Joshi, and M. Mirhosseini, "Stabilizing remote entanglement via waveguide dissipation", PRX Quantum **5**, 030346 (2024).

[194] F. Schäfer, T. Fukuhara, S. Sugawa, Y. Takasu, and Y. Takahashi, "Tools for quantum simulation with ultracold atoms in optical lattices", Nature Reviews Physics **2**, 411–425 (2020).

[195] G. Chen and A. Frisk Kockum, "Simulating open quantum systems with giant atoms", Quantum Science and Technology **10**, 025028 (2025).

[196] K. Fan, I. V. Shadrivov, and W. J. Padilla, "Dynamic bound states in the continuum", Optica **6**, 169–173 (2019).

[197] X. Tang, R. He, C. Chen, Z. Huang, and J. Guo, "Quasi-bound states in the continuum in a metal nanograting metasurface for a high figure-of-merit refractive index sensor", Opt. Express **32**, 762–773 (2024).